MONTE CARLO MOLECULAR SIMULATION OF BINARY FLUID-PHASE EQUILIBRIUM USING HETEROGENEOUS MIXING PARAMETERS

by

Suren Moodley

[B.Sc. (Eng.), M.Sc. (Eng.)]

In fulfilment of the degree Doctor Philosophæ,

Chemical Engineering, University of KwaZulu-Natal

27 February 2012

Supervisors: Dr. E. Johansson, Prof. K. Bolton and Prof. D. Ramjugernath

PREFACE

The work presented in this thesis was performed at the University of KwaZulu-Natal, Durban and the University of Borås, Sweden from January 2009 to January 2012. The work was supervised by Dr. E. Johansson, Prof. K. Bolton and Prof. D. Ramjugernath.

As the candidate's supervisor I, Prof. D. Ramjugernath, agree/do not agree to the submission of this thesis.

Signed: …….

DECLARATION

I ..... declare that:

(i) The research reported in this thesis, except where otherwise indicated, is my original work.

(ii) This thesis has not been submitted for any degree or examination at any other university.

(iii) This thesis does not contain other persons' data, pictures, graphs or other information, unless specifically acknowledged as being sourced from other persons.

(iv) This thesis does not contain other persons' writing, unless specifically acknowledged as being sourced from other researchers. Where other written sources have been quoted, then:

   a) their words have been re-written but the general information attributed to them has been referenced;

   b) where their exact words have been used, their writing has been placed inside quotation marks, and referenced.

(v) Where I have reproduced a publication of which I am an author, co-author or editor, I have indicated in detail which part of the publication was actually written by myself alone and have fully referenced such publications.

(vi) This thesis does not contain text, graphics or tables copied and pasted from the Internet, unless specifically acknowledged, and the source being detailed in the dissertation/thesis and in the References sections.

Signed: …….

ACKNOWLEDGEMENTS

- I thank my thesis advisors, Dr. E. Johansson, Prof. K. Bolton and Prof. D. Ramjugernath for their advice and guidance during the course of my postgraduate studies (which helped to enhance the quality of this work and to improve my research skills), for allowing me to work independently, and intervening when necessary.
- The National Research Foundation (NRF), South Africa, for the grant-holder-linked bursary through Prof. D. Ramjugernath.
- The Swedish International Development Cooperation Agency (SIDA), for funding my accommodation and subsistence costs in Sweden.
- The University of KwaZulu-Natal, for paying for my travel expenses to and from Sweden.
- The Department of Science and Technology (DST), for providing the funds that were used to purchase the Dell, Inc. server on which all simulations in this work were run.
- Shalendra Subramoney, for use of the Laboratoire CEP/TEP (THERMOPACK) software package to generate some of the phase equilibrium data that was used for comparisons with simulation results.
- On a less formal note, I thank my fellow postgraduate colleagues David Lokhat, Shalendra Subramoney and Wayne Nelson for their fellowship.

ABSTRACT

Accurate phase equilibrium data is essential for designing efficient chemical separations equipment, and molecular simulations (MS) have become a convenient, practical means for obtaining such data. Typically MS of chemical systems use mixing rules to calculate potential energy model parameters for non-bonded unlike-atoms on different molecule-types in all phases in the same manner (i.e. *homogeneously*). Good predictions of phase equilibrium compositions can be obtained for mixtures comprising chemically-similar molecules, but significant deviations from laboratory experiments are observed with increasing dissimilarity between molecules. This work presents a novel approach for accurately predicting binary two-phase fluid equilibrium in isobaric-isothermal Gibbs ensemble Monte Carlo simulations.

The very first steps using *heterogeneous* unlike-pair parameters in each phase (ε_{12}^{V} and ε_{12}^{L}) were taken, using the mixture methane-xenon. It is shown that homogeneous cross-energy (ε_{12} when $\varepsilon_{12}^{V} = \varepsilon_{12}^{L}$) adjustments are incapable of always predicting vapour- and liquid-phase compositions with good accuracy simultaneously at all state points. Increasing ε_{12}, which increases attractive forces between methane and xenon by decreasing the Lennard-Jones potential well depth, led to enhancement of methane solubility in both phases in the two-phase region. The opposite was true when decreasing ε_{12}. In spite of its shortcomings, the ε_{12} approach was used to show its equivalence to the k_{ij} interaction parameter used in equation of state models, its optimum-value temperature-dependence, and a discontinuity of the optimum-value at/near the methane critical temperature. Speculation by other workers of the discontinuity being due to new interactions generated in the supercritical region was verified by analysing potential energies.

The lack of simultaneity of good solubility predictions in both phases was overcome with the heterogeneous approach. It revealed strong coupling between the phases that was attributed to the large difference between the pure components' Lennard-Jones εs, and also that different heterogeneous pairs can give the same compositions i.e. a degeneracy. Keeping ε_{12}^{L} constant and increasing ε_{12}^{V} showed both decreases and increases of methane solubility in both phases that were larger at lower ε_{12}^{L} and smaller at higher ε_{12}^{L}, for a given ε_{12}^{V} change. This was due to the total (vapour + liquid) potential energies determining the overall nature of the forces in the system (i.e. attractive or repulsive).

Finally, a model (based on a recent MS study) for determining optimum heterogeneous pairs that also formally proves the degeneracy of the heterogeneous approach is developed and discussed.

The study proved to be a promising step by using a fresh approach towards addressing the limitations of the homogeneous mixing parameter approach. Although a unique solution is not (always) possible thus making optimum-parameter trends arbitrary, it is still of good practical value for application to more complex mixtures in future studies.

TABLE OF CONTENTS

LIST OF FIGURES

LIST OF TABLES

1. INTRODUCTION

This study reports a novel approach for addressing problems associated with using conventional mixing rules in Monte Carlo molecular simulations of fluid phase equilibria of mixtures. This approach can be used for molecular systems in which the non-bonded van der Waals intermolecular forces are modelled by the ubiquitous Lennard-Jones 12-6 potential energy model (Lennard-Jones, 1924), which is a specific form of the more-generalized Mie potential (Mie, 1903), and the Lorentz (Lorentz, 1881) and Berthelot (Berthelot, 1889) mixing rules (collectively known as the Lorentz-Berthelot mixing rules).

Some of the earliest types of chemical separations were carried out by the Babylonians over four millennia ago in a region then known as Mesopotamia for the manufacture of perfume products (Levey, 1954), while the clearest initial evidence for distillation is attributed to Greek alchemists working in Alexandria, Egypt, approximately two millennia ago (Forbes, 1970). (Although the mixture distilled during this period is not explicitly stated, it is believed that the mixture was sea water, which the alchemists separated to obtain fresh water and salt.) Ever since, significant progress has been made as alchemy turned into chemistry, which in turn merged with other sciences to form chemical engineering; this has made the transformation of laboratory-scale separation processes into the industrial scale feasible. Along with the advancements in these subjects, chemical separation equipment of ever-increasing complexity has been developed as well: from the batch distillation alembic (an alchemical still) of the Greeks, which was later modified by the Persian polymath Geber (who developed modern distillation), to the continuous distillation Cellier Blumenthal still (Forbes, 1970).

A crucial aspect in the design of chemical separations processes such as distillation is the acquisition of accurate phase equilibrium data. Aside from laboratory experiments, such as conventional phase equilibrium measurements in conjunction with a chemical analysis technique, e.g. gas chromatography (for example, see Joseph *et al*. (2001) and Naidoo *et al*. (2008)), molecular simulation provides an alternative means for studying the properties of coexisting phases of matter and generating phase diagrams. It can provide great insight into the microscopic structure of the different forms of matter, but only if reliable methods for

describing and calculating the interactions between the matter constituents are available; after all, the properties that different phases of matter exhibit are necessarily due to the characteristic interactions amongst the molecules. With the current global trend of being more environmentally-friendly, while at the same time reducing the cost of designing, manufacturing and setting up expensive laboratories, molecular simulations are no longer seen as just complementary to experiments, but rather as a genuine, practical means for obtaining reliable thermodynamic data *in lieu* of experimental data. Within this field, one uses molecular dynamics (MD) if the dynamical properties, e.g. diffusion coefficients and viscosity, of a system are sought, in which case the classical equations of motion are repeatedly solved as the atoms or molecules follow a deterministic trajectory in space. On the other hand if one requires the equilibrium properties of a system, then the preferred simulation method is the stochastic Monte Carlo (MC) technique, wherein random numbers and acceptance/rejection criteria for different trial moves determine the trajectory of the system in Gibbs phase space – this permits the simulation to perform 'unphysical' trial moves (Frenkel & Smit, 2002) that speeds up the system's approach to equilibrium. It should be noted that MD can also be used to study systems at equilibrium, but the approach to equilibrium may take an extremely long time, making it impractical for research purposes (Frenkel & Smit, 2002).

While accurate phase equilibrium predictions can be made via MC molecular simulations for the two-phase coexistence of pure (single-component) systems, and for two- and multiphase mixtures consisting of chemicals sharing similar or the same chemistry (e.g. alkane mixtures), significant deviations from experiment are observed when asymmetric and non-ideal mixtures are studied, for example, mixtures compromising alkane and alcohol molecules. This is primarily due to the non-bonded molecular interactions between different (pseudo-)atomic groups not being modelled accurately enough and hence calculated. Several 'mixing' rules (to be discussed in Chapter 2) that attempt to describe these interactions correctly have been formulated and used in simulation studies but most of these rules by themselves are not accurate enough, and require the use of additional modifications, usually in the form of multiplying factors, which are usually obtained through step-wise refinement over several simulations until an acceptable deviation from experimental data is observed. Even when using these correction factors that are applied to the mixing rules, large deviations are still observed in highly non-ideal systems, especially in one of the phases.

The prediction of phase equilibrium properties of mixtures via molecular simulations has improved significantly over the past three decades due to the advent of faster (yet cheaper)

computational power, and of equal importance, the development of different molecular simulation methods, for example, Gibbs ensemble Monte Carlo (GEMC) (Panagiotopoulos, 1987 and Panagiotopoulos *et al*., 1988), Gibbs-Duhem integration (Kofke, 1993a and Kofke, 1993b) and Grand Equilibrium (Vrabec and Hasse, 2002). A common element amongst all of these methods is the potential energy model, or force field, which is used to calculate the interaction energy of the system's molecular configurations during a simulation. As stated above, these models predict the equilibrium properties of the pure chemical species, or classes of chemically-similar molecules, for which they were developed with a high degree of accuracy and are also capable of predicting the phase equilibria of mixtures containing such compounds belonging to the same homologous series with similar accuracy. Therefore the observation of deviations between simulation and experiment is undoubtedly due to the inadequacies of the mixing rules to calculate the interactions between the unlike atoms of different molecules in each phase accurately, however complex these rules might be, if it is accepted that the force field parameters reproduce the experimental pure component properties of the molecules for which they were developed with good accuracy. This has also been observed in the author's previous works on the simulation of binary (*n*-hexane/water and ethane/ethanol systems – see Moodley *et al*. (2010a)) and ternary (methane/*n*-heptane/water, *n*-butane/1-butene/water and *n*-hexane/ethanol/water systems – see Moodley *et al*. (2010b)) vapour-liquid-liquid equilibrium of complex polyatomic mixtures.

Many binary and two-phase fluid systems for which the corresponding experimental data are modelled via the myriad of equations of state use the so-called 'combined', or gamma-phi, method (Smith *et al*., 2001). This accounts for departures from an ideal system that obeys Raoult's law by using different thermodynamic models to describe each phase, and this means that the interactions in both phases are modelled uniquely.

Thus it is the purpose of this work to apply a similar approach and investigate the effects of varying the appropriate force field parameter(s) in each phase, with a view to more accurate predictions of phase compositions in molecular simulations. It is interesting to note that the choice of a set of combining rules has a significant effect on thermodynamic properties, even when 'all-atoms' (in contrast to 'united-atom') force fields which explicitly model all types of atoms are employed to model molecular interactions, are used (Delhommelle & Millié, 2001). A good example of why interactions should be calculated differently in each phase is the vapour-liquid coexistence of pure water, in which water has a different dipole moment in each phase. Strauch & Cummings (1992) reduced the magnitude of partial charges on water molecules in

the vapour phase, while keeping liquid-water partial charges unchanged from the original Simple Point Charge (Berendsen *et al*., 1981) force field and in doing so, improved the results of the initial Gibbs Ensemble Monte Carlo simulations that used the same dipole moment in each phase (de Pablo *et al*.,1990).

It has been known since the early 1990s that correction factors applied to the Lorentz-Berthelot energy and size rules can improve simulation results to better-agree with experiment (Möller *et al*., 1992) and numerous studies have implemented such factors to improve the results of simulations to give better agreement with experiment or equations of state (to be discussed in Chapter 2). Recent studies concerning Lennard-Jones mixtures have also concluded that corrections to the LJ energy cross-parameter are important for 'fine-tuning' of simulation results (i.e. improving quantitative agreement between simulations and experiments), while deviations from the Lorentz rule for the size cross term affect simulation results significantly by giving rise to qualitative changes in a mixture by affecting the heights and widths of the first peaks of radial distribution functions (Boda & Henderson, 2008 and Rouha & Nezbeda, 2009), also to be discussed further in Chapter 2.

By modelling the cross-energy interactions in each phase uniquely (which in this work shall be referred to as "heterogeneous unlike-energy parameters"), it is hoped that better agreement between simulated and experimental compositions will be obtained because accurate phase equilibrium data is necessary for designing efficient chemical separation equipment. Going through the scientific literature, there appears to be no studies that have attempted to use different unlike energy parameters in each phase of two-phase (or higher) fluid systems. Hence modelling the cross-energy interactions in each phase uniquely is one of several novel features of this work that contributes original research to molecular simulations.

In spite of the limitations when using the same energy parameter in each phase of a two-phase system (which in this work shall be referred to as the "homogeneous unlike-energy parameter"), this work will also show the analogy between the homogeneous unlike-energy parameter and the binary interaction parameter that is used in equation of state (EoS) modelling, and also provide a brief insight into the phenomenon of the discontinuity of the optimum interaction parameter at the critical temperature of the reference component of a binary system, which, also to the knowledge of the author and at the time of this work being carried out, has not been reported explicitly in the scientific literature and is also an original aspect of this work.

By building on a recent study (Vlcek *et al.*, 2011), this thesis also presents the development and implementation of a model and a method that consolidates the initial purely numerical approach of using heterogeneous unlike-energy parameters. It also explains the inadequacies of the approach used in this study, and is also an additional novel aspect of this work.

The document is structured as follows. In Chapter 2 a very brief description of the theoretical aspects that are central to the proposed work, statistical mechanics and molecular simulation, is given. In Chapter 3 a literature survey is presented, detailing previous studies that have used different types of mixing rules (and highlights their limitations), including several recent molecular simulation studies that have presented methods for finding optimum mixing parameters as well as studies that have used automatic parameterization of force field parameters. Chapter 4 discusses the modelling approach and methodology that was used. The results of the work and a discussion of the insights based on these results are given in Chapter 5. Concluding remarks and recommendations for future work are provided in Chapters 6 and 7, respectively.

2. THEORY OF MOLECULAR SIMULATIONS

This chapter is the author's humble attempt at providing an overview of the principles of statistical mechanics, potential energy models, mixing rules and the Gibbs ensemble Monte Carlo (GEMC) method – these form the mathematical framework used in this study. As such, only the essential aspects of these topics are discussed but references to the corresponding comprehensive works are provided.

2.1 Statistical Mechanics and the Monte Carlo Method

Statistical mechanics is a formalism used to study the properties of macroscopic systems by relating them to the systems' microscopic constituents and configurations. A key idea in this subject is that of an 'ensemble'. Given a system in a certain macroscopic state, an ensemble is a collection of all possible microstates which correspond to that macrostate (see Figure 2-1).

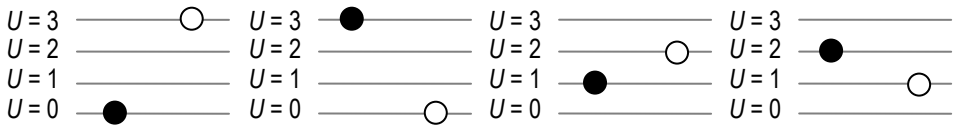

Figure 2–1 – Illustration of a four-state system consisting of two distinct particles, which are represented by the filled and open circles. If one specifies the total energy of the macroscopic system as $U = 3$ (here the energy units are arbitrary), then four microscopic configurations are possible. When the energy U, total number of particles N, and total system volume V are fixed (or kept constant) then this corresponds to the micro-canonical, or NVE, ensemble.

Another idea that is central to molecular simulation studies is the "ergodic hypothesis". Instead of trying to replicate an infinite number of microstates on something as finite as a computer's memory, one may consider a single micro-system and how it evolves with 'time'. The ergodic hypothesis states that "**…in the course of such a 'natural evolution' of the system any permitted microstate will be reached (or closely approximated) with the same relative**

frequency…" (Vesely, 2005). The ergodic hypothesis has an important consequence: for the calculation of thermodynamic averages over the microstates it does not matter if averages are taken over states randomly picked from an ensemble, or over the successive states of one single, isolated system. The corollary of the ergodic hypothesis is stated succinctly as:

$$\text{ensemble average} = \text{time average}, \tag{2-1}$$

where 'average' refers to the thermodynamic average of a required quantity. Thus, one expects, provided that sufficient sampling time in a MD simulation and correct sampling of phase space in a MC simulation occurred, that these two different methods yield the same results.

The ensemble average of a quantity A is defined as

$$\langle A \rangle_{ens} = \frac{\sum_{\vec{\Gamma}} w_{ens}(\vec{\mathbf{\Gamma}}) A(\vec{\mathbf{\Gamma}})}{Q_{ens}}, \tag{2-2}$$

where $w_{ens}(\vec{\mathbf{\Gamma}})$ is the 'weight' of a particular microstate being in a certain configuration $\vec{\mathbf{\Gamma}}$,[1] and $Q_{ens} = \sum_{\vec{\mathbf{\Gamma}}} w_{ens}(\vec{\mathbf{\Gamma}})$ is the ensemble partition function which is a sum over all the possible states of a system, and is unique for each type of ensemble. It may also be thought of as a normalizing factor for the probability p_{ens} of finding a system in a particular state or configuration. For example, the partition function for the NVT ensemble, in which the number of particles, system volume and temperature are all constant, is

$$Q_{NVT} = \sum_{n} \exp\left(-\beta U_n\right), \tag{2-3}$$

[1] This is a multidimensional vector that consists of all of the particles' positions and momenta, which are coordinates in Gibbs phase space. In the context of MC simulations, where the kinetic energy is factored out of the partition function, this vector contains only the positions of all particles within the system.

where the summation is over all states at V and T, $\beta = 1/kT$ (k is the Boltzmann constant) and U_n is the total potential energy of the microstate at V and T. In macroscopic systems consisting of many interacting particles, the spacing of energy levels is usually less than the thermal energy kT and may be treated as a continuum (Widom, 2002). Thus the summation in Equation 2.2 becomes an integral in the classical sense,

$$Q_{NVT} = \frac{1}{h^{3N} N!} \int\int ... \int \exp\left(-\beta U\left(\mathbf{p}^N, \mathbf{r}^N\right)\right) d\mathbf{p}_1 d\mathbf{p}_2 ... d\mathbf{p}_N d\mathbf{r}_1 d\mathbf{r}_2 ... d\mathbf{r}_N \,, \tag{2-4}$$

where h is Planck's constant, $N!$ is a correction for indistinguishable particles, and $\mathbf{p}^N$ and $\mathbf{r}^N$ refer to the momenta and coordinates of all N particles. As can be seen in Equation 2-4, integrating the partition function poses an enormous computational task due to its high dimensionality and so an efficient numerical technique is required for the Monte Carlo method since, for the evaluation of the integrand for a dense liquid, the majority of points the Boltzmann factor is extremely small (Frenkel & Smit, 2002). To this end, the Metropolis method, a type of importance sampling that samples those points in phase space that contribute significantly to the integral, according to a probability distribution that is dependent on the type of ensemble being studied, is implemented.

The Monte Carlo method of molecular simulation is so-named due to its use of random numbers for determining the type of perturbation to apply to a system (i.e. a move type – see Section 2.2.1), and also for deciding whether the move must be accepted or rejected according to acceptance criteria that are based on probability distributions, which in turn are based on the ensemble of interest. Thus, a quality random number generator is required. Ideally, the period of the generator must be much larger than the number of Monte Carlo cycles that are to be performed, so as to avoid patterns which would impose a bias on the simulation. (In one Monte Carlo cycle, N moves are attempted, where N is the number of particles used in the simulation.) Excellent, detailed treatments of the subject are given by Allen & Tildesley (1987), Frenkel & Smit (2002) and Ungerer *et al*. (2005).

2.1.1 The Metropolis Method

In general it is not possible to evaluate integrals of the form $\int \exp[-\beta U(\mathbf{r}^N)]\mathrm{d}\mathbf{r}^N$ when using direct Monte Carlo sampling. The Metropolis method of sampling involves the construction of a random walk through phase space where the probability distribution is non-negligible. Frenkel & Smit (2002) use the analogy that this method is akin to determining the average depth of the river Nile by taking measurements within the Nile *only*, whereas the method of random sampling would sample all of Africa to determine the same average depth. A detailed treatment is given by Frenkel & Smit (2002) and for brevity is not repeated here. Essentially, the method states that the probability of performing a trial move from an old state to a new state is equal to the probability of the reverse move. Metropolis *et al*. (1953) devised an efficient strategy for the sampling of phase space that ensures if the new molecular configuration has a lower energy than the old configuration then the move is accepted. This ensures that an equilibrium state is continuously approached in the chemical system during the equilibration period of a simulation, since the potential energy of each new state progressively decreases (provided that the trial move is accepted). Once an equilibrated system has been realised, the system's properties fluctuate around their equilibrium ensemble averages.

2.2 Ensembles

Two popular ensembles in MC simulations are the isotropic-isochoric-isothermal (NVT) and the isotropic-isobaric-isothermal ensembles (NpT). As their names imply, these ensembles both maintain a fixed number of particles (N), and temperature (T). The total system volume (V) is fixed in an NVT simulation and the total system pressure (p) is fixed in an NpT simulation, where the volume of the simulation box is varied until it fluctuates around its equilibrium ensemble average and thepressure constraint is satisfied (see Figure 2-2).

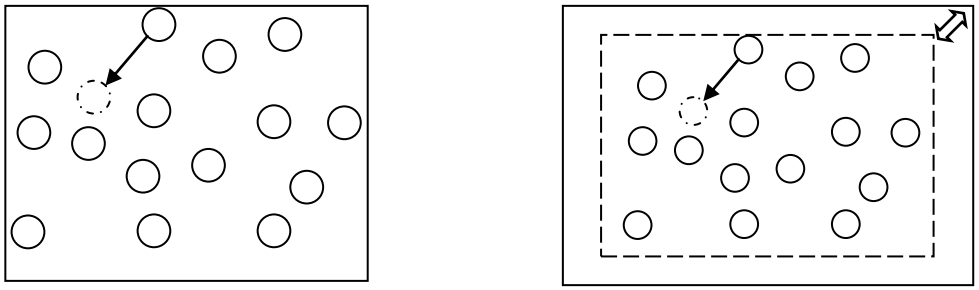

(*a*) (*b*)

Figure 2–2 – Schematic of the *NVT* and *NPT* ensembles. In the *NVT* ensemble (*a*) only particle displacements are permitted, whilst in the *NPT* ensemble (*b*) the total system volume is allowed to change as well.

In chemical thermodynamics, two or more phases (homogenous regions of matter with constant composition) are in equilibrium when their pressures, temperatures, and additionally, the chemical potentials of each species in each phase are all identical. These satisfy, respectively, mechanical, thermal, and chemical equilibrium. In order to determine the number of system variables (e.g. pressure, temperature, volume, or composition) that one is free to choose before the chemical system is 'fully specified', the Gibbs phase rule ($F = 2 - P + C$, where F is the number of degrees of freedom, P is the number of phases and C is the number of chemical species) is used.

2.2.1 The Gibbs ensemble

The Gibbs ensemble (Panagiotopoulos, 1987 and Panagiotopoulos *et al.*, 1988) allows for the direct determination of phase coexistence of pure chemical systems and of mixtures from knowledge of the intermolecular interactions. The advantage of this method over indirect phase equilibrium simulations techniques and direct techniques that involve modeling surfaces due to contact between phases, is that there is no physical contact between the two thermodynamic regions and thus no interfaces to model.

Since this study concerns itself with investigating the effects of using unique cross parameters between unlike atoms (or atomic, or pseudo-atomic groups, depending on the force field

representation of the molecules being simulated) in each phase of a two-phase system, the relative merits and demerits of choosing one simulation method (specifically, one ensemble) over another will not be discussed. The Gibbs ensemble Monte Carlo (GEMC) method has proven its worth as the bulk of phase equilibrium studies have implemented it, and although recently other techniques have been developed and used, for example, the Grand Equilibrium method (Vrabec & Hasse, 2002) and Virtual Gibbs ensembles (Escobedo (1999) and Shetty & Escobedo (2002)), the NpT -GEMC method remains the most widely-used. Some other ensembles that implement the Monte Carlo method are the isotension-isothermal (Parrinello & Rahman (1980 and 1981)) and grand-canonical (first implemented by Norman & Filinov (1969)) ensembles. Another technique that is highly efficient for phase equilibria predictions is transition-matrix Monte Carlo (Shen & Errington, 2005), which combines transition-matrix Monte Carlo and grand canonical methods. One important feature of this method is its ability to predict the entire fluid-phase diagram of a binary mixture at fixed temperature using just one simulation.

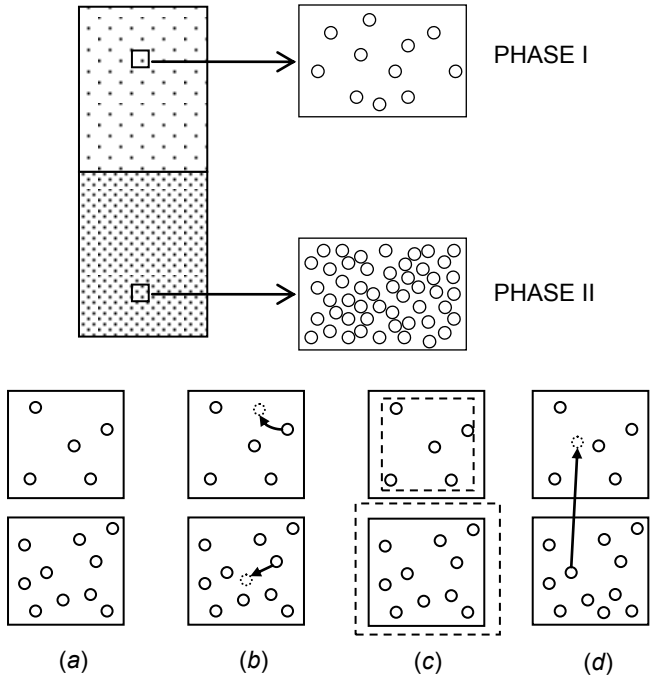

Figure 2–3 – Schematic of a two-phase chemical system and the different types of standard trial moves that are used in a Gibbs ensemble simulation: (*a*) original configuration, (*b*) particle displacements, (*c*) volume changes, and (*d*) particle swaps. For simplicity, monatomic molecules are shown.

In a Gibbs ensemble simulation, different trial moves are performed (see Figure 2-3) and are either accepted or rejected according to criteria that are derived from thermodynamic arguments

and fluctuation theory. A detailed treatment is given by Panagiotopoulos (1987) and Landau & Lifshitz (1980).

The acceptance criteria in the *NpT* ensemble for the three main move types are:

1. Particle displacements

The acceptance rules can be derived by imposing the condition of "detailed balance" – this means the probabilities of a trial move and its reverse trial move must be equal. Assume that the new state *n* is obtained from the original state *o* by displacing a randomly selected particle within a single simulation box. The acceptance rule for a particle displacement is:

$$acc(o \to n) = \min\left(1, \exp\left\{-\beta\left[U\left(\mathbf{s}_{\text{new}}^{n_{\text{I}}}\right) - U\left(\mathbf{s}_{\text{old}}^{n_{\text{I}}}\right)\right]\right\}\right), \tag{2-5}$$

where $\mathbf{s}_{\text{new}}$ and $\mathbf{s}_{\text{old}}$ refer, respectively, to the particle coordinates of the new and old configurations using the scaled coordinates formalism and the n_{I} superscript denotes that the randomly displaced particle resides in box I. This acceptance rule is identical to the conventional *NVT* ensemble acceptance criterion.

2. Particle insertions

The acceptance rule for removing a particle of species *i* from box I and inserting the same particle in box II is written for a multi–component mixture as (Frenkel and Smit, 2002):

$$acc\left(o \to n\right) = \min\left\{1, \frac{n_{\mathrm{I},i}\left(V - V^{\mathrm{I}}\right)^{n_{\mathrm{II}}}}{\left(n_{\mathrm{II}} + 1\right)V^{\mathrm{I}}} \times \exp\left[-\beta U\left(\mathbf{s}_{\mathrm{new}}^{n_{\mathrm{I}}+n_{\mathrm{II}}}\right) - \beta U\left(\mathbf{s}_{\mathrm{new}}^{n_{\mathrm{I}}+n_{\mathrm{II}}}\right)\right]\right\}. \qquad (2\text{-}6)$$

3. Box volume changes

The particle insertion and particle displacement acceptance criteria for the *NpT*–Gibbs ensemble are identical to the acceptance criteria for its *NVT* counterpart; however, for mutual exchange of volume between any two phases (here denoted as phases I and II), the acceptance criterion is different. For an increase in the volume of phase I of ΔV_{I}, $V_{\mathrm{I}}^{\mathrm{new}} = V_{\mathrm{I}}^{\mathrm{old}} + \Delta V_{\mathrm{I}}$ (Panagiotopoulos *et al.*, 1988):

$$acc\left(o \to n\right) = \min\left[1, \exp\left(\begin{array}{l} -\beta\Delta U_{\mathrm{I}} - \beta\Delta U_{\mathrm{II}} + N_{\mathrm{I}} \ln\dfrac{V_{\mathrm{I}} + \Delta V_{\mathrm{I}}}{V_{\mathrm{I}}} \\ +N_{\mathrm{II}} \ln\dfrac{V_{\mathrm{II}} + \Delta V_{\mathrm{II}}}{V_{\mathrm{II}}} - \beta P\left(\Delta V_{\mathrm{I}} + \Delta V_{\mathrm{II}}\right) \end{array}\right)\right]. \qquad (2\text{-}7)$$

For a pure chemical system, the NVT variant of the Gibbs ensemble, using two simulation boxes, is used to study its phase coexistence (see Figure 2–3); usually, this is done at several different temperatures for a predefined number of particles and total system volume. Obviously, these parameters must be judiciously selected so as to not obtain the same vapour and liquid densities for two or more sets of N, V, and T.

For systems containing large, polyatomic molecules, more advanced techniques are required because the probability of complete transferring such molecules from the vapour phase (or a low density phase) to the liquid phase (or a high density phase) in a single swap move is very low. To address this, the configurational-bias Monte Carlo method (Siepmann & Frenkel, 1992) was developed. Using this method, a molecule is grown atom–by–atom into those areas of a dense fluid that have lower energy positions, and this 'bias' is then corrected afterwards, effectively leading to a large increase in acceptance rates for polyatomic molecule insertions.

When the vapour-liquid or liquid-liquid (or multiphase) coexistence of a *mixture* is to be simulated, then the ensemble of choice is the NpT ensemble. This ensemble allows for direct comparison with experimental phase equilibrium measurements due to the system temperature

and pressure being fixed. Provided that the simulation occurs within a system's two- or multiphase region, then the desired number of phases should be obtained – this, however, depends on how accurately the set of force fields that are used in the simulation can represent the non-bonded intermolecular interactions.

2.3 Molecular interactions, force fields and mixing rules

A force field, or potential energy model, describes the potential energy of a system of particles. It consists of mathematical functions that model the various types of intra- (bonded) and intermolecular (non-bonded) interactions in the system.

The actual terms that a force field consists of depends on the rigour of the molecular model. (To date, all force fields have been developed only for pure chemicals or classes of chemical.) For example, a united-atom force field typically "lumps" the hydrogen atoms that are bonded to carbon or oxygen atoms onto the carbon or oxygen atoms to give a single "pseudo-atom" – numerous united-atom force fields have been developed for many different types of inorganic and organic molecules – some prominent models are **Tra**nferable **P**otentials for **P**hase **Eq**uilibria – **U**nited-**A**tom (TraPPE-UA – see Martin & Siepmann (1998a), Martin & Siepmann (1998b), Martin & Siepmann (1999), Wick *et al*. (2000), Chen *et al*. (2001), Kamath *et al*. (2004) and Stubbs *et al*. (2004)), **R**evised **N**ath, **E**scobedo, and **d**e Pablo (NERD – see Nath *et al*. (1998) and Nath *et al*. (2000) (Version 1), Nath *et al*. (2001a), Nath & Khare (2001b) and Nath (2003) (Version 2), and Khare *et al*. (2004) (Version 3)), and **O**ptimized **P**otentials for **L**iquid **S**imulations **u**nited **a**tom (OPLS-ua – see Chandrasekhar *et al*. (1984), Cournoyer & Jorgensen (1984), Jorgensen *et al*. (1984), Jorgensen & Swenson (1985), Jorgensen (1986a), Jorgensen (1986b), Jorgensen & Briggs (1988) and Jorgensen *et al*. (1990)). For example, methanol would be represented by two pseudo-atoms – (—CH_3) and (—OH) and methane would be represented as a single interaction site – (—CH_4). This improves computational efficiency by reducing the simulation time for equilibrium to be attained because fewer particle interactions are computed. Furthermore, it reduces the complexity of the molecule by having fewer intramolecular interactions (see below). This coarse graining approach has become necessary for the simulation of many types of molecules, especially large, complex proteins because explicitly modelling every atom of a large molecule leads to unreasonably long simulation times.

In contrast, an all-atom (or explicit-atom) force field is one in which all the atoms in a molecule are explicitly modelled – for example, TraPPE-Explicit Hydrogen (TraPPE-EH – see Chen & Siepmann (1999) and Rai & Siepmann (2007)), **C**hemistry at **HAR**vard **M**acromolecular **M**echanics (Charmm27 – see MacKerell Jr. *et al*. (1998) and Foloppe & MacKerell Jr., (2000)), and OPLS-**a**ll **a**tom (OPLS-aa – see Pranata *et al*. (1991), Kaminski *et al*. (1994), Jorgensen *et al*. (1996), Damm *et al*. (1997), Jorgensen & McDonald (1998), McDonald & Jorgensen (1998), McDonald *et al*. (1998), Rizzo & Jorgensen (1999), Mahoney & Jorgensen (2000) and Kaminski et al. (2001)). While these force fields are associated with longer equilibration times than united-atom force fields for a given molecule, they offer a higher level of accuracy.

The total potential energy (U) of a system may be written as a sum of two parts,

$$U_{\text{total}} = U_{\text{intra}} + U_{\text{inter}}, \tag{2-8}$$

where U_{intra} is the contribution of intramolecular interactions and U_{inter} is the contribution of intermolecular interactions. Each contribution can be split further into different types of contributions, depending on the structure of the molecule of interest and its inherent chemistry. These parameters are dependent on the chemistry of the molecule of interest and are usually predicted using *ab initio* quantum mechanical methods where the Schrödinger equation is solved for the molecule whose parameters are sought. A good discussion is given by Jensen (2007). Force fields are further "fine-tuned" by fitting the model parameters to large experimental datasets, thus making most force fields semi-empirical. Ungerer *et al*. (2000) and Bourasseau *et al*. (2003) give detailed treatments of the optimization of alkane and olefin force fields, respectively.

Regarding intramolecular interactions, typically three main types are modelled. These are bond-bending, bond-stretching, and dihedral angle (or torsion) perturbations (see Figure 2-4). Note that the Lennard-Jones interactions also form part of intramolecular interactions (not shown in the diagram).

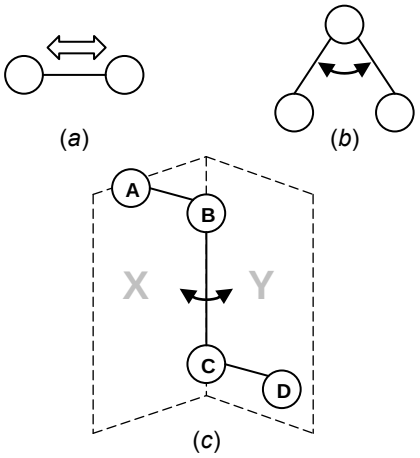

Figure 2-4 - The various intramolecular interactions that contribute to the potential energy of a given molecular configuration. From top left (clockwise): (*a*) bond stretching (*b*) bond bending (*c*) torsion energy. The circles represent individual atoms and the solid lines that join the circles represent chemical bonds.

The stretching and bending interactions are usually modelled by Taylor series around 'rest' lengths and angles, respectively, as

$$U_{\text{str}} = \frac{1}{2} k_{\text{str}} (l - l_0)^2 \text{, and} \tag{2-9}$$

$$U_{\text{bend}} = \frac{1}{2} k_{\text{bend}} (\theta - \theta_0)^2 , \tag{2-10}$$

where the ks refer to stretching and bending constants, and the ls and θs refer to lengths and angles, respectively. For torsion or 'twisting' energy to be present, there must be at least four bonded atomic groups in the molecule (see Figure 2-4). The angle formed by the planes A and B in the figure is referred to as the dihedral angle (ϕ). The orientation of the molecule is of no consequence when measuring the dihedral angle and so the energy interactions may be defined by a periodic function, specifically, a cosine series, which is typically of the form

$$U_{\text{tors}} = c_0 + c_1[1 + \cos\phi\,] + c_2[1 - \cos 2\phi\,] + c_3[1 + \cos 3\phi\,], \tag{2-11}$$

where the cs are constants.

Intermolecular interactions, all of which are electromagnetic by nature, fall into three categories that depend on the ranges of intermolecular separations (Kaplan, 2006). The three ranges of interactions are (Kaplan, 2006):

1. Short, where the potential is repulsive and, due to overlapping of molecular electronic shells, electronic exchange dominates. (This is explained by the Pauli Exclusion Principle.)

2. Intermediate, in which the repulsive and attractive forces coexist and cancel each other at the van der Waals minimum, which imparts stability to the molecular system.

3. Long, where the forces are attractive and electronic exchange is negligible.

Within the context of molecular simulations these interactions are usually represented by a potential energy model/function (also called a force field) that contains information about the system that it describes through numerical parameters (Stone, 2008). For computational expediency, most of these potentials treat the interactions as additive two-body (or pair-wise) interactions. The main contributions to the intermolecular energies that are described by different terms in the potential energy models are (Stone, 2008):

1. The exchange (or exchange-repulsion or van der Waals repulsion) term, due to the overlapping of the electronic shells.
2. The dispersion term (or van der Waals attraction or London force), which is an attractive interaction "**arising from correlated fluctuations of the electrons in the interacting molecules**" (Stone, 2008).
3. The electrostatic term that describes the interaction between the charge distributions of the molecules.
4. Induction, which is the distortion of the electron density of a molecule in response to the electric field of other molecules in its vicinity.
5. Charge transfer, where transfer of electron density from one molecule to another can lead to the initial stage of chemical bonding. This is part of the induction term, but it is treated separately sometimes.

The intermolecular interactions are split in two parts – a van der Waals component that describes the non–polar interactions, and a Coulombic component that describes the charged-particle interactions.

The Lennard-Jones 12–6 potential (Lennard-Jones, 1931) is a simple mathematical formula that models this behavior:

$$U_{\mathrm{LJ}}^{ij}\left(r_{ij}\right)=4\varepsilon_{ij}\left[\left(\frac{\sigma_{ij}}{r_{ij}}\right)^{12}-\left(\frac{\sigma_{ij}}{r_{ij}}\right)^{6}\right], \tag{2-12}$$

where σ_{ij}, ε_{ij} and r_{ij} are the depth of the potential well, the distance at which the intermolecular potential is zero, and the separation between two atomic sites i and j, respectively (see Figure 2-5). The attractive $\left(\sigma/r\right)^{6}$ term (which represents a dispersion force) is quantum mechanical in its origin since dispersion interactions decrease with distance as $1/r^{6}$ (Kaplan, 2006), while the repulsive $\left(\sigma/r\right)^{12}$ term has the exponent 12 "due to mathematical convenience." (Kaplan, 2006) Other non-bonded pair-wise potential energy models of note, which are more complex than the Lennard-Jones potential, are the 12–6–4 (Mason & Schamp, 1958), *m*–6–8 (Klein & Hanley, 1970) and Stockmayer (1941) potential models. The justification for using the Lennard-Jones potential is given in Chapter 4.

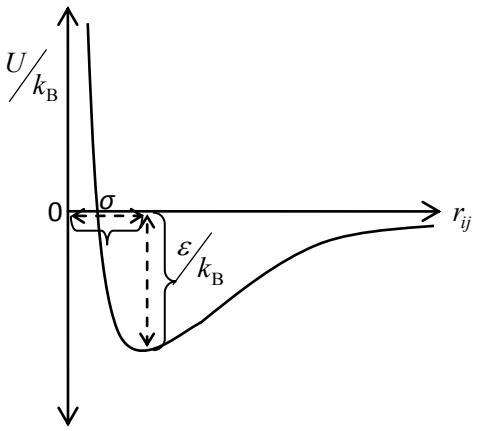

Figure 2-5 - Illustration of the potential energy well of a Lennard–Jones fluid.

The Coulomb interactions, relevant to systems of molecules that contain charged or partially charged species, are calculated using Coulomb's law of electric interaction between two charged bodies:

$$U_{\text{Coulomb}}^{ij} = \frac{q_i q_j}{4\pi\varepsilon_0 r_{ij}}, \tag{2-13}$$

where q_i and q_j are the charges on interacting sites i and j, while $\varepsilon_0 = 8.854\times10^{-12}$ $C^2.N^{-1}$ m^{-2} (also F. m^{-1}) is the permittivity of free space. Being a long-range interaction, the contribution of electrostatic interactions in a system cannot be ignored. More advanced techniques are required when calculating the total contribution of electrostatic interactions in a system; to this end, the Ewald summation method (de Leeuw (1980a, 1980b and 1980c)) for point charges is used. A comprehensive quantitative treatment of induction and charge transfer interactions, which are not central to this work and are only modeled in very refined force fields (this is also justified in Chapter 4), is given by Kaplan (2006).

A mixing rule (also called a combining rule) is a formula for calculating a parameter of a mixture (which is here understood to be a single phase containing two different types of chemical species) from knowledge of the corresponding parameter of the individual chemical species. More specifically for phase equilibrium calculations, a mixing rule is used to calculate the *interaction* parameter(s) between two different interaction sites between the molecules in a mixture. These combining rules find application in various equations of state models and in MC and MD simulations. Mixing rules are used to calculate the non-bonded intermolecular interactions between two atomic groups; note that these atomic groups can be on the same molecule.

The accuracy of the cross-energy parameters as determined by the mixing rules is very important because it contributes to calculations of the properties of a phase, which are dependent on the composition of the phase. Hence, obtaining the correct chemical composition

of a phase in a thermodynamic systems, which are dependent on the potential energy models of the pure components and the mixing rules, cannot be overstated. The parameters that are of interest when using mixing rules are the (Lennard-Jones – see Chapter 3) size (σ) and energy (ε) parameters. The usual method for calculating the combined parameters of heterogeneous pairs in molecular simulations is through the Lorentz (Lorentz, 1881), an arithmetic average, and Berthelot (Berthelot, 1889), a geometric average, rules:

$$\sigma_{ij} = \frac{\sigma_{ii} + \sigma_{jj}}{2}, \tag{2-14}$$

and

$$\varepsilon_{ij} = \sqrt{\varepsilon_{ii}\varepsilon_{jj}}\ . \tag{2-15}$$

More complex variations of these have been used (this will be discussed in Chapter 3), but in this study the Lorentz-Berthelot rules were chosen due to their simplicity and because the focus of this study was to test a new approach towards obtaining more accurate simulation results. In any case, the more complex mixing rules still use the same unlike-size and unlike-energy parameters in each phase, which is what this study tries to overcome by using different cross-energy terms in each phase.

Consider a mixture containing two types of molecules, A and B, and each molecule consists of two different pseudo-atomic groups (Figure 2-6).

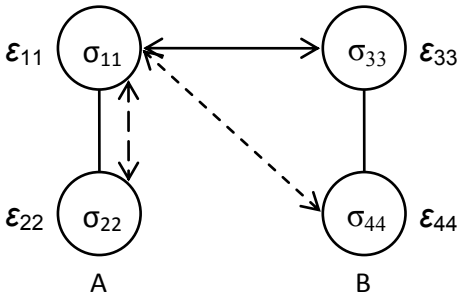

Figure 2–6 – Schematic of the various non-bonded interactions for two different molecules. For clarity, the self-interactions are not shown. The circles represent individual atoms and the solid lines that join the circles represent chemical bonds.

The size and energy interactions between two 'like' atomic groups are denoted by σ_{ii} and ε_{ii}, respectively, while interactions between unlike group pairs are denoted by σ_{ij} and ε_{ij}. For such a mixture, each pseudo-atomic group has three energy and three size *unlike*-pair parameters. Since there are four different pseudo-atoms, there are $4\times(3+3)/2=12$ unlike-pair parameters (the division by two is necessary since $\varepsilon_{ij}=\varepsilon_{ji}$ and $\sigma_{ij}=\sigma_{ji}$). In general, for a mixture containing X distinct (pseudo)-atomic groups, there will be $X\times\left[(X-1)+(X-1)\right]/2=X(X-1)$ unlike-pair parameters. This illustrates that for mixtures of complex molecules that consist of many different types of chemical functional groups, the modeling of unlike interactions becomes increasingly important.

3. LITERATURE REVIEW OF STUDIES THAT USED DIFFERENT MIXING RULES, AND OPTIMUM POTENTIAL ENERGY PARAMETERS

Molecular simulations have been applied successfully to the study of multi-component phase equilibrium in numerous studies but have relied on the use of mixing rules to calculate interactions between unlike atomic sites. As explained in Chapter 1, except for mixtures comprising chemically similar molecules, significant deviations from experimental data are observed between simulation and experiment. Several studies have employed empirical multiplying factors for the interaction parameters between those pseudo-atomic groups that dominate the contribution of non-bonded interactions to the total potential energy of the system, but such parameters are only obtained via successive modifications of the (constant) multiplying factors over several simulations – this is time-consuming and tedious. Typically, the simplest method for adjusting unlike molecular interactions in a binary Lennard-Jones system is to change the cross-energy parameter. Increasing only the cross-energy parameter results in the solubility of the more volatile component increasing in each phase (decreasing the parameter has the opposite effect). Changing only the unlike size parameter is not so straightforward, since Boda & Henderson (2008) and Rouha & Nezbeda (2009) showed that large-enough changes lead to the mixture's qualitative behaviour being altered. In this chapter, a survey of studies that have used modified/adjusted non-bonded cross-interaction parameters, or numerical methods for the parameterisation of force fields of pure chemicals (this will be used as part of the background for the model and method to be used in this study – see Chapter 4), or have reported notable deviations from experimental data, are summarised.

Sadus (1993) examined the influence of molecular shape and combining rules for unlike interactions on the critical phase transition of four non-polar type III binary mixtures (tetrafluoromethane/n-heptane, and sulfur hexafluoride/[either n-octane, n-nonane, or n-undecane]). The critical properties of these mixtures were predicted by using two equations of state: the Carnahan-Starling hard sphere model (Carnahan & Starling, 1969) and the Boublik-Nezbeda representation of non-spherical molecular geometry (Boublik, 1981). These models differ by a non-sphericity parameter α that is present in the Boublik-Nezbeda EoS; when $\alpha = 1$, the Carnahan-Starling EoS is obtained. Very good quantitative agreement between theory and

experiment was obtained over a wide range of densities, temperatures and pressures. Aside from reaching conclusions about the modelling of the shape of the n-alkane molecules that were studied, it was found that correct determination of the parameters characteristic of unlike interactions significantly influenced the predicted critical properties. The conformal parameters f_{es} and h_{es}, which can be obtained from the van der Waals mixing rules ($A_{\text{mix}} = \sum\sum x_i x_j A_{ij}$, where A_{mix} is a mixture property and x is a mole fraction) and are proportional to the strength of intermolecular potential and internuclear separation, respectively, are only accurate when the site differences between component molecules are not large. An adjustable parameter (in the form of a simple multiplying factor) reflecting the strength or weakness of unlike interactions was used in the van der Waals mixing rules for f_{es}; without the parameter, significant deviations from experimental data were observed.

Errington *et al.* (1998) used GEMC simulations to determine methane/water and ethane/water phase equilibria from 300 K to 570 K, and from sub-atmospheric pressure up to 3000 bars. Water was modelled by the extended simple point charge (SPC/E) and modified extended simple point charge MSPC/E (Boulougouris *et al.*, 1998) potential models, while the alkanes were modeled by the Transferable Potentials for Phase Equilibria (TraPPE-UA) force field (Martin & Siepmann, 1998). In a second set of simulations, the exp-6 potential model (Buckingham, 1938) was used to calculate the van der Waals interactions for all chemical species. Isobaric-isothermal (NpT) GEMC simulations were used to determine the Henry's law constants of the alkanes in water; where instabilities were encountered in these simulations, constant volume (NVT) simulations were used instead. It was found that the SPC/E and MSPC/E models were in good agreement with experimental data, though at higher pressures the exp-6 model was more accurate in the vicinity of the pure water critical point. In general, at high pressures, deviations were observed between the experimental and simulation ((M)SPC/E+TraPPE-UA, and exp-6) data.

Delhommelle & Millié (2001) used NpT-GEMC simulations to compute vapour-liquid equilibria and liquid properties of binary mixtures comprising rare gases modelled by effective pair potentials. Three sets of combining rules were used: Lorentz-Berthelot, Kong (1973), and Waldman-Hagler (1993). It was shown that: (1) the choice of a set of combining rules has a significant effect on thermodynamic properties, (2) the Lorentz-Berthelot combining rules yield significant deviations from experiment, and (3) the Kong rules provided a better, though not

adequate, description of mixture properties. A brief discussion was given in which it was pointed out that even when 'all-atoms' (as opposed to 'united-atom') force fields, which explicitly model, for example, hydrogen atoms in alkanes, are employed to model molecular interactions, the choice of combining rule is still significant. It was mentioned too that models that use a united atoms representation are sometimes 'dissimilar enough to be sensitive to the choice of the set of combining rules'. Delhommelle & Millié (2001) also state that if the pure components' Lennard-Jones size parameters do not differ by much then the Lorentz mixing rule suffices for obtaining the unlike-size parameter.

Using temperature scaling Gibbs ensemble MC simulations, Zhang & Duan (2002) studied the VLE of a methane/ethane mixture. Using the LB rule in its conventional form, excellent agreement between simulations and experiment was obtained. This was partly due to methane and ethane belonging to the same homologous series as well as the workers proposing a new set of LJ parameters for ethane. It was mentioned, though, that consideration was given to a study by Möller *et al.* (1992) in which correction factors of 1.0009 and 1.0025 were applied to the energy and size rules, respectively, as follows:

$$\varepsilon_{ij} = k_{1,ij}\sqrt{\varepsilon_i \varepsilon_j}\,, \tag{3-1}$$

and

$$\sigma_{ij} = k_{2,ij}\left(\sigma_i + \sigma_j\right)\big/2\,. \tag{3-2}$$

In Equations 3-1 and 3-2, $k_{1,ij}$ and $k_{2,ij}$ are the mixing coefficients for the Berthelot and Lorentz combining rules, respectively. However it was argued by Zhang & Duan that these deviations from unity were small enough not to affect their results since the error from simulation noise was probably larger.

Zhang & Siepmann (2005) studied the pressure dependence of the vapour-liquid-liquid equilibria (VLLE) of two ternary alkanes/perfluoroalkanes/CO_2 mixtures (*n*-decane/*n*-perfluorohexane/CO_2 and *n*-hexane/*n*-perfluorodecane/CO_2). Satisfactory results were obtained only after modifications of the both the size and energy cross-parameters for each binary pairing, although no details on the actual optimization procedure were provided in the publication. The comparisons of the simulations were made with a limited range of

experimental data, and mostly with the SAFT-VR (statistical associating fluid theory of variable range) equation of state.

Docherty *et al.* (2006) used GEMC simulations to calculate the excess chemical potential of methane in water over a wide temperature range. Water was modeled by the TIP4P/2005 model, while methane molecules were represented as simple Lennard-Jones beads. The experimental chemical potentials were not reproduced when using the Lorentz-Berthelot combining rules, but it was observed that the deviations were systematic. Accurate results were obtained when a positive deviation (approximately +7%) from the Berthelot energy cross-parameter was implemented – this indirectly accounted for the polarization energy between methane and water. The large excess chemical potential that was initially observed was postulated to be a result of either a too large diameter or too low well depth, or a combination of both, for methane-water interactions. The workers decided to change the value of the well depth *only*, since the accuracy of the data prevented simultaneous changes to both the size and energy parameters. By increasing the non-bonded interaction energy parameter, the interaction energy between the dipole moment of water and the induced dipole of methane was implicitly accounted for.

Lenart & Panagiotopoulos (2006) used grand canonical Monte Carlo simulations with histogram reweighting to determine the critical loci of methane/ethane and methane/water mixtures. These mixtures display different classes of criticality, with methane/ethane displaying type I criticality (i.e. continuous mixing between both components over the entire composition range) and methane/water displaying type IIIb criticality (i.e. a discontinuity is present in the critical locus). The dispersion interactions were modelled with the modified Buckingham exp-6 potential model (Buckingham, 1938), and heterogeneous interactions between different atom types were calculated by using the Lorentz-Berthelot rules. Additionally, the repulsion factor for the Buckingham potential was described by $\alpha_{ij} = \sqrt{\alpha_{ii}\alpha_{jj}}$. Further to the Lorentz-Berthelot rule, the Kong and Sadus combining rules were used for the methane/water mixture. The water and alkane models were both developed by Errington and Panagiotopoulos (1998a, 1998b, and 1999), and the study showed that the methane/ethane mixture quantitatively predicted the experimental results using the conventional LB mixing rules. However, the same combining rules for the methane/water mixture gave only a qualitative description of the critical behavior. It was found that the Lorentz-Berthelot + Sadus combined description provided the best prediction of the experimental results when compared to the other combining rules that were used in the study. It was suggested by the workers that the addition of an *empirical* parameter to

improve the energy and size parameters may yield simulation results that are closer to experiment, but at a cost, as this would render the models non-predictive.

Schnabel *et al*. (2007) systematically investigated the influence of the unlike Lennard-Jones parameters on vapour-liquid coexistence of CO/C_2H_6 and N_2/C_3H_6 mixtures. The performance of eleven combining rules - Lorentz–Berthelot (Lorentz, 1881; Berthelot, 1889), Kohler (Kohler, 1957), Hudson–McCoubrey (Hudson *et al*., 1960), Fender–Halsey (Fender *et al*., 1962), Hiza (Hiza & Duncan, 1969; Hiza & Duncan, 1970; Hiza & Robinson, 1978), Sikora (Sikora, 1970), Smith–Kong (Smith, 1972; Kong, 1973), Halgren (Halgren, 1992), Waldman–Hagler (Waldman & Hagler, 1993), and Al-Matar & Rockstraw (types *A* and *B*) (Al-Matar & Rockstraw, 2004) – each of varying complexity, was also examined. They argued that unlike LJ parameters can be directly adjusted to a single experimental data point. Twenty-five combinations of different LJ cross parameters (size and energy) were used to simulate the CO/C_2H_6 mixture with minimum and maximum deviations of -4% and 4%, respectively, while thirty simulations over the same range of deviations were performed for the N_2/C_3H_6 mixture. The results indicated that the mixture bubble density was accurately obtained even when using an arithmetic mean to calculate the LJ size cross-parameter, and that the density was insensitive to variations of the LJ energy cross-parameter. The vapour pressure was found to be dependent on both types of cross parameters, with considerably lower sensitivity for vapour composition. This study recommends the adjustment of the unlike LJ size parameter to experimental vapour pressures. A similar study in which only the LJ energy cross terms were adjusted to a single experimental vapour pressure corresponding to different binary mixtures was performed by Vrabec *et al.* (2005). Using the adjustment procedure, excellent agreement between experiment and simulation was obtained for C_2H_6/C_2H_4, C_2H_6/C_2H_2, and C_2H_4/C_2H_2 (binary) mixtures. In fact, very good results were obtained from a simulation of the corresponding ternary $C_2H_6/C_2H_4/C_2H_2$ mixture with no altering of the corrected LJ energy cross-terms from the binary simulations.

Boda & Henderson (2008) studied the effects of deviations from the LB mixing rule on a simple LJ mixture at two state points ($p^* = 0.017$ and $T^* = 0.7$, for $x_1 = 0.0625$ and 0.5) using nine combinations of ξ_{12} (= $1+\delta_\varepsilon$) and η_{12} (= $1+\delta_\sigma$), where $\delta_{\varepsilon,\sigma} = \{-0.2, 0, 0.2\}$ where ξ_{12} and η_{12} were the LJ multiplying factors for the unlike energy and size parameters, respectively (much like the $k_{1,ij}$ and $k_{2,ij}$ multiplying factors in Equations 3-1 and 3-2). This study found that radial distribution functions (rdfs) are weakly dependent on the unlike energy parameter and it also

showed that there is a strong dependence of the rdfs on the size parameter i.e. affecting the heights and widths of the first peaks. This suggests the possibility that different qualitative fluid behavior depends more on deviations from the unlike LJ size parameter, than on the energy parameter.

Rouha and Nezbeda (2009) studied simple LJ mixtures to examine whether deviations from the LB rule may produce qualitatively different mixture properties (e.g. properties such as those exhibited by mixtures of strongly associating fluids). A systematic study was undertaken to evaluate the partial molar quantities (using a method based on Tikhonov regulation to evaluate derivatives (Lubansky *et al.*, 2006)), of a LJ mixture at selected combinations of the LJ cross parameters that produced qualitative changes in the thermodynamics of the mixture. Both size and energy parameters of the individual components were identical but cross interactions were varied for several different combinations of the parameters, over the entire concentration range [0, 1]. This study concluded from observations of the excess volumes and enthalpies, partial molar volumes, and rdfs, that manipulation of the energy cross-parameter is important for 'fine-tuning' of the results (i.e. improving quantitative agreement between simulation and experiment), but deviations from the Lorentz rule (for the LJ size cross term) affects results significantly by giving rise to qualitative changes in the mixture.

Vrabec *et al.* (2009) did a comprehensive study to describe the VLE of 267 binary systems using the grand equilibrium method (Vrabec & Hasse, 2002). For each binary system, a state independent binary parameter (i.e. a multiplying factor; see Equation 3-1) was adjusted to a single experimental vapour pressure corresponding to that mixture. It was found on average that the LJ unlike energy parameter was altered by less than 5%. Although the correction factor was adjusted to only one experimental data point (viz. the mixture's vapour pressure, at a specified temperature), it had hardly any effect on the bubble density and dew point composition. Since the experimental dew point composition was not included in the adjustment, the simulated dew point data was fully predictive and provided superior results to adjusted cubic equations of state. The workers stated that one may argue that the binary interaction parameter (and consequently, the mixture model) might be valid only at the temperature where it was fitted to the vapour pressure; to address this, they studied 53 binary mixtures for two to a maximum of four isotherms, and for a mixture of CO/CH_4, excellent results were obtained over a 55K range. Similar results were obtained over a 100K range for chlorodifluoromethane/CS_2.

Faller *et al.* (1999) developed an automatic parameterisation method for force fields in molecular simulations. By incorporating the simplex method of optimization in molecular dynamics simulations, they were able to fine-tune the Lennard-Jones size and energy parameters for four *pure* liquids (2-methylpentane, tetrahydrofurane, cyclohexene, and cyclohexane). The optimized parameters were obtained by minimizing a 'target function' that was the square root of the weighted sum of relative squared deviations,

$$f_{target}\left(\{p_n\}\right) = \sqrt{\sum_i w_i \left(1 - \frac{P_i\left(\{p_n\}\right)}{P_{i,target}}\right)^2}\ , \tag{3-3}$$

where $P_{i,target}$ is the experimental value of property P_i which in turn is dependent on the parameters of interest $\left(\{p_n\}\right)$, and w_i is a weighting factor which is determined by how easy it is to reproduce property i. The experimental properties to which the Lennard-Jones parameters were fitted in this study were the heats of vapourization (for the energy parameters) and the liquid densities (for the size parameters). They noted that when the force field parameters were changed with respect to an old equilibrated configuration, the new system had to re-equilibrate with respect to the new parameters, before another set of parameters were calculated. They also noted that due to the 'noise' inherent in all simulations, one should not strive to reproduce experimental data to a high precision.

Recently, Müller *et al.* (2008) used the method proposed by Faller *et al.* (1999) as part of their work in developing a force field, with subsequent parameter fine-tuning, for ethylene oxide. During the molecular dynamics simulations, the Lennard-Jones energy and size parameters were also fitted to the experimental heat of vapourization and liquid density of ethylene oxide at 375 K and 1428.5 kPa, respectively. They noted, when compared to tabulated ε - and σ - values of carbon and oxygen, that their parameter set was novel as it was outside the initially estimated parameter space, and thus represented one solution to the optimization problem.

In a study of the solubility and structure of water in n-alkanes and polyethylene, Johansson *et al.* (2007) used an empirical multiplying factor of 1.30 (which was obtained after a systematic investigation that tested several values of correction factors) for the Lennard-Jones energy

parameter to better represent interactions between TraPPE-UA alkanes SPC/E water interactions, since the unmodified geometric average gave water solubilities in alkanes that were much lower than experimental values. However, the agreement between simulation and experiment for alkane solubility in water was worsened.

A slightly different approach to optimizing the molecular interactions for Lennard-Jones-based pure fluids to improve agreement (by reducing the deviations) between simulation and experiment, using alkane/perfluoroalkanes as an example, was used by Potoff & Bernard-Brunel (2009). By varying the repulsive exponent of the Lennard-Jones potential (and keeping the attractive "6" exponent constant), the pure alkane (ethane to tetradecane) and pure perfluoroalkane (perfluoromethane to perfluorooctane) were optimized to reproduce experimental saturated liquid densities to within 1%, and experimental vapour pressures to within 3% (alkanes) and 6% (perflouroalkanes). Thereafter, by using the Lorentz-Berthelot mixing rules the optimized pure models were tested to determine their performance in binary mixture simulations. Slight deviations that were more pronounced in the vapour phase were observed for *n*-propane/*n*-pentane at 360.93 K, and the deviations were especially higher at 410.93 K, which is in the region of supercritical propane. For the ethane/perfluoroethane mixture, the Lorent-Berthelot mixing rules provided very poor agreement with experiment and satisfactory agreement with experiment was obtained only after using a multiplying factor of 0.955 for the Berthelot (energy) parameter. Again, while excellent agreement was obtained for the liquid phase, deviations in the vapour phase were observed in the ethane-rich and perflouroethane-rich regions of the phase diagram. Another pure component force field parameter optimization method for the non-bonded Lennard-Jones parameters that is worth mentioning here is the method of van Westen *et al*. (2011). Using the perturbed chain statistical associating fluid theory equation of state (PC-SAFT) (Gross & Sadowski, 2001), which is an analytical equation of state, an objective function based on deviations from experiment of the vapour pressures, enthalpies of vapourisation and liquid densities was minimized – this approach was found to be "orders of magnitude" faster than conventional simulation approaches. The PC-SAFT-based objective function proved to be an excellent approximation of the real objective function and only a few subsequent simulations were required for the optimization to converge.

To summarize, the following is noted, with reference to the review that has been presented:

1. Automatic parameterization of non-bonded force field parameters is possible and has been performed in real-time in molecular dynamics simulations, but no similar studies that use Monte Carlo simulations have been reported. Such parameterizations of these interactions have been done with respect to pure fluids (liquids) and not mixtures.

2. Monte Carlo simulation studies of the phase equilibrium of mixtures that have used adjusted parameters, have done so by either successive modification of the adjustment factors, or have required several independent simulations.

3. Fitting of the Lennard-Jones energy and size parameters to experimental data has been done to heats of vapourisation (or as shown by studies of simulations of mixtures, the mixture's vapour pressure) and liquid densities.

4. For fine-tuning of force fields the unlike-energy parameter is usually adjusted, and changing the unlike-size parameter effects qualitative phase behaviour changes.

5. The Lorentz rule (arithmetic average) for calculating the unlike LJ size parameter is adequate when the LJ size parameters of the pure components do not differ significantly.

These salient points will be discussed further in Chapter 4 where the rationale for this work's methodology is developed.

4. MODEL & METHOD

This chapter formulates and justifies the methodology that was used in this study. An overview of molecular and intermolecular interactions is given first, along with the selection of the chemical system that was used in all simulations in this work. Following that, a decision is made on the parameters of the potential model that needed to be modified for the purposes of this work, based on the Literature Review (Chapter 3), and the weakness of automating the search for optimum heterogeneous parameters is also discussed. Finally, the approaches used in this work to accomplish the new proposed method are given.

4.1 Intermolecular interactions

Since this study is concerned with presenting a novel approach for treating the unlike intermolecular interactions uniquely in each phase of a two-phase fluid equilibrium system, the potential models of the pure components of the system must give excellent agreement between the pure component phase coexistence simulations and the corresponding experimental data. Furthermore, because the use of unique unlike interactions in each phase is being attempted, it is prudent to consider a mixture of "simple" chemicals that can be represented by a computationally economical potential model that does not contain too many adjustable parameters. At the same time, it must be ensured that the potential energy model provides an acceptable physical model of the system and, ideally, does not have too many types of intermolecular interaction terms (which would make the simulations computationally expensive).

The system methane/xenon was chosen for this study because it meets the requirements mentioned above. There is also reliable experimental vapour-liquid equilibrium data for this system over a wide range of temperatures (Dias *et al*., 2004), and it is well-represented by the Peng-Robinson (Peng & Robinson, 1976) equation of state – this means that the temperature range of its vapour-liquid phase coexistence can be extended in order to study the phase behaviour at temperatures slightly below the critical temperature of pure methane. Both

molecules are represented as simple monoatoms by their potential models (Gray & Gubbins, 1984, Panagiotopoulos, 1989, and Martin & Siepmann, 1998) and for methane, bond bending, bond stretching and torsion energies are not considered. The potential energies of both types of chemicals are modelled by the Lennard-Jones 12-6 force field. Certainly, the Lennard-Jones potential is a first-order approximation because it considers the van der Waals repulsion and attraction two-body interactions only. These, however, generally account for most of the overall non-bonded intermolecular energy especially in systems that contain no polar molecules, and/or have very small induction effects, as is the case with inert gases and hydrocarbons (Stone, 2008), which is precisely the system that is being studied here. Thus for pure chemical systems containing molecules that are symmetric, not easily polarisable, neutral (i.e. have no permanent dipoles, or higher) and are known to have very little induction effects, it can be assumed that whatever discrepancies exist between simulation and experiment (keeping in mind that a pair-wise additive potential is being used) can be attributed to three-body and higher terms. Provided that the qualitative equilibrium properties of a mixture, e.g. the shape of its phase envelope at the macroscopic conditions of interest, can be predicted even if only roughly (in the context of molecular simulations), then this potential model provides a computationally efficient and powerful tool to predict fluid phase equilibrium, if combined with a fresh approach to modelling the unlike interactions.

4.2 Deciding what unlike-molecule interactions parameters to modify

Chapter 3 reported studies that were considered useful for determining the parameters that needed to be adjusted for the fine-tuning of the unlike-interaction force field parameters. It also reported a few works that during the initial stages of this study, seemed to be useful for automating the search for the optimum parameters that would minimise the deviation between simulations and experimental data.

Irrespective of the complexity of the mixing rules that are used to calculate unlike-pair interaction parameters in a simulation, it is clear that that the accuracy of simulations is limited unless adjustable parameters associated with the mixing rules are adjusted when simulating complex chemical mixtures comprising several different types of atoms. In fact, for highly non-ideal chemical mixtures the inaccuracies are so large because the unlike atomic interactions can be dominant enough so as to produce vastly different qualitative phase behaviour from what is observed in reality. For example, Moodley (2008) studied the three-phase coexistence of a

ternary n-hexane/ethanol/water mixture using NpT-GEMC simulations and the TraPPE-UA and SPC/E force fields, and the study showed that the qualitative shape of the simulated phase envelope progressively deviated from the experimentally observed shape as the concentration of ethanol was increased over several simulations. Even more worrying is that the deviations were not systematic. In other words, misrepresentation of the unlike non-bonded interactions can give simulation results that are in stark contrast to the observed chemistry of a mixture.

Except for the work of Zhang & Siepmann (2005), all studies reviewed in Chapter 3 focused on the simulation of binary mixtures and the adjustment of the corresponding non-bonded parameters. In particular, the majority of those studies adjusted the Lennard-Jones energy (or potential energy well depth) parameter between unlike pairs of atoms – as pointed out in the Chapters 1 and 3, this parameter is of interest when fine-tuning or optimizing the interaction energies between different non-bonded types. Hence in this work the focus will be on the adjustment of the energy cross parameters in each phase. It should be noted that although Zhang & Siepmann (2005) studied the three-phase coexistence of ternary mixtures, they adjusted the non-bonded interaction parameters with respect to every possible binary system (alkane/perfluoroalkane, alkane/CO_2, and perfluoroalkane/CO_2 mixtures). Unfortunately their GEMC simulation results for the ternary system were compared to the results of another predictive method (SAFT-VR EoS) and thus it is difficult to infer from their study whether the GEMC results were accurate when compared to experimental data of the same system, even though the binary simulations that used the optimized interaction parameters were in very good agreement with the corresponding experimental data. This highlights the deficiency of not only three-phase coexistence studies, but also of ternary mixture studies that involve the adjustment of non-bonded interactions between unlike atomic groups. Similarly, Vrabec *et al*. (2005) also used adjusted parameters from binary simulations to study the ternary vapour-liquid equilibrium of $C_2H_6/C_2H_4/C_2H_2$ at 277.79 K and 3.54 MPa, and obtained very good agreement with both experiment and the Peng-Robinson EoS (Peng & Robinson, 1976) – this does not provide a conclusive argument, though, that adjustments of energetic parameters for binary combinations are sufficient to accurately simulate ternary (or higher) mixtures that are composed of the different molecules from the binary mixtures.

Rowlinson & Swinton (1982) state that it is unwise to attempt to explain or calculate the properties of mixtures from a knowledge of the pure component properties (and hence, parameters) only – this is precisely what conventional mixing rules (for example, the ubiquitous

Lorentz-Berthelot rules) do. One needs to incorporate experimental information in order to obtain good models for mixtures (Haslam *et al*. 2008). It is through the introduction of correction factors that the mixture experimental information is imparted onto systems that would otherwise rely solely on pure-component model information.

As pointed out by Galindo *et al*. (2006) in their study of the excess chemical potential of methane in water, by adjusting the Lennard-Jones energy parameter between methane and water, they were able to implicitly account for the polarization energy of the two species, even though non-polarizable potential models were used in that study – this again reinforces the decision to adjust the Lennard-Jones unlike-energy parameter in this work, since by calculating the optimum parameters (or correction factors) between non-bonded atomic groups in molecular simulations, one can gain far greater insights into the chemistry of different molecular systems at equilibrium, irrespective of the number of chemical species or coexisting phases. Certainly, quantum mechanical methods are more rigorous and accurate, and do not require a priori knowledge of experimental data (Sandler 2003), but such methods will remain impractical for studying large chemical systems that contain complex molecules for many years to come, due to the large amounts of computational power required. This current method attempts to offer a means to improving current, practical methods.

The NpT –GEMC simulation was the chosen method of computation since it allows for the calculation of the phase equilibrium of mixtures at fixed temperature, pressure and total number of molecules without having to model the vapour-liquid interface, which is usually complex and subject to finite-size effects. It also allows direct comparison of the simulated data with experimental phase equilibrium data. The important details of this method were given in Chapter 2.

4.3 Automation of finding the optimum heterogeneous parameters

The Nelder-Mead simplex method of optimization (Nelder & Mead, 1965) has been used to good effect in studies for determining optimum force field parameters (Faller *et al*., 1999 and Müller *et al*., 2008). However, this method was used to optimize the force field parameters for pure compounds only and also by using homogeneous size and energy parameters, and to date

no studies have been reported on the automatic parameterization of cross-interactions (between unlike atomic group in mixtures). Thus, the implementation of the simplex method in this study for the automation of the cross-parameters was seen, initially, as a possible solution.

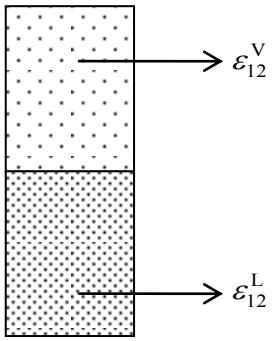

Figure 4-1 – Schematic of the approach used in this work. Unlike previous approaches that used the same Lennard-Jones cross-energy parameter in both simulation boxes, this work uses unique cross-energy parameters in each simulation box.

Unfortunately the simplex method was not viable because of the very nature of the model, i.e., using heterogeneous energy parameters. The problem was that while the simplex method attempted to minimize the error between simulation and experimental mole fractions by using different energy cross-parameters in each simulation box, it had no control over the numerical difference between the two parameters, and when the difference between the parameters was too large, a single liquid phase or phase-swapping were observed. Introducing a constraint on the difference would have been pointless because the only way to determine the maximum allowable difference for two-phase equilibrium would have been to run several simulations in which unlike differences between the parameters were tested, in which case the approach discussed at the end of this thesis would suffice. In any case, notwithstanding knowing what the maximum allowable difference is (*a priori* or not), the simplex method would not have been able to determine what the unique solution (optimum heterogeneous parameter pair) to the problem is because it turns out that there is no unique solution. This will be shown in both the preliminary investigation, which was purely numerical in its approach, and then through a more rigorous approach that was done at the end of this study (Chapter 5).

4.4 Approach to the problem and execution of simulations

The Monte Carlo for Complex Chemical Systems (MCCCS) Towhee program (http://towhee.sourceforge.net/) was modified to use different energy cross-parameters, ε_{12}^{V} and ε_{12}^{L}, in each simulation box for two-box isobaric-isothermal Gibbs ensemble Monte Carlo (NpT-GEMC) simulations (see Appendix C for the list of modifications made to the relevant subroutines, as well as additions to the code). This was done by multiplying the Lorentz-Berthelot unlike-energy parameter, $\varepsilon_{12} = \sqrt{\varepsilon_{11}\varepsilon_{22}}$, by the factors B^{V} and B^{L} in the designated vapour and liquid simulation boxes, respectively, so that $\varepsilon_{12}^{V} = B^{V}\sqrt{\varepsilon_{11}\varepsilon_{22}}$ and $\varepsilon_{12}^{L} = B^{L}\sqrt{\varepsilon_{11}\varepsilon_{22}}$. The force field parameters for methane and xenon are tabulated in Table 4-1. These molecules are represented as single interaction sites with no Coulombic charges – hence, only the Lennard-Jones 12-6 potential was used to calculate the interaction energies. The pure component Lennard-Jones parameters were not fine-tuned because the pure components' properties are already in excellent agreement with experiment.

Atom, or interaction, type	ε / [K]	σ / [Angströms]
methane-methane	148	3.73
xenon-xenon	183.29	3.91
methane-xenon (Lorentz-Berthelot)	227	3.82

Table 4–1 – Lennard-Jones potential model parameters for methane (Martin & Siepmann, 1998) and xenon (Gray & Gubbins, 1984 and Panagiotopoulos, 1989).

Firstly B^{V} was set equal to B^{L} for several values around unity to observe the effects of a homogeneous energy cross-parameter at eight different temperatures below and above the critical temperature of pure methane at specific pressures (see Table 4–2).

T / [K]	165	172	180	185	189.78	208.28	236.17	260.62
p / [kPa]	1200	1500	1750	2000	2073	2411	4559	5105
y_1	0.9418	0.9239	0.8951	0.8796	0.8348	0.6908	0.5778	0.3123
x_1	0.59	0.56	0.5	0.49	0.4792	0.2871	0.3317	0.1678

Table 4–2 – Experimental and equation of state-generated data (Dias *et al.*, 2004) which were used in this study. y_1 and x_1 are, respectively, the vapour and liquid mole fractions of methane, T is the temperature and p is the pressure.

The pressures that were selected at each temperature correspond to those which allow for the largest two-phase region in the experimental and equation of state-generated two-phase envelopes, and thus allowed for a large range of correction (B) factors to be studied at each two-phase state point. Here, the Peng-Robinson equation of state (Peng & Robinson, 1976) was used to generate the phase envelopes below 189.78 K since it provides an excellent fit to the experimental data at temperatures greater than or equal to 189.78 K. Once the results of these simulations were obtained, square grids of B^{V} and B^{L}, based on the 'optimum' values from the homogeneous simulations, were generated and once again, these values were used in further simulations to determine the effects of the heterogeneous cross-energy parameters in each phase. Except at 172.5 K and 236.17 K, where a 9×9 grid of factors was used, all other state points used a 5×5 grid (see Chapter 5 for the justification). Seven hundred molecules were used in each simulation along with 1.0-1.5 % box volume moves, 10-20 % swap moves and the remainder of the Monte Carlo moves were centre-of-mass translations. Pre-equilibration periods consisting of at least 5×10^3 MC cycles (where one MC cycle consists of N MC moves, where N is the total number of molecules) were used, to ensure that at least 50% of all box volume changes and translations were accepted. Thereafter, equilibration periods consisting of 2×10^5 to 3×10^5 MC cycles were used, followed by productions runs of at least 1.5×10^5 MC cycles. Lennard-Jones interactions were truncated at $2.84\sigma_{\mathrm{Xe}}=11.1044$ Angströms (Frenkel & Smit, 2002) and analytical tail corrections were used beyond this distance. The results of both homogeneous and heterogeneous simulations were quantified by using different error calculations for the individual phase composition deviations, and then the combined (total) deviation, from experiment. For individual phase composition deviations, a relative error,

$$\%\ \text{relative error} = 100\% \times \frac{X^{\text{sim}} - X^{\text{exp}}}{X^{\text{exp}}}, \tag{4-1}$$

where X^{sim} and X^{exp} refer to simulated and experimental solubilities (vapour or liquid), was used while the combined deviation of the two phases was calculated as

$$\text{Total error} = SSQD = \left(\frac{y_1^{\text{sim}} - y_1^{\text{exp}}}{y_1^{\text{exp}}} \right)^2 + \left(\frac{x_1^{\text{sim}} - x_1^{\text{exp}}}{x_1^{\text{exp}}} \right)^2, \tag{4-2}$$

where $SSQD$ is the sum of the squared relative deviations and the y_1 and x_1 symbols refer to the vapour and liquid compositions of methane, respectively.

As mentioned in Chapter 1, despite the shortcomings of the traditional homogeneous approach, further investigations were done to determine the temperature dependence of the global optimum homogeneous parameters. The same simulation methodology mentioned above was used at several pressures at each temperature (150 K, 165 K, 180 K, 189.78 K, 223.81 K and 248.15 K and also at several other state points that are described in Chaper 6.

Apart from the simulated solubilities, other simulation properties of interest were the potential energies, number densities and specific densities. The importance of these properties will become apparent in Chapter 5.

5. RESULTS & DISCUSSION

This chapter is structured as follows. The results of simulations using homogeneous Bs are discussed first in which it is shown that the homogeneous Lennard-Jones energy parameter is inadequate for giving good predictions of solubilities in the vapour and liquid phases simultaneously. The temperature dependence of the optimum homogeneous energy parameters is also explained. This is followed by a discussion of the heterogeneous $\left(B^{\mathrm{V}}, B^{\mathrm{L}}\right)$ simulations where apart from showing the improvements that the heterogenous parameter approach offers, the implications on the system's energy and solubilties are explained too. Finally a model and method that consolidates the findings of the heterogeneous parameter approach is presented and results obtained from it are discussed. Tables and figures that are referred to within the text are presented at the end of the chapter. At the outset, it should be mentioned that in spite of several thousand simulations being executed in the course of this study, the bulk of the results from these simulations were discarded since the initial parts of this study involved a lot of trial and error, and debugging of code. Supplementary numerical data that were used for generating some of the graphs are given in Appendix A.

5.1 Homogeneous energy parameters

5.1.1 Initial investigations

Graphical results are presented in Figures 5-1, 5-2 and 5-3 and numerical data is tabulated in Table 5-1. As can be seen, increases in B resulted in increasing solubility of the reference component, methane, in each phase. This effect is more pronounced in the liquid phase than in the vapour phase, as the same incremental changes of B results in a much larger change of the solubility of methane in the liquid box and has also been observed in Grand Equilibrium simulations (Vrabec & Hasse, 2009), where small changes in vapour compositions were observed and the vapour pressure varied linearly with changes in the unlike energy parameter. This is to be expected since vapour phase densities in these simulations were mostly two orders of magnitude smaller than the coexisting liquid densities; thus fewer interactions with other

(vapour) molecules, coupled with more long-range interactions not contributing to the potential energy, lead to smaller changes in the solubilities of each component. This apparently monotonic trend is not indefinite and is valid in the two-phase region only. Below the lower limit of the two-phase region, a complete vapour, distributed over both simulation boxes, was observed while above this limit, a complete liquid was similarly observed, in most cases in one simulation box only. Again, this is due to much weaker liquid interactions dominating towards lower values of B, while stronger interactions persist at the higher values – eventually, these weak (or strong) interactions result in a transition to a complete vapour (or liquid). Such transitions to single phases were observed in the initial simulations that used a smaller potential energy truncation radius to get a qualitative idea of how large deviations from the Berthelot rule affect the system, but in a computationally efficient manner.

Another explanation for the aforesaid solubility response of methane in each phase to changes of B is to consider the Lennard-Jones potential energy model. Decreasing B is equivalent to increasing the potential well depth (ε_{12}), thus increasing the repulsive forces in the two-phase system and diminishing the attractive forces to form a vapour. The opposite is true when B is increased, in which case a liquid is formed due to dominant attractive forces. Therefore decreasing B in two-phase NpT -GEMC simulations is equivalent to approaching the mixture's dew point, and beyond this point a complete vapour forms. Similarly, increasing B progressively shifts the mixture's bubble point, until complete liquefaction occurs; at 165 K, 172.5 K and 180 K, the liquid-phase composition of methane approached those of the overall methane compositions that were used in the simulations at those conditions. At the same time, the number of vapour molecules decreased until complete liquid formation occurred; that is, the system entered the single phase region below the mixture's bubble line. When compared with the other temperatures (185 K – 260.62 K) the liquid composition curves at 165 K, 172.5 K and 180 K are not linear especially at higher B values, since at $B=1.00$ at 260.62 K, the "vapour" density exhibits large fluctuations and beyond this point, a complete liquid forms. Thus, the B-interval in which the liquid-phase methane composition approached the overall mixture methane composition progressively decreased with increasing temperature and pressure because the (average) width of the phase envelope for the mixture becomes smaller with increasing temperature, due to in the supercritical methane temperature range. Note how, from the relative errors of methane solubilities in each phase, a homogeneous B is inadequate for predicting the experimental solubilities in both phases with good accuracy simultaneously. At all state points the combined absolute error of the vapour and liquids compositions is much lower at a B that gives the lowest liquid composition error than at a B that gives the lowest vapour phase error,

due to the much larger changes in methane solubility with B in the liquid phase. The errors that are expressed as sums of the squared relative deviations, for the most part, belie the large deviations between experiment and the simulation results at their minima (which correspond to 'optimum' BS). For example, at 260.62 K the simulation minimum error point gives a total absolute error equal to 10.84 %, which is much larger than when expressed in the alternate form mentioned above. At this temperature-pressure pair it was also noted that linear extrapolation to a theoretical 'zero-error' B is not possible as this false optimum is located in the region that results in complete liquid formation.

This justified the further investigation of the effects of varying B independently in each simulation box, and to determine whether the homogeneous energy correction factor bottlenecks mentioned above could be overcome. It is also worth mentioning that the optimum correction factors that were found at each temperature-pressure pair are only local optima and are not transferable to other pressures, for each temperature. To illustrate this point, it was noted that for additional simulations at 172.5 K, the optimum B $(=0.99)$ at 1400 kPa is much different to the optimum correction factor $(B=1.02)$ at 2200 kPa.

5.1.2 Temperature and pressure dependence of optimum homogeneous B

In spite of the abovementioned inadequacies of the homogeneous energy correction factor approach, further work was done to determine the temperature and/or pressure dependence of the optimum homogeneous energy correction factors, since an overwhelming majority of simulation studies of mixture fluid phase equilibrium have used the same unlike Lennard-Jones parameters, specifically the energy parameter, at all temperatures/pressures of interest by assuming 'transferability' of the parameters. The results are shown graphically in Figure 5-4 and numerically in Table 5-2. In Figures 5-4(a) to 5-4(d), only simulated data corresponding to the unadjusted Berthelot parameter ($B=1$) are shown – the optimum B for each simulated NpT state point was used for calculating the global optimum B for each temperature to establish the temperature dependence of the energy parameter, but further simulations at these temperatures (165 K to 189.78 K) based on the global optimum B were not done since the Berthelot value provides a reasonably good fit.

As can be seen, at low temperatures (Figures 5-4(a) to 5-4(d)) the simulated vapour compositions, having small statistical uncertainties, are in excellent agreement with experimental data and equation of state predictions. However at 189.78 K (Figure 5-4(d)) slight deviations between simulation and experiment become apparent over the entire pressure range and the trend persists at higher temperatures, with positive deviations that become larger with increasing pressure. This observation seems contrary to Figure 5-4(f), where the vapour composition seems to be in better agreement with experiment at the highest simulated pressure, when compared with the lower pressures at this isotherm – however, at this state point, there are large, overlapping uncertainties in both the vapour and liquid compositions and hence, densities. Therefore, this was not a reliable result and was discarded when calculating the global optimum B for this temperature. In fact, for all temperatures greater than 223.81 K the simulated systems tended towards instability at high pressures (near the mixture critical point) when using the Berthelot energy parameter. The critical temperature of pure methane is 190.4 K (Perry & Green, 2007) and that of xenon is 289.7 K (Smith *et al*., 2001). The instabilities are not unexpected since Gibbs ensemble simulations near the critical points of both pure substances and mixtures are not very efficient (Panagiotopoulos, 1987). In regards to the simulated liquid compositions using the Berthelot rule, positive deviations from experiment are also observed from moderate to high temperatures at all pressures, but negative deviations occur at the lower temperatures when pressures are low.

The mostly-positive departures from experimental compositions observed in the phase diagrams, coupled with the observed increase of methane solubility in each phase with increasing B in the first part of this section means that the Berthelot rule gives an energy parameter value that is higher than it should be if better agreement between simulation and experiment is sought. This means the optimum energy parameters for each isotherm should be less than unity in order to reduce the potential well depth and the over-prediction of attractive forces between the unlike molecules. This was investigated by using a weighted-fit for each isotherm, based on the relative volatilities of methane and xenon for different pressures along the same isotherm, to obtain the global homogeneous B at each temperature. A similar procedure was also performed using the width of the phase envelope at each experimental pressure-temperature state that was simulated as the weighting factor. Figure 5-5 shows the variation of the optimum global B with temperature for the two different methods mentioned above.

Using the optimum energy parameters that were obtained from the weighted-relative volatility fitting at 223.81 K and 248.15 K (the temperatures at which the largest deviations from experiment were observed when using the Berthelot energy parameter) it is seen that better agreement with experiment is obtained especially in the liquid phase. However, positive deviations from experiment are still observed in the vapour phase and at 248 K, slight negative deviations are observed for the liquid phase with increasing pressure. Thus with increasing pressure methane molecules have a preference for the vapour phase when using a single homogeneous B^{opt} for a given temperature. It is also worth noting that at the highest pressure at 248.15 K, a stable system was obtained with the lower, revised B^{opt}, which is expected because the original Berthelot value was too high to yield stable vapour-liquid coexistence. This is consistent with the observation at 260.62 K mentioned at the beginning of this section, where at or beyond the Berthelot energy parameter ($B \geq 1$) fluctuations in densities, and hence system instabilities, occurred. These observations imply that when a weight-averaged temperature-dependent homogeneous energy parameter is used for the calculation of phase diagrams, satisfactory agreement with experiment also depends on the pressure at the thermodynamic state of interest. In this regard equation of state modelling of the fluid phase equilibrium of mixtures usually outperforms molecular simulation due to an EoS using a much larger number of adjustable parameters.

Figure 5-5(a) also reveals trends for the temperature-dependence of the optimum global Bs. The tendency is for B^{opt} to decrease with increasing temperature, before and after the discontinuity at or near the critical temperature of methane (the more volatile component). This is in line with the observation that when using the Berthelot energy parameter ($B = 1$) the positive deviations from experiment get larger as the temperature is increased, and thus B^{opt} should follow the opposite trend. The trends of the optimum global Bs obtained from the second fitting procedure are not apparent because of the nature of the weight that was used to obtain these optimum Bs. Relative volatilities contain important thermodynamic information of a mixture, while the width of the phase envelope of a mixture by itself is seemingly arbitrary.

At constant pressure, there are also variations of B^{opt} with temperature that are comparable in magnitude to the variations observed in the constant temperature simulations discussed above. It seems that the tendency is for the optimum parameters to decrease with temperature at the moderate pressure (3000 kPa) and to increase with temperature at the higher pressure (5000

kPa), although despite extremely long production runs at 248.15 K, the value of the optimum B did not change appreciably upon analysing the simulation data. Considering that at 1800 kPa no definite trend of B^{opt} could be discerned as well (to be discussed in section 5.1.3), this means that while there is a dependence of B^{opt} on temperature and pressure in simulations (indeed, equations of state have such dependences too), it is more frugal to calculate and discuss such parameters in terms of temperature only. Note that at 150 K, the methane/xenon experimentally-observed vapour-liquid equilibrium region does not extend over the entire composition range of methane. However, for the purpose of demonstrating the temperature-dependence of the optimum energy parameter, this temperature was chosen since it is sufficiently far away from 165 K so as to observe a difference in the optimum energy parameter values at these two temperatures. One possibility for why solid-liquid equilibrium was not observed in these simulations at 150 K can be explained through the parameterization of the original pure component force fields. The parameters were fitted to vapour and liquid thermophysical properties and no such solid properties were used. Note too, that in order to simulate solid phases accurately in the Gibbs ensemble, additional free-energy models of the solid phase must be generated - see Sweatman & Quirke (2004).

5.1.3 A possible explanation for the discontinuity at 189.78 K

Although the range of optimum Bs corresponding to the temperature range that was studied is seemingly small, it is evident that there is a discontinuity at 189.78 K which is slightly lower than the experimentally observed critical temperature of pure methane, which is 190.4 K (Perry & Green, 2007). This means the TraPPE-UA potential energy model for methane slightly under-estimates its experimentally-observed critical temperature. Indeed, the work of Martin & Siepmann (1998) reports a reduced critical temperature ($T_c^* = T_c / \varepsilon_{CH_4}$) of methane of 1.294 ± 0.009 and at the lower limit of this value, the critical temperature of methane is 190.18 K but this is still a (slightly) higher value than that at which the discontinuity is observed; however the same study also stated that the systematic error associated with the uncertainty of the critical scaling exponent β (this should not be confused with the statistical mechanics quantity $\beta = 1/k_B T$) is roughly 1%, and roughly 2% if one considers finite simulation sizes. Using the former modest error estimate of 1%, the critical temperature of TraPPE-UA methane is then 188.23 K – this is lower, albeit very slightly, than the temperature at which the discontinuity of the optimum B is observed and thus it can be concluded that the observation of

the deviation between the simulation and the experimental methane critical temperature is consistent with previous work and not due to any error that might have come out in this work. Similar discontinuities at the critical temperatures of the more-volatile component have been reported, based on equation of state modelling of experimental data, for the k_{12} binary interaction parameters of R227ea/CO_2, R134a/CO_2, methane/butane (Valtz *et al.*, 2003) and SO_2/R227ea (Valtz *et al.*, 2004) mixtures. Therefore based on Figure 5-5(a) and as stated by Valtz *et al.* (2003), it is incorrect to extrapolate temperature-dependent optimum binary interaction parameters that are fitted only to temperatures below or above the volatile component's critical temperature, to temperatures on the corresponding opposite sides of the critical point. Valtz *et al.* (2003) also state, with reference to the discontinuity, that "**...the phenomenon ... is certainly due to the absorption of a supercritical gas in a liquid very different to that of a subcritical gas. Maybe it generates new interactions that lead to a significant jump in the values of the binary interaction parameters.**" This hypothesis was tested at a single pressure (1800 kPa) that has both sub- and supercritical methane in its temperature range (172.5 K, 180 K, 185 K, 189.78 K, 208.29 and 223.81 K). Initially, the standard Berthelot energy parameter was used in each simulation because although there are pressure- and temperature-dependencies of the B^{opt} for each (P,T) pair, the temperature dependence of B^{opt} at constant pressure is slightly smaller than the pressure dependence of B^{opt} at constant temperature. In any case, due to this isobar having small composition ranges or being in the dilute regions at the initial temperature range that was studied that included 165 K and 236 K, meaningful composition trends could not be established at the minimum (165 K) and maximum (236 K) temperatures when varying the unlike energy parameter at these temperatures due to finite-size effects (even when using 1500 total molecules). Therefore it was assumed that unreliable optimum energy parameters might have introduced unnecessary uncertainty to the results.

Figure 5-7 provides evidence for the assertion of there being "new interactions" in the supercritical liquid since again at 189.78 K there is a distinct increase (spike) in the liquid-phase potential energy after a monotonic decrease of the liquid energy with subcritical methane temperature increases. Despite the simulation uncertainties of potential energies being large (this is in fact typical in both Monte Carlo and molecular dynamics molecular simulations), Figure 5-7 shows that the uncertainties of the average vapour- and liquid-phase potential energies at all temperatures are sufficiently small to infer trends of these potential energies with respect to sub- and supercritical methane. It appears that at constant pressure, increasing the

system temperature within the subcritical methane temperature range effects quite a steep energy decrease in the liquid phase while there are very small changes to the vapour phase energy. Thus, the attractive forces in the liquid phase become stronger with increasing temperature; equally one can say that the repulsive forces get weaker. At 189.78 K, there is a sharp increase in the liquid-phase potential energy – this indicates that a strong repulsion force is present at, or just after, the onset of methane criticality and most likely the cause of the discontinuity that is observed. At this point one can also say that there is a sudden weakening of the attractive forces in the liquid. Beyond this point there are no large changes in the liquid-phase potential energy, though the attractive forces persist, but there is a steady decrease of the potential energy of the vapour phase, indicating that attractive forces in the vapour phase get stronger (or the repulsive forces get weaker) with increasing temperature above the critical temperature of methane, and thus increasing the solubility of xenon, the 'solute', in this phase. Interestingly there is also a sudden increase in vapour potential energy at 185 K. To confirm that this was not an "outlier" in the data, the simulations were repeated using the optimum energy parameters for each temperature and it is seen that the overall trend persists even with the "correct" energy parameters.

One approach to understand the effects of the discontinuity phenomenon that was explained above is to study the phase densities on either side of the discontinuity. Figure 5-8 consolidates the energy trends shown in Figure 5-7. Below 189.78 K, the very small increases of potential energy in the vapour correspond to small changes of vapour density, while the steep decrease of the liquid-phase energy, which indicates increasing attractive system energy, corresponds to a steady increase of the liquid density with increasing temperature. At and beyond the discontinuity (189.78 K), it is clear that for a given temperature interval, there is a significantly sharper increase of the supercritical-methane vapour density, which corresponds to the steady decrease of vapour potential energy in Figure 5-7, when compared to the same interval on the subcritical side of the discontinuity. The slope of the vapour density-temperature curve also increases with temperature and this agrees well with supercritical fluid (SCF) theory in that for a gas that is above its critical point, liquids become much more soluble in the gas phase due to the gas density being much higher and comparable to the density of a liquid (Petrucci *et al*., 2006).

A question that arises is whether the discontinuity, in the context of these simulations, is the result of methane-methane, methane-xenon or xenon-xenon interactions (or combinations thereof). Considering that the vapour and liquid potential energy profiles in Figure 5-7 were obtained by using different values for scaling the methane-xenon interactions (first the

unadjusted Berthelot parameter and then the optimum homogeneous unlike-energy parameter for each temperature), and that the revised potential energy profile that was obtained was merely shifted vertically upwards along the potential energy axis, it can be concluded that the discontinuity is not due to the unlike interactions (otherwise, there would have been noticeable shifts along the temperature axis too). The experimental critical temperature of pure xenon, 289.7 K (Smith *et al.*, 2001), is much higher than the highest temperature that was used in this part of the work (223.81 K) and it is not expected that the simulated critical temperature of xenon will differ from the experimental by much, since the xenon force field gives excellent agreement with experiment for the pure component simulations. That is not to say within the context of these simulations that xenon-xenon interactions did not contribute to the discontinuity at all, but rather that the evidence is in favour of the discontinuity being due to methane-methane interactions since the phenomenon is observed at or near the critical temperature of pure methane.

5.2 Heterogeneous energy parameters

Independent changes of the unlike energy parameter in each phase lead to the observation of interesting coexisting phase behaviour at the chosen thermodynamic state points. Initially, 9×9 (square) grids of equally spaced Bs were used at 172.5 K and 236.17 K to get a refined set of data. These temperatures are, respectively, significantly below and above the critical temperature of pure methane. The size of the B interval for the initial 236.17 K simulations was reduced because a significant number of simulations resulted in either large periodic density fluctuations in both phases or liquid-liquid equilibrium, and the focus of this work was vapour-liquid equilibrium only. Also, 5×5 grids were tested and it was found that cubic spline interpolation provided as good a representation of the data as it did for the larger grids (see Figure 5-9). Therefore, it was decided to use the more computationally economical 5×5 grids for the remainder of the state points. The results of these simulations are shown in Figure 5-10, where the effects of heterogeneous correction factors on the sum of the relative deviations squared are shown. While this representation of the error belies the total absolute error, it was still used because it provided a smooth 'function' with which a reasonable qualitative overview of the simulation deviations at different combinations of cross-energy correction factors could be gained. As can be seen, the minimum errors, and hence optimum B pairs are located close to the line $B^{\mathrm{V}} = B^{\mathrm{L}}$. Importantly it is seen that, for example, at 260.62 K for which the total absolute error is 10.84 % when using a homogeneous correction factor, a pair of heterogeneous

correction factors reduced the error to 3.96 % at the point $(B^{V}, B^{L}) = (0.9853, 0.9856)$. Furthermore, at 236.17 K the total absolute error has been reduced to 4.35 % at $(B^{V}, B^{L}) = (1.0045, 1.0060)$, from the initial error of 8.17 %, which was obtained using a single homogeneous energy parameter. While the reductions of the errors might not seem substantial, they nevertheless emphasize the suggestion of this work, that is, to model the unlike energy interactions in each phase uniquely. The simulations at 260.62 K proved mostly unstable especially when the differences between the correction factors were large, in spite of decreasing the range of factors that were initially studied; this is directly related to the much smaller homogeneous correction factor range that gave stable VLE at this pressure and temperature.

An interesting observation from Figure 5-10 is the location of the areas of the largest errors. For 165 K to 185 K (Figures 5-10(a) – 5-10(d)), the subcritical temperatures of methane, the maximum errors are located in regions where the vapour phase energy correction factors are larger than the corresponding liquid phase factors and these are regions where the numerical differences between the factors are large. In contrast, for temperatures 189.78 K to 260.62 K (Figures 5-10(e) – 5-10(h)), the regions of maximum errors are located where the liquid phase energy correction factors are larger than the vapour phase factors. This can be attributed to the discontinuity that was described in the homogeneous simulations section of this chapter and is perhaps suggestive of a trend for the sub- and supercritical heterogeneous energy correction factors. Again at 189.78 K, which is less than the experimental critical temperature of pure methane (190.4 K), the location of the maximum errors is in the same region as those of the supercritical temperatures. However, as explained in Section 5.1.3, the critical temperature of pure methane has been shifted to a lower value in the context of this work.

While the numerical results of the grid simulations do not indicate any sub- or supercritical methane trends in terms of the optimum heterogeneous parameters, it should also be borne in mind that these numerical results are based on actual, discrete simulation datasets and were not interpolated (or extrapolated) to any theoretical minima. However, later in this chapter a new model for the relationship between unlike-atom potential energies and the phase-dependent energy parameter perturbations is presented. It will be shown that the anticipated trends discussed above are not necessarily valid, since different pairs of the vapour and liquid energy parameter correction factors at a single pressure and temperature can be construed as being "optimum". All simulation errors at all state points that were studied were dominated by the

liquid phase (Figure 5-11 is an example at 172.5 K and 1500 kPa) and this was also observed when homogeneous correction factors were used.

The variations of the vapour and liquid compositions with B^{V} at constant values of B^{L} at 172.5 K are shown in Figures 5-12. At constant B^{L}, increasing B^{V} causes a monotonic decrease (within the range of B^{V} that was used) of methane solubility in both phases, with larger changes observed in the liquid phase. In both phases, the overall changes in solubility over the range of B^{V} are larger at lower values of constant B^{L} than at higher values of B^{L}. The opposite of the aforesaid observations is true when B^{V} is constant and B^{L} is varied, with the difference being in both phases the overall changes in solubility over the range of B^{L} are larger at higher values of constant B^{V} than at lower values of B^{V}. The reasons for these observations are as follows. At constant B^{L}, increasing B^{V} results in a decrease of the vapour phase potential energy and an increase of the attractive forces in this phase. At the same time, increases of the liquid phase potential energy, which corresponds to a more repulsive nature being present in this phase, are observed (Figure 5-13). However, the total (system) potential energy, or "net" energy, is dominated by the liquid phase potential energy due to it being larger in magnitude, and being repulsive, results in a decrease of methane solubility in both phases. This agrees with the homogeneous simulations that were discussed earlier in this Chapter in which, due to the Berthelot energy parameter yielding too high solubilities when compared to experiment, the homogeneous factors were decreased to less than the Berthelot value (i.e. less than unity) to reduce the excess attractive nature (or increase the repulsive nature) of the system. Referring to Figure 5-13 again, it is seen that for the range of B^{V} that was used, larger changes of the potential energy contributions (due to the perturbations B^{V} and B^{L} around the Berthelot rule) occur at lower values of B^{L}, while smaller changes are observed when is B^{L} higher; this is perhaps the reason why larger changes in solubilities are observed when B^{L} is low, since the potential energy "driving force" is larger.

Similar trends are observed at 236.17 K (4559 kPa) (see Figure 5-14), but here sharp changes in the vapour and liquid compositions between $B^{V} = 0.994$ and 1.0015 for $B^{L} = 1.0015$ to 1.006 are observed. These are regions wherein the differences between the correction factors are large, and this causes sharp changes in density and hence, composition. Especially when

$B^{\mathrm{L}} = 1.006$ there are several sharp changes in compositions. These observations suggest that adjusting the simulated compositions is not controlled simply by the correction factors used in each simulation box, but also by the differences between the factors in each phase. Notice too, that the composition profiles are shifted along the abscissa of the diagrams at different constant values of the vapour and liquid correction factors. Again, similar trends with respect to the potential energy of each phase that were observed for the system at 172.5 K are observed here too, but because of the slightly larger grid used at this state point, there are both increases and decreases of mole fractions with increasing B^{V} at constant B^{L}.

It was also found that different combinations of heterogeneous energy cross-parameters do not necessarily map uniquely into the solubility and hence, error, spaces. At 185 K, the co-ordinates $(B^{\mathrm{V}}, B^{\mathrm{L}}) = (0.9825, 0.9875)$ (a) and $(0.9850, 0.9900)$ (b) both yielded, within excellent statistical uncertainty, the same vapour (0.9154 ± 0.005 and 0.9153 ± 0.004) and liquid compositions (0.5932 ± 0.001 and 0.5933 ± 0.001), respectively. Incidentally, for each set of coordinates the difference between the vapour- and liquid-phase correction factors is the same ($\Delta = 0.05$) and upon further inspection, it is seen that the corresponding liquid potential energies (-0.59708×10^6 K $\pm 0.36352 \times 10^4$ K (a) and -0.59798×10^6 K $\pm 0.24131 \times 10^4$ K (b)) and vapour potential energies (-0.81926×10^3 K $\pm 0.26304 \times 10^3$ K (a) and -0.80110×10^3 K $\pm 0.21361 \times 10^4$ K (b)) are in excellent agreement with each other. This observation by itself is enough to conclude that there exist several $(B^{\mathrm{V}}, B^{\mathrm{L}})$ pairs for a certain NpT state point, each having distinct individual B^{V} and B^{L} values (but whether having the same difference between each pair of values remains to be seen) that give the same solubilities and energies in each phase of a two phase system – technically, one can state that there is a degeneracy associated with the heterogeneous energy parameter approach. This will be proved later in this chapter as well when a new unlike-atom potential energy model that utilises heterogeneous energy parameters is presented.

The findings discussed so far can be explained more formally, and since Monte Carlo molecular simulations are driven by the changes of a system's potential energy, the obvious starting point for such an explanation is to discuss the coexisting vapour and liquid potential energies. A very recent study (Vlcek *et al.*, 2011) developed a computational scheme for the determination of the optimum unlike Lennard-Jones parameters (size and energy) and optimum electrostatic charges

for a system exhibiting very low mutual solubility – carbon dioxide/water – by using a rigorous statistical mechanical treatment. Like all parameter-optimization studies preceding it, the aforesaid work used homogeneous corrections factors for the system of interest.

In order to elucidate the above remarks, it is instructive to consider not just the potential energies of the system being investigated at each $(B^{\mathrm{V}},\ B^{\mathrm{L}})$ pair, but the *contribution* made by every such pair to the potential energy of the reference Lorentz-Berthelot system in which $(B^{\mathrm{V}},\ B^{\mathrm{L}}) = (1,1)$. In this argument, the grid simulations at three different pressures (3121 kPa, 4559 kPa and 5290 kPa) at 236.17 K shall be used. Before presenting the argument, though, the method implemented by Vlcek *et al*. (2011) will be explained briefly, although their method of optimizing the electrostatic interactions will be omitted since the mixture that was used in this work contained no molecules with permanent electrostatic charges.

A lengthy derivation by Vlcek *et al.* (2011) shows that the equation that relates, or 'couples', the coexisting phases in a two-phase binary system is

$$\frac{\rho_1^{\mathrm{V}}(0)}{\rho_1^{\mathrm{V}}(\theta)} \times \left\langle \exp\left[-\beta \sum(\theta)\right] \right\rangle_{\mathrm{V}} = \frac{\rho_1^{\mathrm{L}}(0)}{\rho_1^{\mathrm{L}}(\theta)} \times \left\langle \exp\left[-\beta \sum(\theta)\right] \right\rangle_{\mathrm{L}} \quad , \tag{5-1}$$

where 0 and θ refer to the unperturbed and perturbed systems respectively, ρ is the *number* density of the reference component in a phase (having units of $\text{number of molecules of component 1/unit volume}$), $\beta = 1/k_{\mathrm{B}}T$ in which k_{B} is the Boltzmann constant and T is the system temperature, and the $\langle \ldots \rangle$ refer to ensemble averages. The equation was derived by first imposing the condition for chemical equilibrium i.e. the chemical potential of each species must uniform throughout the system – this is true for both the perturbed and the unperturbed (Lorentz-Berthelot) systems. Then, using the coupling parameter approach (Fischer et al. (1989) and Chialvo (1991)) for the unlike size and energy parameters, along with the definition of the *NpT* partition function for both the perturbed and unperturbed systems, the chemical equilibrium condition was expressed in a form that related the perturbation of the unlike-pair LJ interaction parameters to the changes in the concentration (number density) of the reference species in both phases i.e. Equation 5-1.Using results from a

study by Chialvo (1991), Vlcek *et al*. (2011) also presented a relationship between the contribution made by the perturbation, θ, to the potential energy of the reference system (where $B=\eta=1$, i.e. homogeneous correction factors). The relationship is

$$\sum(\theta)=\varphi^{\mathrm{REF}}\left(B+2\eta^{6}-\eta^{12}-2\right)+\psi^{\mathrm{REF}}\left(\eta^{6}-\eta^{12}\right)/6 \quad , \tag{5-2}$$

where $\sum(\theta)$ is the contribution of the unlike-atom perturbation θ to the system's total potential energy, φ^{REF} is the total unlike-atom potential energy when $B=\eta=1$ (obtained from a single simulation), $\psi^{\mathrm{REF}}=\sum_{j\neq i}\left(r_{ij}\,\partial u_{ij}\left(r_{ij},\theta=0\right)/\partial r_{ij}\right)_{\theta=0}$ also when $B=\eta=1$ (also obtained from a single simulation), η is the Lennard-Jones size correction factor and B is the Lennard-Jones energy correction factor. Equation 5-2 allows for a very large number of (B,η) pairs to be tested, using simplex optimization, for example, without the need for the same number of additional simulations using every such pair in order to match the unlike-energy contribution on the left hand side. The unlike energy contribution is obtained from Equation 5-1. Vlcek *et al*. (2011) simplified Equation 5-1 by noting that because CO_2 has a high dilution in the H_2O–rich phase (and vice versa), the chemical potentials of CO_2 in the CO_2–rich and H_2O in the H_2O–rich phases are practically unchanged because of the abovementioned high dilutions; hence, Equation (5-1) was simplified to

$$\frac{x_1(\theta)}{x_1(0)}\approx\frac{\rho_1(\theta)}{\rho_1(0)}=\left\langle\exp\left[-\beta\sum\theta\right]\right\rangle_{\mathrm{L}} \quad , \tag{5-3}$$

where x refers to liquid mole fraction. Hence for the specific case of a binary system containing chemicals with high insolubility in their respective dilute phases, only the Lorentz-Berthelot and target solubilities are required to obtain $\sum(\theta)$ (Equation 5-3), which is then used in Equation 5-2 to obtain the first approximation of the optimized unlike Lennard-Jones parameters. The second iteration would use the first approximation as the new reference system, and the procedure would continue until the desired tolerance is reached (in the case of CO_2/H_2O, two iterations were sufficient for every NpT state that was simulated). As with

most perturbative methods, the perturbed system must be sufficiently close to the unperturbed system in order to get meaning results. As an example, the work of Vlcek *et al*. (2011) showed that the optimized LJ unlike size and energy parameters (σ,ε) for carbon (in CO_2)-oxygen (in H_2O) interactions in the final iteration were (2.8412 Å, 0.5511 kJ/mol), while the unperturbed Lorentz-Berthelot system values were (3.0995 Å, 0.6597 kJ/mol) – relative to the LB system, these changes were -8.33% and -16.46%, respectively. In the context of this work, as was shown in section 5.1.1 of this chapter, the extreme cases of large perturbations resulted in systems that were not two-phase systems.

5.3 New model and method stemming from this work

In the context of this part of the current work (heterogeneous energy parameters), $\eta = 1$ because no corrections were applied to the Lennard-Jones unlike-size parameter. Thus Equation 5-2 reduces to

$$\sum(\theta) = \varphi^{\mathrm{REF}}(B-1) \quad . \tag{5-4}$$

Equation 5-4 contains only a homogeneous energy correction factor and the contribution of the unlike molecules to the base/reference system's total potential energy is also contained within a single constant, φ^{REF}. This equation needs to be modified to contain the vapour and liquid correction factors, as well as the reference unlike potential energy in each phase to describe the contribution of each perturbation to the unlike potential energy in that phase. Chialvo (1991) showed, using exact mathematical expressions, that the total contribution of unlike atoms to the potential energy of a two-phase system is a linear combination of the departures from the Lorentz-Berthelot mixing rules. Since $\eta = 1$ the total potential energy consisting of the 'base case' Lorentz-Berthelot system and the homogeneous energy parameter perturbation (departure from the Berthelot rule) is (Chialvo, 1991)

$$\begin{aligned} U\left(\mathbf{r}^N, B\right) &= U\left(\mathbf{r}^N\right)_{\mathrm{LB}} + (B-1)U_{12}\left(\mathbf{r}^N\right)_{\mathrm{LB}} \\ &= U\left(\mathbf{r}^N\right)_{\mathrm{LB}} + \varphi^{\mathrm{REF}}(B-1) \end{aligned} . \tag{5-5}$$

This is an important result because it implies that the linearity of Equation 5-4 is still preserved when an additional energy parameter is introduced and as shown below, this relationship is valid for the system studied in this work.

Hence, this work proposes the following modified form of Equation 5-2 that models the contributions of the vapour- and liquid-phase perturbations, $\left(B^{\mathrm{V}}-1\right)$ and $\left(B^{\mathrm{L}}-1\right)$, to the vapour and liquid unlike-atom total potential energies for a binary Lennard-Jones system:

$$\left(\sum\theta\right)^{\mathrm{V}} = \varphi^{\mathrm{V}}_{B^{\mathrm{V}},\,\mathrm{REF}}\left(B^{\mathrm{V}}-1\right) + \varphi^{\mathrm{V}}_{B^{\mathrm{L}},\,\mathrm{REF}}\left(B^{\mathrm{L}}-1\right), \tag{5-6}$$

$$\left(\sum\theta\right)^{\mathrm{L}} = \varphi^{\mathrm{L}}_{B^{\mathrm{V}},\,\mathrm{REF}}\left(B^{\mathrm{V}}-1\right) + \varphi^{\mathrm{L}}_{B^{\mathrm{L}},\,\mathrm{REF}}\left(B^{\mathrm{L}}-1\right), \text{ and} \tag{5-7}$$

$$\left(\sum\theta\right) = \left(\varphi^{\mathrm{V}}+\varphi^{\mathrm{L}}\right)_{B^{\mathrm{V}},\,\mathrm{REF}}\left(B^{\mathrm{V}}-1\right) + \left(\varphi^{\mathrm{V}}+\varphi^{\mathrm{L}}\right)_{B^{\mathrm{L}},\,\mathrm{REF}}\left(B^{\mathrm{L}}-1\right). \tag{5-8}$$

In Equation 5-6 $\left(\sum\theta\right)^{\mathrm{V}}$ is the total contribution of the perturbations $\left(B^{\mathrm{V}}-1\right)$ and $\left(B^{\mathrm{L}}-1\right)$ to the potential energy of the vapour phase, and $\varphi^{\mathrm{V}}_{B^{\mathrm{V}},\,\mathrm{REF}}$ and $\varphi^{\mathrm{V}}_{B^{\mathrm{L}},\,\mathrm{REF}}$ are the total unlike-atom energies contributed to the vapour phase potential energy when $B^{\mathrm{V}}=1$ and $B^{\mathrm{L}}=1$ respectively. Equation 5-7 is the corresponding liquid phase model, and Equation 5-8 is simply the sum of Equations 5-6 and 5-7. Although Equation 5-8 will not be used directly in the following discussion, it emphasises the preservation of the linearity of the anticipated contributions of the perturbations.

Considering that the work of Vlcek *et al*. (2011) was published during the advanced stages of this work, and that obtaining the $\varphi^{\mathrm{V,L}}_{B^{\mathrm{V,L}},\,\mathrm{REF}}$ directly from further simulations would have first required a considerable programming effort, it was decided to test the proposed model by using existing grid simulation data at 236.17 K at three different pressures (3121 kPa, 4559 kPa and 5290 kPa).

For each grid-simulation dataset, the contributions of the perturbations $\left(B^{\mathrm{V}}-1\right)$ and $\left(B^{\mathrm{L}}-1\right)$ to the total *unlike* energy were obtained by simply subtracting the homogeneous "base case" *total* system energy from the total system energies of the corresponding perturbed systems. Following that, multivariable linear regression (using MATLAB®) gave the $\varphi^{\mathrm{V,L}}_{B^{\mathrm{V,L}},\,\mathrm{REF}}$. Obviously, the approach being described relies on the perturbed systems having accurate potential energies with low simulation uncertainties and ideally the $\varphi^{\mathrm{V,L}}_{B^{\mathrm{V,L}},\,\mathrm{REF}}$ should be obtained directly from the actual "base" system simulation (as explained in the previous paragraph), but it will be shown that this approach is sufficient to explain the degeneracy of energy states mentioned earlier in this chapter.

The results of the regressions carried out at (236.17 K, 3121 kPa) and (236.17 K, 4559 kPa) are shown in Figures 5-15 to 5-18. As can be seen, the proposed model is indeed validated by the high coefficient of determination (R^2) equal to 0.9779 and the sum of residuals (-1.0914×10^{-11}) using a 95% confidence interval is sufficiently close to zero. The five data points used for the regression at 4559 kPa are based on simulations that used heterogeneous energy parameters close to the Berthelot value, and the model did not give a good representation of the initial data set (consisting of all 81 simulations, see Figure B-7 in Appendix B) because, as shown in Figure 5-14, there are no monotonic trends for the compositions of each phase which are directly related to the system's potential energy. In fact, Figure 5-14 shows a few inflections at certain B^{L} values, which are more pronounced in the liquid phase – this indicates a transition between different coexisting vapour-liquid states.

Using the same range of vapour and liquid energy correction factors on a smaller (5×5) grid at 236.17 K and at a lower pressure (3121 kPa), a similar excellent fit is obtained ($R^2=0.9700$

and sum of residuals = 2.4425×10^{-15}). Clearly, at constant temperature, a system at a lower pressure is less sensitive to the same range of heterogeneous energy parameters than a system at a higher pressure – these smoother trends are shown in Figures B-8 to B-12 in Appendix B where several quantities (specific densities, energy contributions, methane number densities and methane composition profiles) obtained from the simulations at 236.17 K at the different pressures are provided, to give an understanding of how the same range of heterogeneous perturbations effect different changes in these quantities at different pressures. According to the residual case order plot, using a 95% confidence interval, the fifth simulation is an outlier to the data; this state point has the maximum difference between the $(B^{\mathrm{V}},\ B^{\mathrm{L}})$ pair and large system fluctuations are therefore expected. Unfortunately, at the highest pressure that was tested at 236.17 K, most simulations resulted in system compositions that were far-removed from the target compositions, much like the inflections discussed above for Figure 5-14 and hence it would be of little use to compare these results to the results of the 3121 kPa and 4559 kPa simulations.

Now that the proposed energy model has been validated, the next step is to show how to put the model into practise by combining it with the work of Vlcek *et al.* (2011), specifically, Equation 5-1, which is the general relationship between both phases. While the development of the model proposed in this work was simplified by not applying perturbations to the Lennard-Jones size parameter, complications arise when trying to relate the total potential energy of the system to the number densities. Obviously, the simplifying assumptions made for the CO_2 / H_2O system cannot be used here since methane/xenon are highly miscible in both the vapour and the liquid phases, though less-so in the supercritical methane region.

The following is proposed. Equation 5-1 is rearranged to contain the *ratio* of vapour and liquid unlike-energy contributions,

$$\frac{\left\langle \exp\left[-\beta\sum(\theta)\right]\right\rangle_{\mathrm{V}}}{\left\langle \exp\left[-\beta\sum(\theta)\right]\right\rangle_{\mathrm{L}}} = \frac{A_{\mathrm{L}}}{A_{\mathrm{V}}}, \tag{5-9}$$

where $A_{\mathrm{L}} = \rho_1^{\mathrm{L}}(0)/\rho_1^{\mathrm{L}}(\theta)$ and $A_{\mathrm{V}} = \rho_1^{\mathrm{V}}(0)/\rho_1^{\mathrm{V}}(\theta)$. Thus, a relationship between the number densities on the right hand side and the heterogeneous energy correction factors, via Equations

5-6 and 5-7, on the left hand side is obtained. One point of concern is the vapour number density of the reference component, methane. In all simulations, the liquid number density varied linearly with the liquid mole fraction; the variations are shown in Figures 5-19 and 5-20 for the two systems being discussed viz. (236.17 K, 3121 kPa) and (236.17 K, 4559 kPa). However the trend is not so apparent for the vapour number density and mole fraction of methane. Fortunately in this discourse, both the target ($\rho_1^{\mathrm{V}}(\theta)$) and the reference ($\rho_1^{\mathrm{V}}(0)$) number densities were within the linear range of the relationships shown in Figures 5-19 and 5-20.

The difference between the two sides of Equation 5-9 is plotted as a function of the heterogeneous energy correction factors for the (236.17 K, 3121 kPa) and (236.17 K, 4559 kPa) systems in Figures 5-21 and 5-22 using their respective $\varphi_{B^{\mathrm{V,L}},\,\mathrm{REF}}^{\mathrm{V,L}}$s obtained from the regressions described above. The contours labelled "0" indicate the first-approximation lines containing $(B^{\mathrm{V}},\ B^{\mathrm{L}})$ coordinates that *should* be close to the target solubilities for the respective systems.

For the 236.17 K system at 3121 kPa, three coordinates along the "zero" line were selected and used as the energy correction factors in three separate simulations. The results are tabulated in Table 5-3.

The experimental mole fractions of methane in the vapour and liquid phases at (236.17 K, 3121 kPa) are 0.1510 and 0.4201, respectively. While the solubilities obtained from the simulations are certainly far from the target solubilities (it should also be remembered that like the original method described by Vlcek *et al.* (2011), the target solubilities were not realised upon the first iteration), what is promising is that three different simulations that used different heterogeneous energy correction factors gave, within their simulation uncertainties, roughly the same compositions. Indeed, the differences between each pair of values used here (0.015, 0.0152 and 0.0153, respectively) are not equal but sufficiently close to each other to infer equality of results of all three simulations, unlike the observation discussed earlier in this chapter for 185 K, for which different pairs of correction factors having *the same* difference gave identical results. The non-constant difference is attributed to the though excellent, but slightly imperfect fitting of the contributions of the perturbations to the $\varphi_{B^{\mathrm{V,L}},\,\mathrm{REF}}^{\mathrm{V,L}}$s due to the simulation uncertainties of the potential energies. Considering that the system to which the proposed model and method has

been applied, methane/xenon, is highly sensitive to perturbations of the unlike energy parameter, and the fact that the left hand side of Equation 5-9 is also numerically sensitive due to its exponential nature, the reasons given above are valid.

Similarly, at 4559 kPa, four simulations were executed by using values along the "0" as well as the "0.2" lines, to show that the method works along different contours of Equation 5-9. The results are tabulated in Table 5-4. Note that some of the correction factors used here are out of the range of the corresponding values whose energies were used in the fitting procedure described earlier, but these out-of-range heterogeneous pairs are still in the neighbourhood of the original pairs.

Once again, it is seen that the heterogeneous pairs selected from the contour plot, this time along two different lines, are in excellent agreement with each other along the same contour. It only makes sense to compare the results obtained when using those values from the "0" line with experimental mole fractions at this pressure ($x_1 = 0.3317$ and $y_1 = 0.5778$). The simulation values are in good agreement with experiment after the first iteration, though the uncertainties of the liquid solubilities are high – this is perhaps due to the large differences between the correction factors which impart certain instabilities to the systems.

Obviously the approach described above does not give a direct (or immediate) answer for the optimum energy correction factors, since, like the model and method from which is was developed (which itself was later simplified to Equations 5-3), it requires a few more iterations that would require the determination of the $\varphi^{V,L}_{B^{V,L},\,REF}$s either through regression of data from simulations around the newly acquired 'reference' states (like in this work), or directly through a single simulation (which, as stated previously, would require considerable programming effort to isolate the unlike interactions due to each correction factor in each phase). The number density–mole fraction profiles are not expected to change since the simulation pressure and temperature are constant (see Figure 5-19 and 5-20).

What the approach *has* done is that it has formally proved the degeneracy of energy states when using heterogeneous parameters for a single NpT simulation, which was observed in Section 5.2. It has also shown that the numerical difference between each such pair is virtually the same. Thus it appears there is no unique solution to the problem of finding a pair of phase-dependent

unlike-energy parameter correction factors that minimises the error between simulation and experiment. Furthermore, the method shown above has been applied to a two-phase system that has components with high mutual solubilities (certainly, it is a simple system with only two types of intermolecular forces being present) and thus the method has provided a slightly more general framework for determining optimum energy correction factors for Lennard-Jones mixtures when compared to the study of Vlcek *et al.* (2011), which used simplifying assumptions based on the chemistry of the carbon dioxide/water mixture.

5.4 Tables and graphs

See next page.

		B	y_1		y_1 error / [%]	x_1		x_1 error / [%]	TAE / [%]
(165 K, 1200 kPa)		0.880	0.9080	0.0078	-3.586	0.2056	0.0241	-65.147	68.73353
		0.900	0.9106	0.0082	-3.318	0.2562	0.0269	-56.576	59.89465
y_1^{exp}	0.9418	0.920	0.9110	0.0059	-3.270	0.3137	0.0168	-46.833	50.10291
x_1^{exp}	0.5900	0.940	0.9211	0.0045	-2.196	0.4356	0.0268	-26.176	28.37133
		0.955	0.9282	0.0047	-1.451	0.4956	0.0211	-15.996	17.44679
		0.970	0.9333	0.0058	-0.901	0.5370	0.0210	-8.976	9.87614
		0.985	0.9394	0.0048	-0.261	0.5659	0.0136	-4.080	4.34153
		1.000	0.9440	0.0025	*0.229*	0.5808	0.0072	-1.559	1.78840
		1.015	0.9458	0.0021	0.422	0.5851	0.0061	-0.829	1.25064
		1.030	0.9489	0.0026	0.749	0.5903	0.0020	*0.047*	0.79596
		1.036	0.9502	0.0038	0.892	0.5906	0.0029	0.102	0.99414
(172.5 K, 1500 kPa)		0.900	0.8891	0.0096	3.761	0.2757	0.0336	50.771	54.53227
		0.950	0.9088	0.0092	1.633	0.4771	0.0192	14.801	16.43375
y_1^{exp}	0.9239	0.955	0.9105	0.0042	1.443	0.4813	0.0170	14.061	15.50388
x_1^{exp}	0.5600	0.970	0.9169	0.0035	0.756	0.5162	0.0164	7.830	8.58580
		0.980	0.9215	0.0087	0.257	0.5449	0.0273	2.701	2.95737
		0.985	0.9228	0.0041	0.108	0.5516	0.0143	*1.493*	1.60104
		0.990	0.9244	0.0090	*-0.064*	0.5488	0.0188	1.999	2.06264
		1.000	0.9282	0.0051	-0.469	0.5687	0.0128	-1.545	2.01342
		1.015	0.9318	0.0028	-0.862	0.5781	0.0082	-3.225	4.08742
		1.030	0.9368	0.0026	-1.398	0.5859	0.0035	-4.620	6.01814
(180 K, 1750 kPa)		0.955	0.8797	0.0074	1.720	0.4260	0.0181	14.802	16.52181
		0.970	0.8866	0.0059	0.943	0.4559	0.0169	8.818	9.76087
y_1^{exp}	0.8951	0.980	0.8918	0.0094	0.367	0.4740	0.0198	5.202	5.56840
x_1^{exp}	0.5000	0.985	0.8971	0.0047	*-0.225*	0.5009	0.0179	*-0.173*	0.39853
		0.990	0.8984	0.0098	-0.369	0.5100	0.0271	-1.991	2.36031
		1.000	0.9042	0.0047	-1.019	0.5275	0.0163	-5.498	6.51716
		1.010	0.9096	0.0024	-1.619	0.5480	0.0072	-9.601	11.21935
		1.020	0.9141	0.0048	-2.118	0.5590	0.0145	-11.804	13.92226
		1.030	0.9175	0.0026	-2.507	0.5676	0.0099	-13.515	16.02165
		1.040	0.9198	0.0094	-2.758	0.5702	0.0193	-14.041	16.79933
		1.050	0.9223	0.0087	-3.045	0.5793	0.0108	-15.865	18.91001
		1.075	0.9291	0.0040	-3.804	0.5886	0.0041	-17.713	21.51750
		1.100	0.9349	0.0041	-4.447	0.5918	0.0023	-18.363	22.81027
(185 K, 2000 kPa)		0.955	0.8639	0.0091	1.778	0.4236	0.0189	13.553	15.33041
		0.970	0.8734	0.0080	*0.700*	0.4581	0.0222	6.505	7.20449
y_1^{exp}	0.8796	0.985	0.8810	0.0061	-0.162	0.4881	0.0178	*0.383*	0.54517
x_1^{exp}	0.4900	1.000	0.8899	0.0058	-1.170	0.5228	0.0139	-6.687	7.85663
		1.010	0.8953	0.0062	-1.782	0.5379	0.0149	-9.771	11.55238
		1.020	0.9000	0.0055	-2.324	0.5495	0.0141	-12.145	14.46911
		1.030	0.9080	0.0050	-3.230	0.5713	0.0124	-16.602	19.83169

Table 5-1 – Numerical results from the initial homogeneous *B* simulations of methane/xenon at various temperatures and pressures. *B* is the Lennard-Jones unlike-energy multiplying factor, y_1 and x_1 are the vapour and liquid mole fractions of methane, respectively (with simulation uncertainties listed in the corresponding columns to the right of the mole fractions), y_1 error and x_1 error are the percent relative errors between simulation and experiment and TAE is the total absolute error.

	B	y_1		y_1 error / [%]	x_1		x_1 error / [%]	TAE / [%]
(189.78 K, 2073 kPa)	0.955	0.8341	0.0073	*0.080*	0.3642	0.0162	24.001	24.08132
	0.970	0.8435	0.0059	-1.043	0.3997	0.0164	16.600	17.64250
y_1^{exp} 0.8348	0.985	0.8500	0.0065	-1.820	0.4290	0.0175	10.481	12.30096
x_1^{exp} 0.4792	0.990	0.8580	0.0102	-2.774	0.4459	0.0203	6.957	9.73099
	1.000	0.8606	0.0054	-3.090	0.4646	0.0148	3.042	6.13259
	1.010	0.8629	0.0068	-3.364	0.4726	0.0147	*1.379*	4.74347
	1.020	0.8699	0.0060	-4.208	0.4899	0.0148	-2.238	6.44566
	1.030	0.8767	0.0060	-5.022	0.5099	0.0147	-6.396	11.41811
	1.040	0.8840	0.0077	-5.894	0.5207	0.0163	-8.655	14.54962
(208.29 K, 2411 kPa)	0.900	0.7191	0.0080	4.095	0.2071	0.0169	-27.879	31.97384
	0.910	0.7166	0.0072	3.741	0.2210	0.0153	-23.023	26.76336
y_1^{exp} 0.6908	0.920	0.7127	0.0071	3.168	0.2315	0.0136	-19.349	22.51733
x_1^{exp} 0.2871	0.930	0.7124	0.0088	3.131	0.2417	0.0129	-15.805	18.93552
	0.940	0.7126	0.0069	3.156	0.2498	0.0136	-12.991	16.14669
	0.950	0.7123	0.0099	3.115	0.2551	0.0139	-11.151	14.26671
	0.960	0.7088	0.0064	*2.609*	0.2649	0.0163	-7.722	10.33137
	0.970	0.7141	0.0098	3.379	0.2707	0.0151	-5.729	9.10815
	0.990	0.7124	0.0093	3.129	0.2948	0.0146	*2.683*	5.81209
(236.17 K, 4559 kPa)	0.955	0.5759	0.0068	*0.329*	0.2710	0.0081	18.295	18.62383
	0.970	0.5903	0.0082	-2.161	0.2969	0.0093	10.494	12.65546
y_1^{exp} 0.5778	0.985	0.5977	0.0085	-3.447	0.3140	0.0098	5.334	8.78082
x_1^{exp} 0.3317	1.000	0.6120	0.0086	-5.922	0.3392	0.0085	*-2.250*	8.17199
	1.010	0.6201	0.0070	-7.315	0.3512	0.0100	-5.893	13.20814
	1.020	0.6269	0.0081	-8.500	0.3632	0.0094	-9.494	17.99378
	1.030	0.6375	0.0111	-10.340	0.3799	0.0128	-14.546	24.88593
(260.62 K, 5105 kPa)	0.880	0.2966	0.0147	5.018	0.0956	0.0072	43.050	48.06821
	0.900	0.3019	0.0156	3.334	0.1064	0.0082	36.605	39.93924
y_1^{exp}	0.915	0.3083	0.0162	1.274	0.1164	0.0092	30.612	31.88602
x_1^{exp}	0.925	0.3084	0.0159	1.255	0.1205	0.0090	28.185	29.43992
	0.935	0.3108	0.0173	*0.475*	0.1252	0.0100	25.389	25.86383
	0.945	0.3221	0.0107	-3.132	0.1355	0.0072	19.266	22.39821
	0.955	0.3209	0.0132	-2.764	0.1394	0.0080	16.905	19.66936
	0.985	0.3314	0.0205	-6.130	0.1599	0.0099	4.714	10.84338
	0.990	0.3362	0.0177	-7.643	0.1621	0.0073	*3.402*	11.04523

Table 5-1 – (continued) Numerical results from the initial homogeneous *B* simulations at various temperatures and pressures. *B* is the Lennard-Jones unlike-energy multiplying factor, y_1 and x_1 are the simulated vapour and liquid mole fractions of methane, respectively (with simulation uncertainties listed in the corresponding columns to the right of the mole fractions), y_1 error and x_1 error are the percent relative errors between simulation and experiment and TAE is the total absolute error.

T / [K]	p / [kPa]	B	y_1		x_1		B^{opt}	y_1^{exp}	x_1^{exp}
150	130.235	1	0.6942	0.0059	0.0731	0.0029	0.9864	0.6990	0.0600
	348.2978	1	0.9049	0.0028	0.2673	0.0094	0.9879	0.8990	0.2400
	702.351	1	0.9679	0.0022	0.6257	0.0142	1.0077	0.9668	0.6400
	900.9612	1	0.9870	0.0015	0.8439	0.0195	1.0041	0.9872	0.8700
165	320.7	1	0.6865	0.0092	0.1090	0.0036	0.9847	0.6918	0.0900
	701.5	1	0.8720	0.0123	0.2942	0.0212	0.9873	0.8711	0.2800
	1200	1	0.9436	0.0022	0.5798	0.0043	0.9961	0.9415	0.5881
	1600	1	0.9753	0.0015	0.8192	0.0123	1.0625	0.9253	0.8363
180	790	1	0.7331	0.0080	0.1828	0.0056	0.9794	0.7301	0.1618
	1001.8	1	0.7962	0.0022	0.2519	0.0045	0.9845	0.7914	0.2300
	1750	1	0.9048	0.0026	0.5335	0.0057	0.9946	0.8955	0.5017
	2500	1	0.9548	0.0030	0.7824	0.0161	0.9920	0.9492	0.7819
189.78	693	1	0.4991	0.0089	0.0846	0.0038	0.9990	0.4877	0.0880
	1128	1	0.7095	0.0110	0.2034	0.0060	0.9981	0.6913	0.1994
	1592	1	0.8005	0.0051	0.3248	0.0113	1.0002	0.7850	0.3239
	2632	1	0.9036	0.0038	0.6196	0.0140	0.9976	0.8800	0.6186
	3231	1	0.9381	0.0014	0.7726	0.0066	0.9866	0.9214	0.7645
	3743	1	0.9630	0.0015	0.8831	0.0066	0.9437	0.9470	0.8822
223.81	1726	1	0.3050	0.0136	0.0725	0.0050	0.9890	0.2961	0.0670
	2345	1	0.4834	0.0116	0.1636	0.0062	0.9915	0.4713	0.1477
	2961	1	0.6001	0.0067	0.2472	0.0047	0.9995	0.5716	0.2444
	3656	1	0.6710	0.0070	0.3393	0.0088	0.9869	0.6508	0.3264
	4330	1	0.7277	0.0027	0.4400	0.0046	0.9939	0.6887	0.4353
	5017	1	0.7642	0.0026	0.5345	0.0066	0.9958	0.7281	0.5308
	5516	1	0.6067	0.0084	0.7861	0.0039	0.9808	0.7376	0.5948
248.15	3109	1	0.2413	0.0034	0.0807	0.0011	0.9800	0.2226	0.0706
	4020	1	0.4037	0.0053	0.1737	0.0033	0.9798	0.3733	0.1591
	4895	1	0.4944	0.0055	0.2621	0.0044	0.9880	0.4563	0.2545
	5482	1	0.5394	0.0130	0.3235	0.0142	0.9814	0.4947	0.3086
	5976	1	0.5222	0.0812	0.4183	0.0783	0.9908	5145.0000	0.3600

Table 5-2 – Numerical results from further simulations of methane/xenon at six different temperatures and several pressures to determine the optimum B at each state point. T is temperature, p is pressure, B is the Berthelot Lennard-Jones unlike-energy multiplying factor, y_1 and x_1 are the simulated vapour and liquid mole fractions of methane, respectively (with simulation uncertainties listed in the corresponding columns to the right of the mole fractions), B^{opt} is the optimum B corresponding to the simulated state point and y_1^{exp} and x_1^{exp} are the experimental vapour and liquid mole fractions, respectively.

Case No.	B^V	B^L	y_1	x_1
1	0.99	1.005	0.1122 (0.0041)	0.3511 (0.0036)
2	0.992	1.0072	0.1133 (0.0034)	0.3540 (0.0064)
3	0.994	1.0093	0.1147 (0.0029)	0.3544 (0.0071)

Table 5-3 – Results of three independent simulations using values obtained from the proposed unlike-energy model for methane/xenon at (236 K, 3121 kPa). Uncertainties of the simulation outputs are shown in parentheses.

Case No.	B^V	B^L	y_1	x_1
1 – line "0"	1.00432	0.994	0.5587 (0.0087)	0.3046 (0.0319)
2 – line "0"	1.00540	0.9952	0.5578 (0.0112)	0.3088 (0.0379)
3 – line "0.2"	0.9752	0.977	0.6155 (0.0077)	0.3327 (0.0082)
4 – line "0.2"	0.9829	0.985	0.6266 (0.0049)	0.3447 (0.0042)

Table 5-4 – Results of three independent simulations using values obtained from the proposed unlike-energy model for methane/xenon at (236 K, 4559 kPa). Uncertainties of the simulation outputs are shown in parentheses.

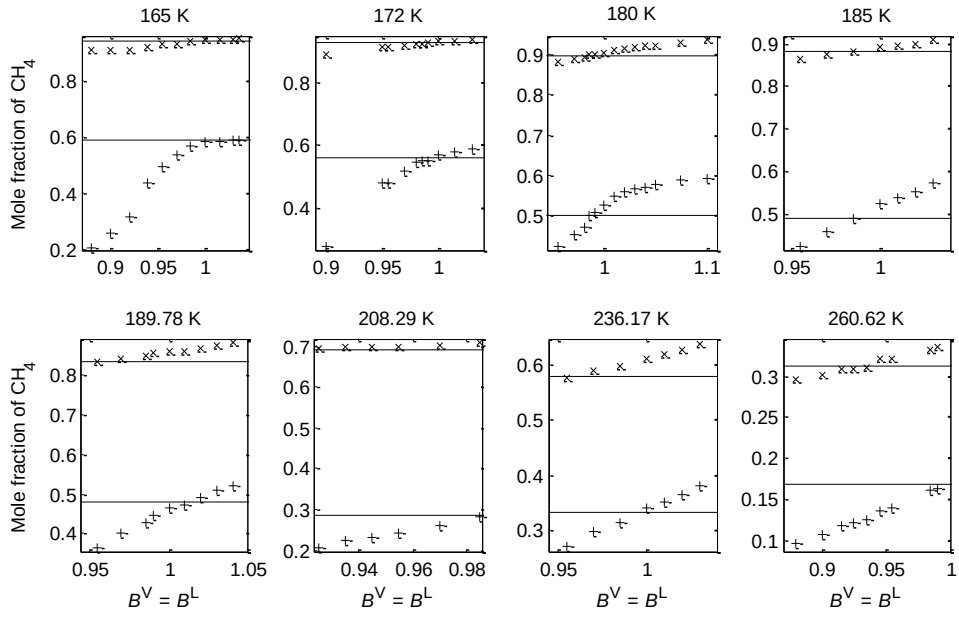

Figure 5–1 – Composition profiles of methane in the vapour (x) and liquid (+) phases for homogeneous correction factor ($B^V = B^L$) simulations. The solid lines of constant composition represent the experimental (target) solubilities.

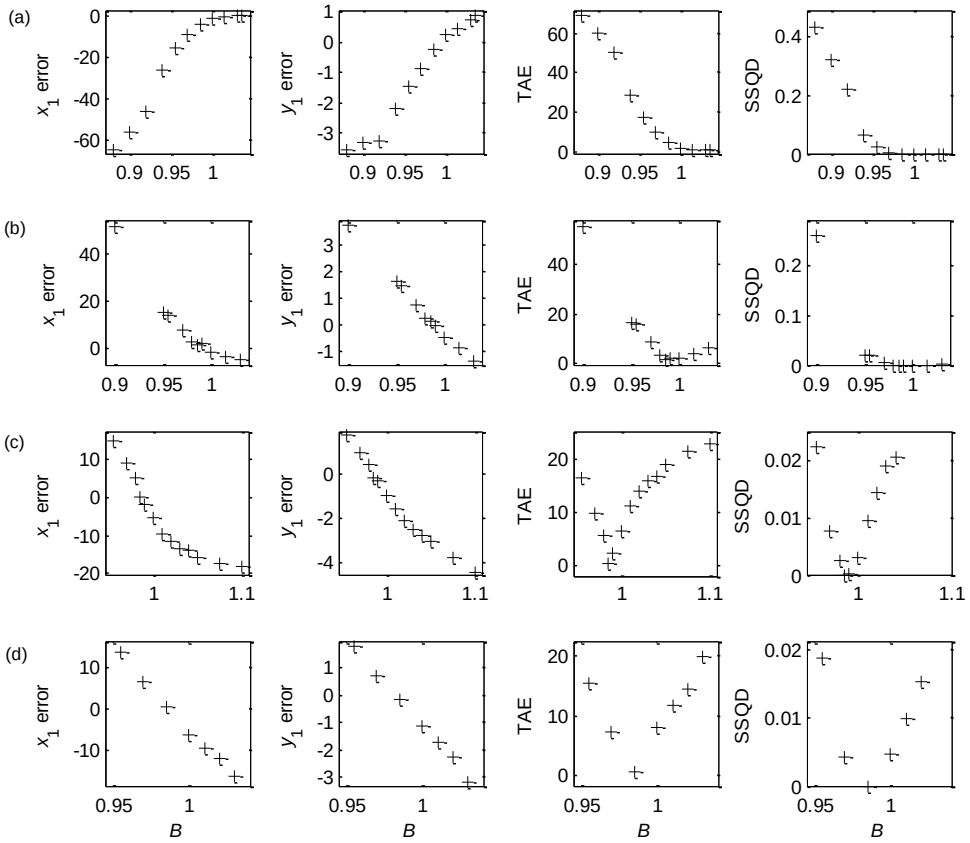

Figure 5–2 – Liquid-phase (x_1), vapour-phase (y_1), total absolute error (*TAE*) and sum of squared deviations (*SSQD*) error plots with respect to methane composition for homogeneous correction factor simulations at (a) 165 K, (b) 172.5 K, (c) 180 K and (d) 185 K.

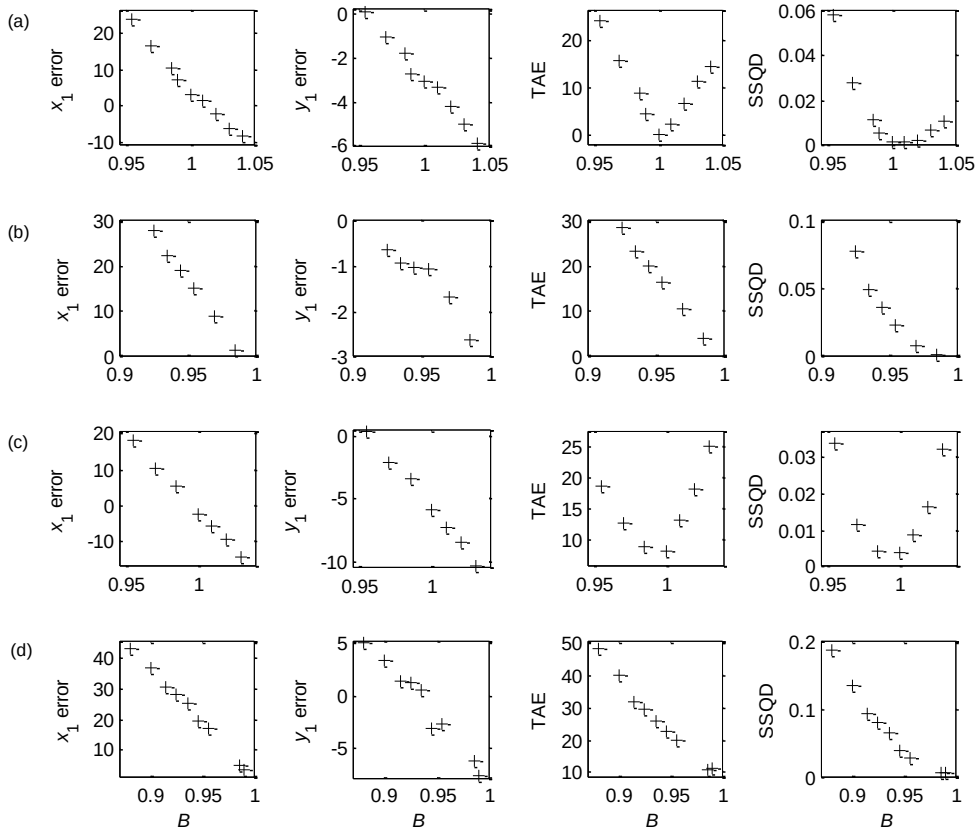

Figure 5–3 - Liquid-phase (x_1), vapour-phase (y_1), total absolute error (*TAE*) and sum of squared deviations (*SSQD*) error plots with respect to methane composition for homogeneous correction factor simulations at (*a*) 189.78 K, (*b*) 208.23 K, (*c*) 236.17 K and (*d*) 260.62 K.

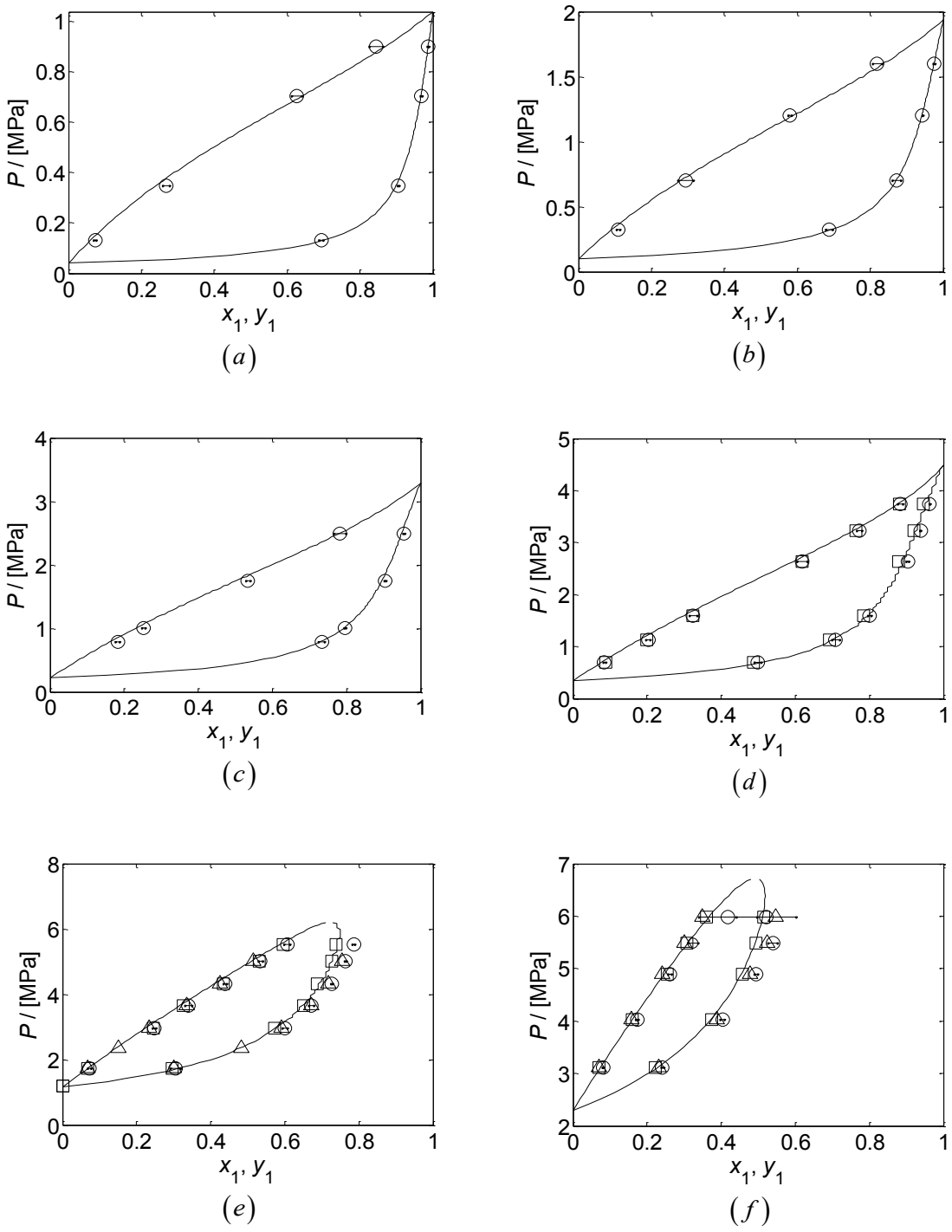

Figure 5–4 - Phase diagrams of the vapour-liquid equilibrium system methane (1)/xenon (2) at (*a*) 150 K, (*b*) 165 K, (*c*) 180 K, (*d*) 189.78 K, (*e*) 223.81 K and (*f*) 248.15 K. Circles represent simulation data using the unmodified Berthelot rule and continuous solid lines are Peng-Robinson predictions based on experimental data (Dias *et al.*, 2004), shown as squares. Triangles in (*e*) and (*f*) represent simulation data using the corresponding temperature-specific optimum (*B*).

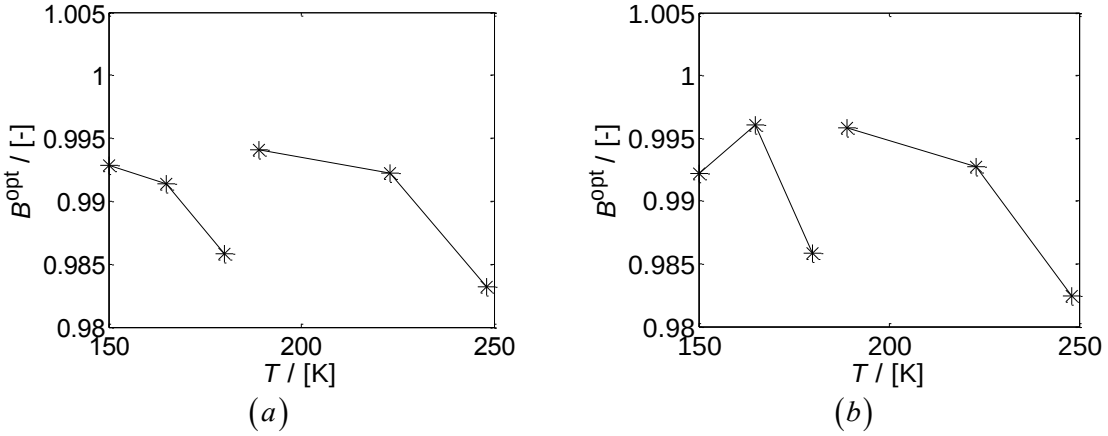

Figure 5–5 - Temperature dependence of optimum homogeneous energy parameter using (*a*) weighted relative volatility and (*b*) weight phase envelope width.

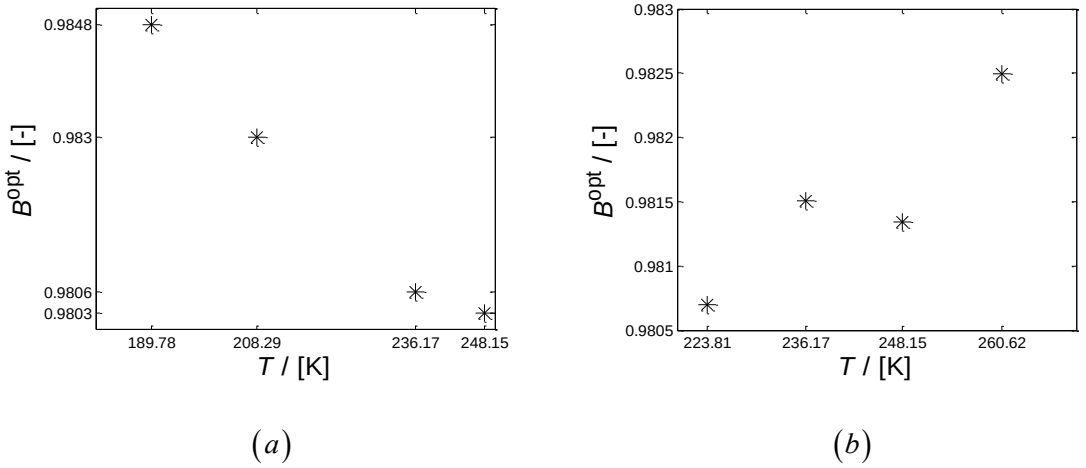

Figure 5–6 - Temperature dependence of optimum homogeneous energy parameter at (*a*) 3000 kPa and (*b*) 5000 kPa.

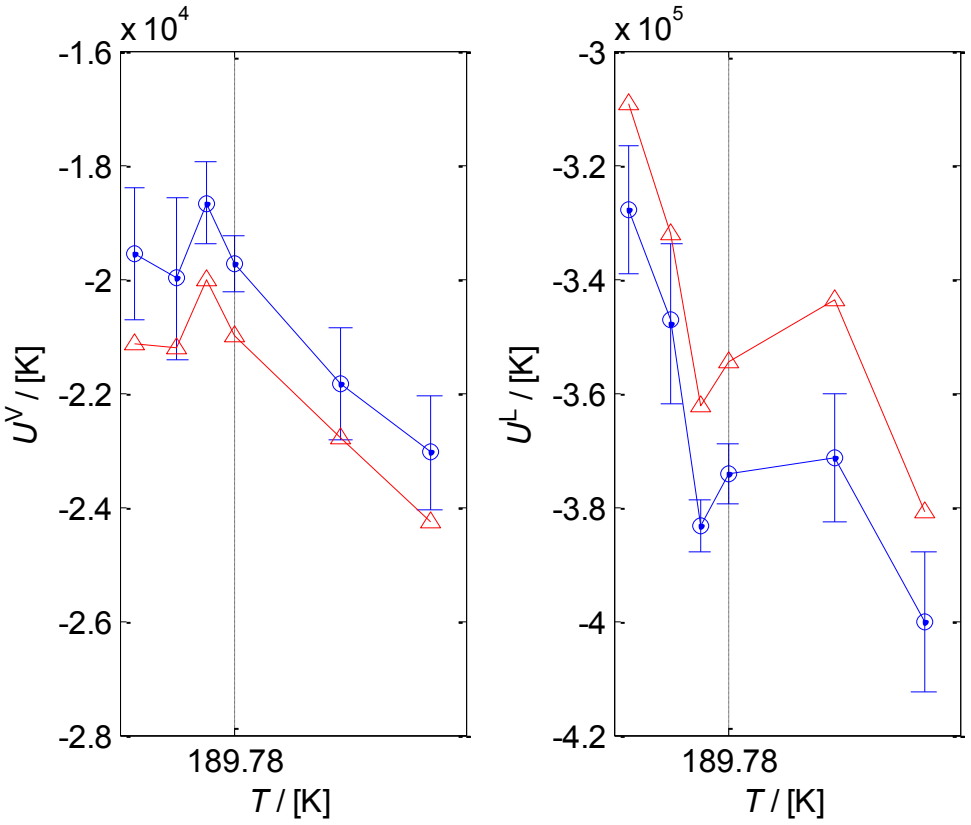

Figure 5–7 - Variation of vapour- and liquid-phase potential energies with temperature at 1800 kPa, using the standard Berthelot energy parameter (circles) and optimum energy parameters (triangles) for each temperature. The dashed lines of constant temperature indicate the location of the discontinuity of the liquid potential energy.

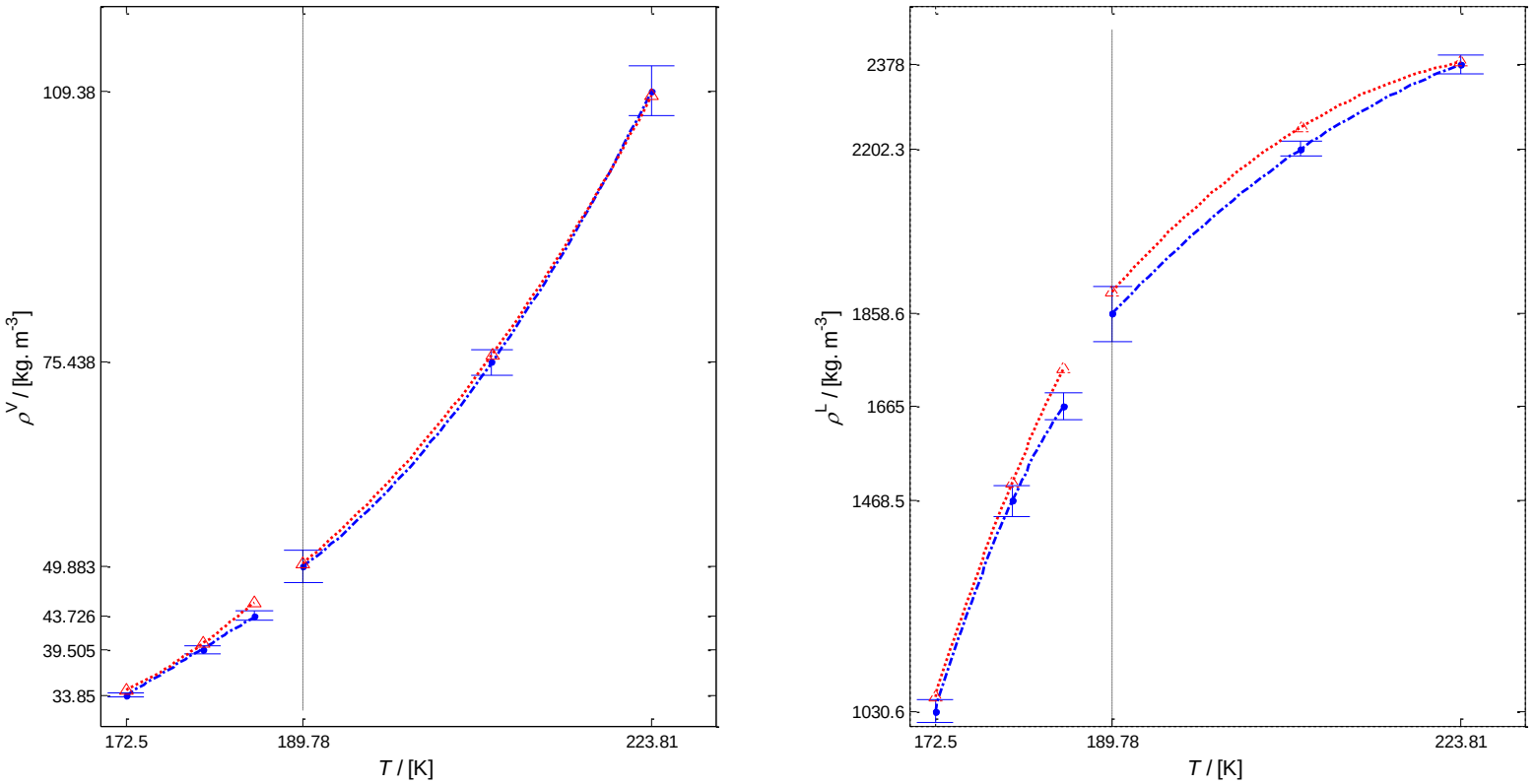

Figure 5–8 - Temperature-dependence of vapour- and liquid-phase densities on both sides of the critical temperature of methane at 1800 kPa, using the standard Berthelot energy parameter (blue dots with error bars) and optimum energy parameters (triangles) for each temperature. The dashed lines of constant temperature indicate the discontinuity. The smooth curves running through the data are added for emphasis and are not based on any theoretical models.

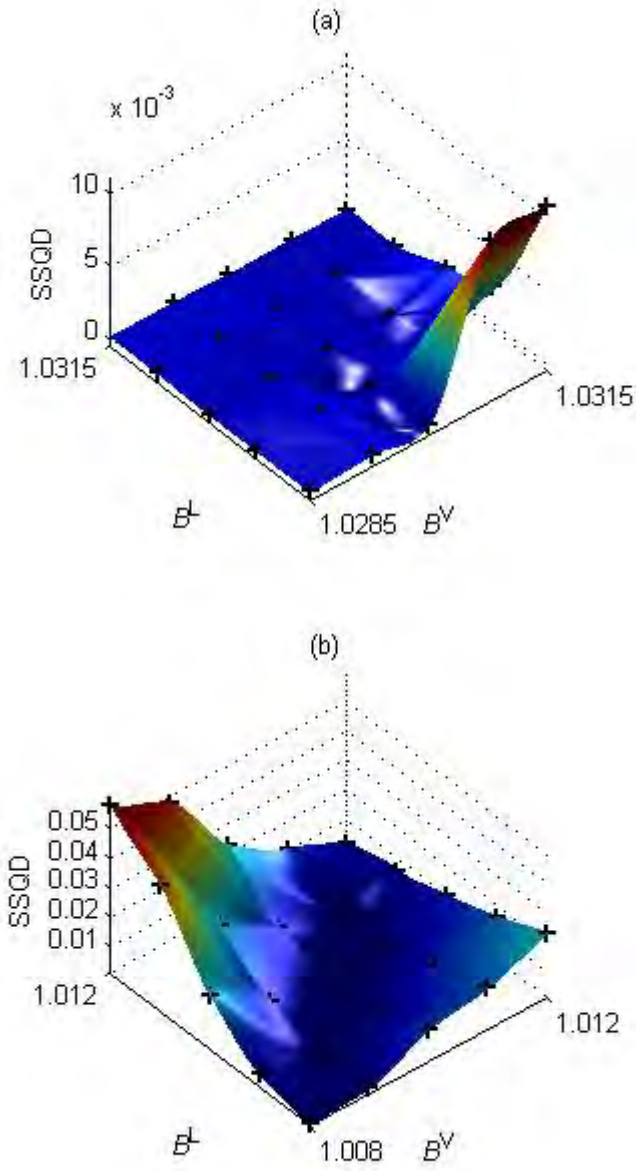

Figure 5–9 - Error surfaces with respect to composition using a sum of squared deviations (SSQD) representation for heterogeneous correction factors ($B^V \neq B^L$) at (*a*) 165 K and (*b*) 189.78 K. Simulation data are shown as black (+) symbols, while the surfaces were generated using cubic spline interpolation.

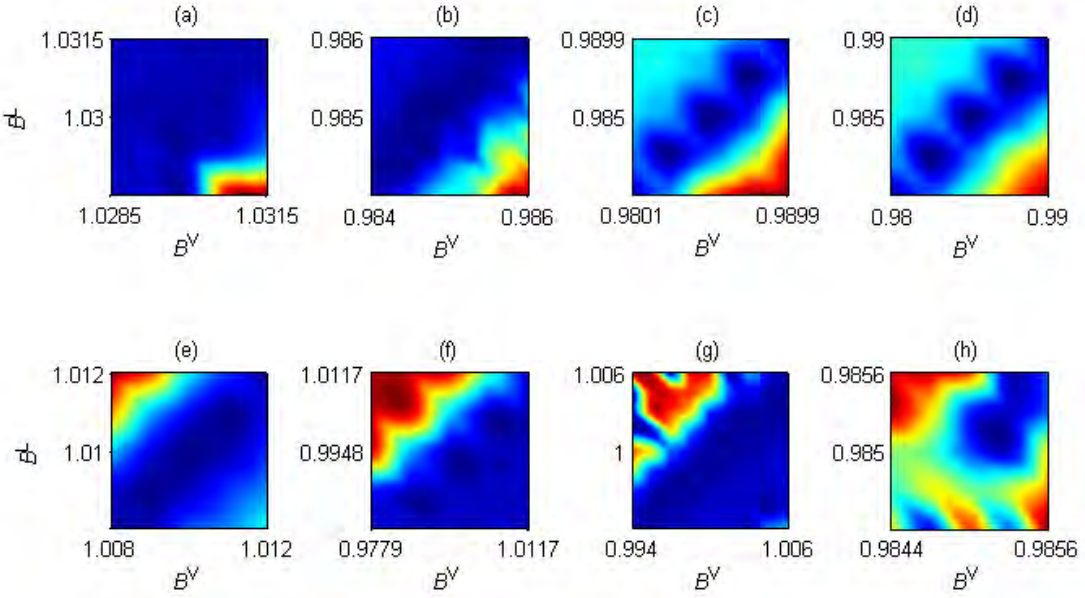

Figure 5–10 - Error surfaces on the B^V-B^L plane with respect to composition using a sum of squared deviations representation for heterogeneous correction factors (B^V-B^L) at (*a*) 165 K, (*b*) 172.5 K, (*c*) 180 K, (*d*) 185 K, (*e*) 189.78 K, (*f*) 208.23 K, (*g*) 236.17 K and (*h*) 260.62 K. The surfaces were generated from simulation data using cubic spline interpolation. Dark blue regions correspond to small errors, while large errors are shown in red.

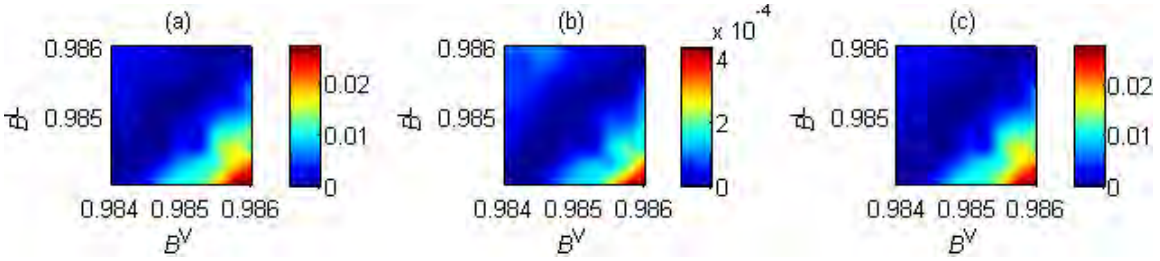

Figure 5–11 - Comparison of the (*a*) liquid-phase and (*b*) vapour-phase composition errors (using a sum of squared deviations representation), and their contributions to the (*c*) total error at (1500 kPa, 172.5 K).

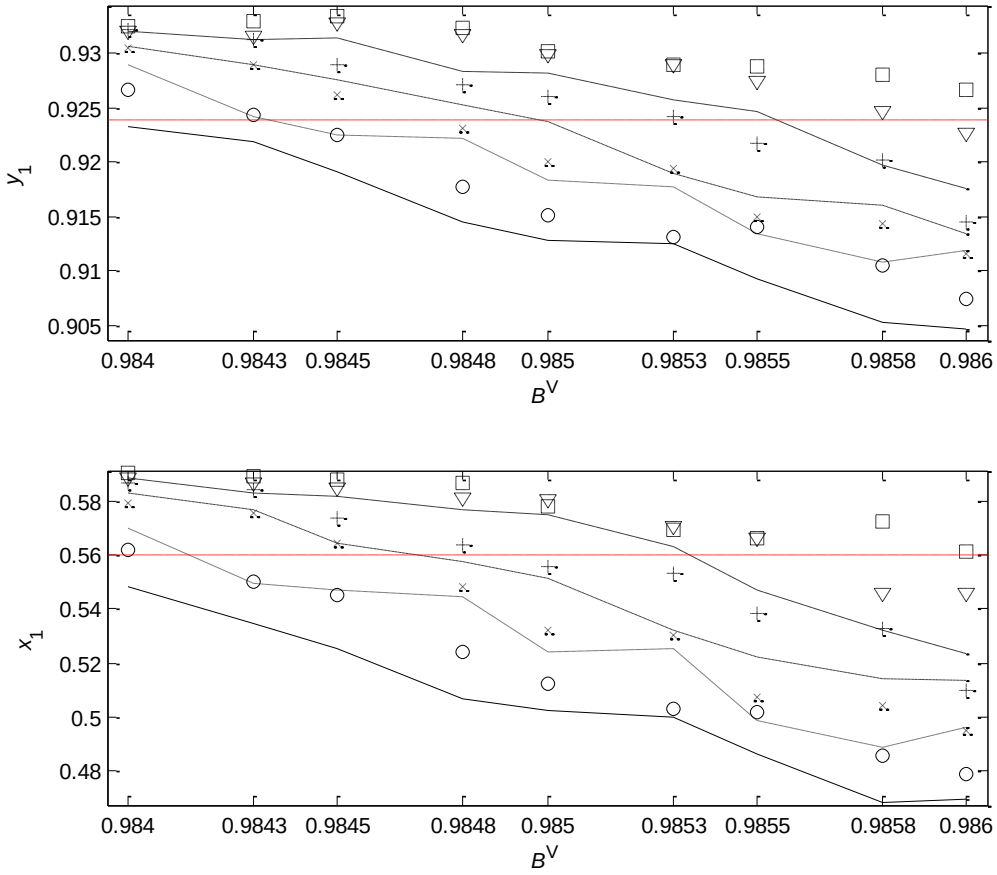

Figure 5–12 - Variation of methane solubility at 172.5 K in the vapor and liquid phases with vapour-phase correction factor B^V at various constant liquid-phase correction factors (B^L): 0.9840 (solid line); 0.9843 (○); 0.9845 (− − −); 0.9848 (×); 0.9850 (— − — −); 0.9853 (+); 9855 (— — —); (0.9858) ▽; 0.9860 (□).The solid lines of constant composition refer to the experimental values.

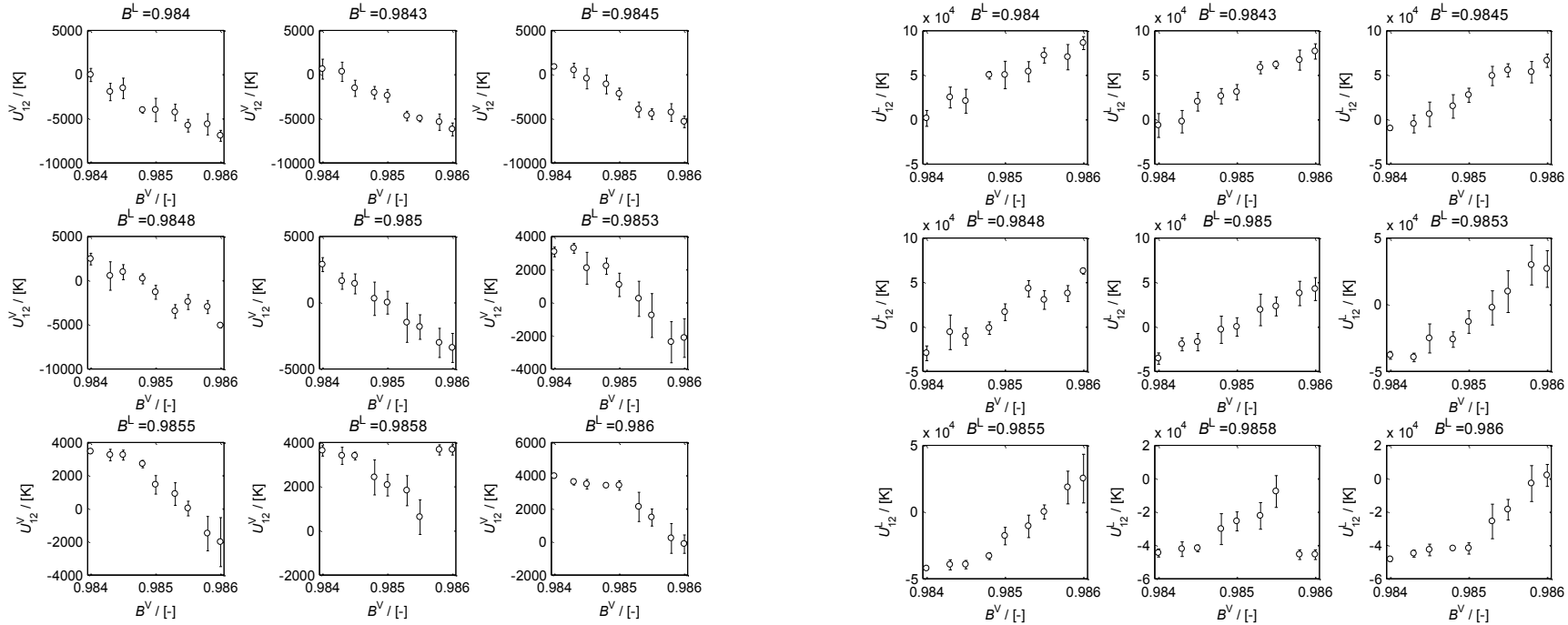

Figure 5–13 - Comparisons of the "excess" vapour and liquid potential energies using $B^V = B^L = 0.985$ as the reference system at (172.5 K, 1500 kPa).

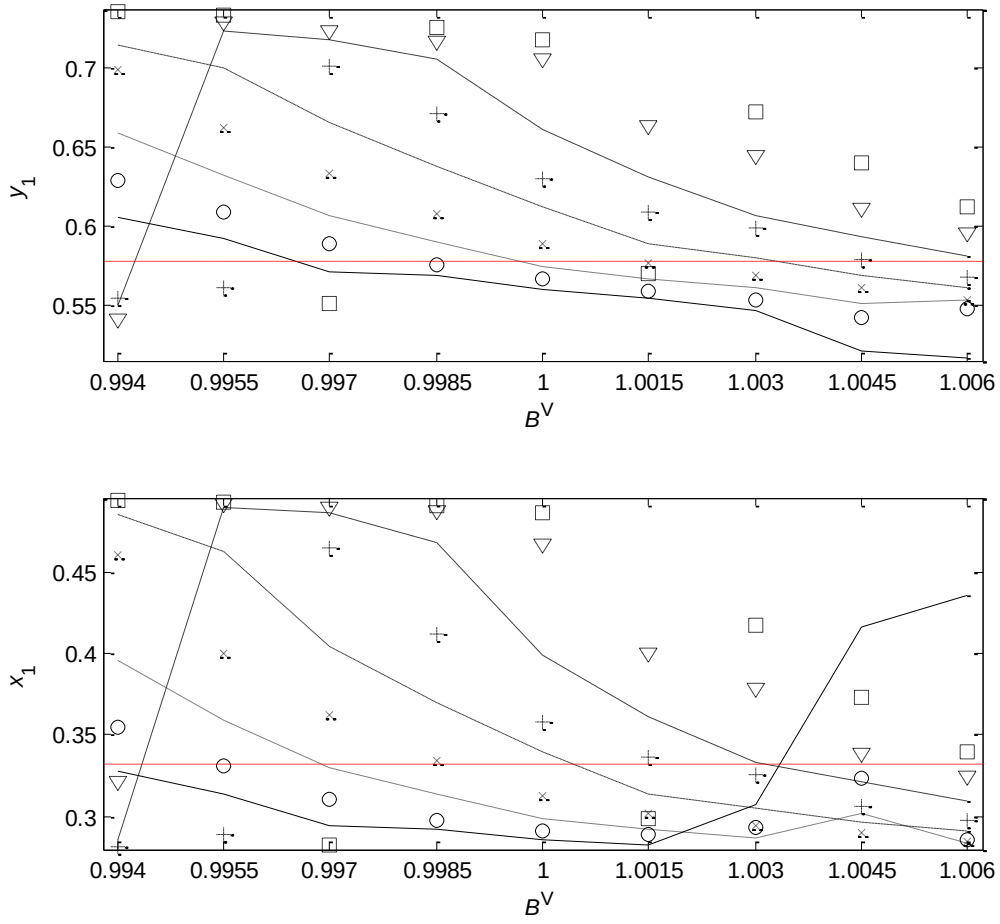

Figure 5–14 - Variation of methane solubility at 236.17 K in the vapor and liquid phases with vapour-phase correction factor (B^V) at various constant liquid-phase correction factors (B^L): 0.9940 (solid line); 0.9955 (○); 0.9970 (– – –); 0.9985 (×); 1.000 (— – — –); 1.0015 (+); 1.003 (— — —); (1.0045) ▽; 1.006 (□). The solid lines of constant composition refer to the experimental values.

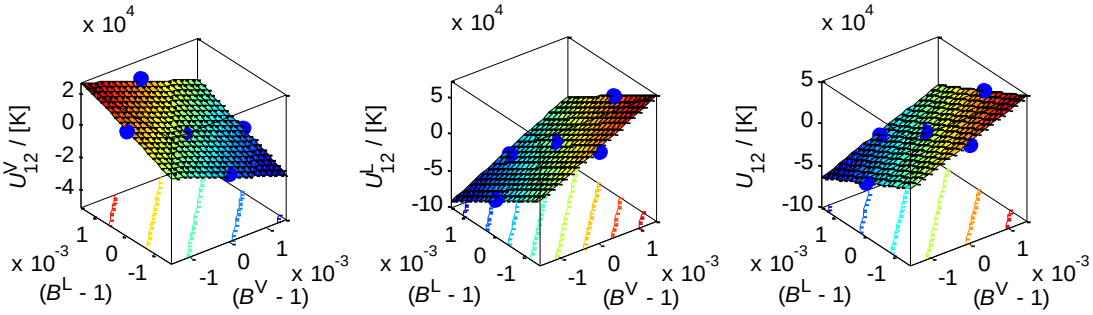

Figure 5–15 - Comparison between the energies at (236 K, 4559 kPa) in the vapour, liquid and overall system (vapour + liquid) due to heterogeneous perturbations from simulations (blue dots) with the surface predicted by the model proposed in this work.

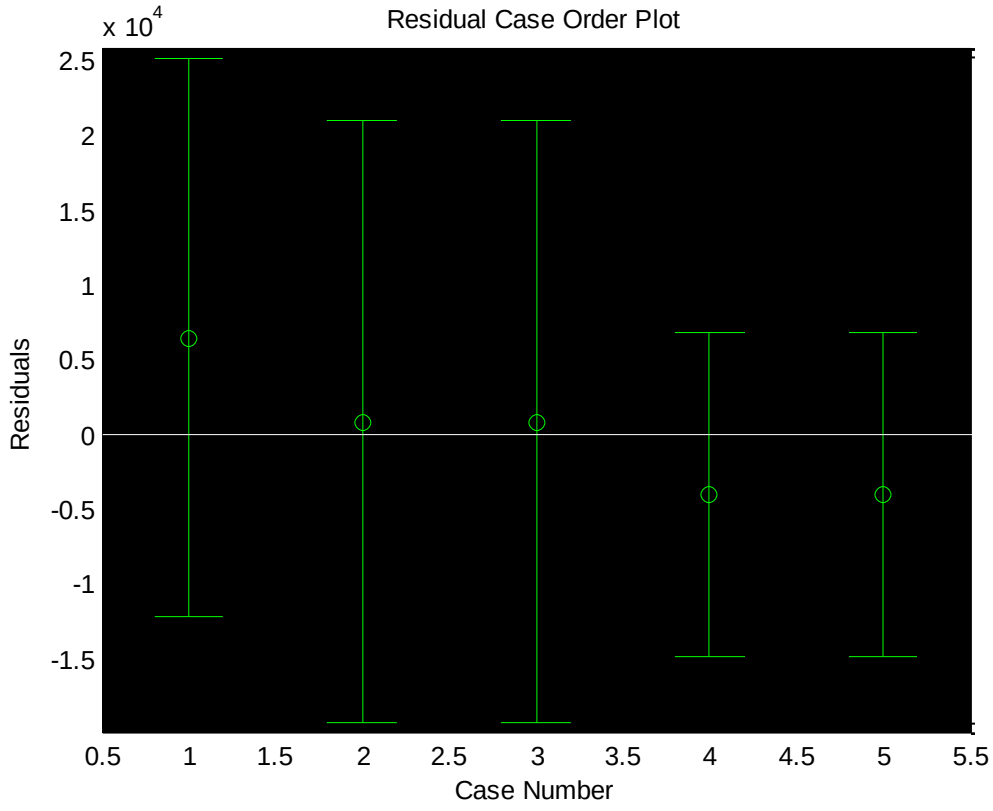

Figure 5–16 - Residual plot for the total system energy at (236 K, 4559 kPa) using a 95% confidence interval.

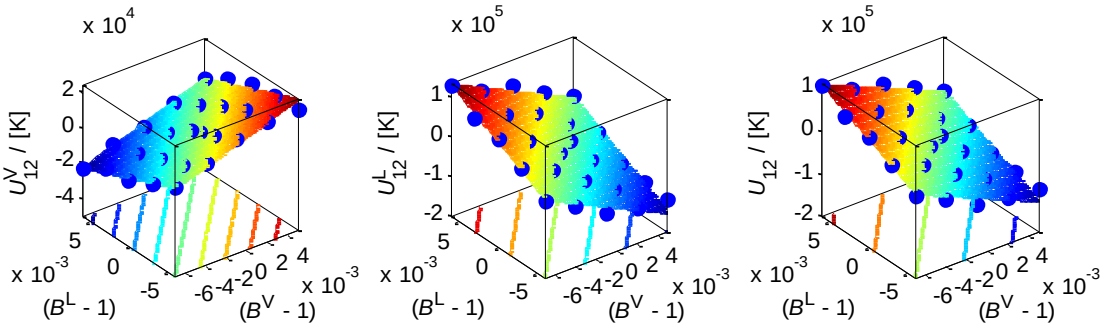

Figure 5–17 - Comparison between the energies at (236 K, 3121 kPa) in the vapour, liquid and overall system (vapour + liquid) due to heterogeneous perturbations from simulations (blue dots) with the surface predicted by the model proposed in this work.

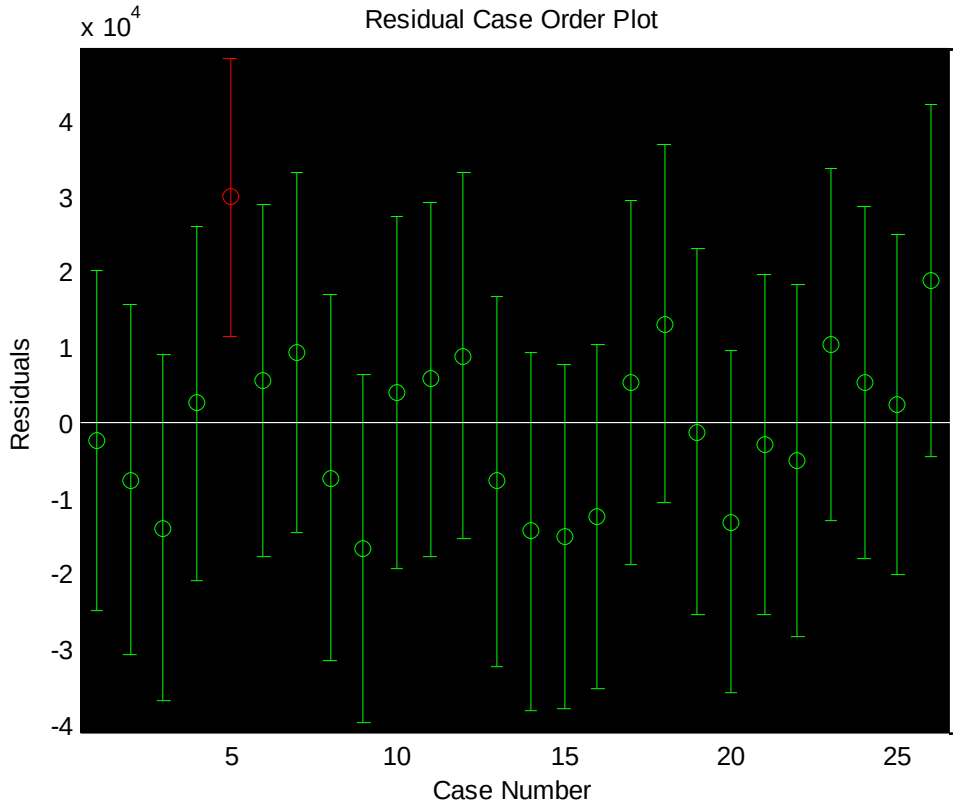

Figure 5–18 - Residual plot for the total system energy at (236 K, 4559 kPa) using a 95% confidence interval.

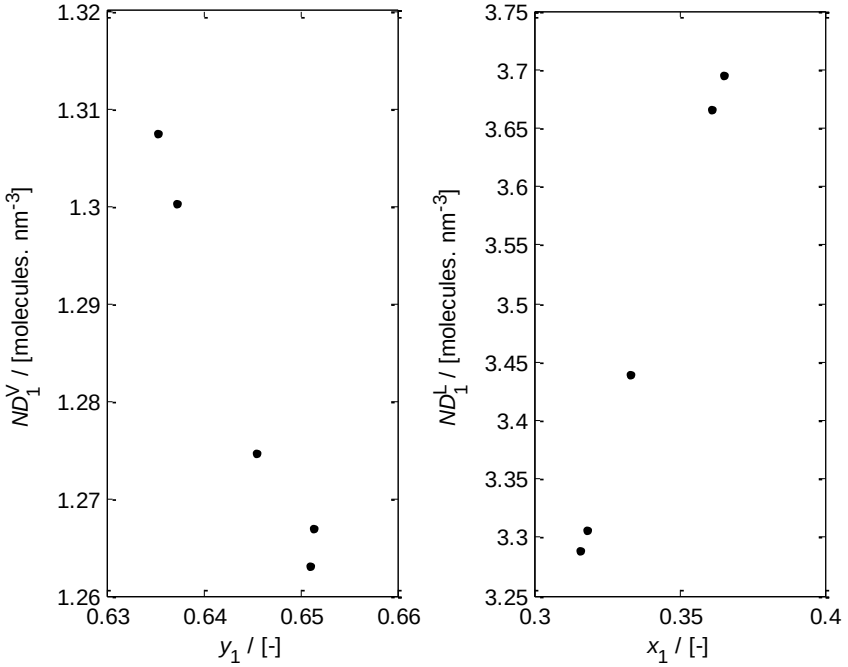

Figure 5–19 - Solubility-number density relationships in the vapour and liquid phase at (236.17 K, 4559 kPa)

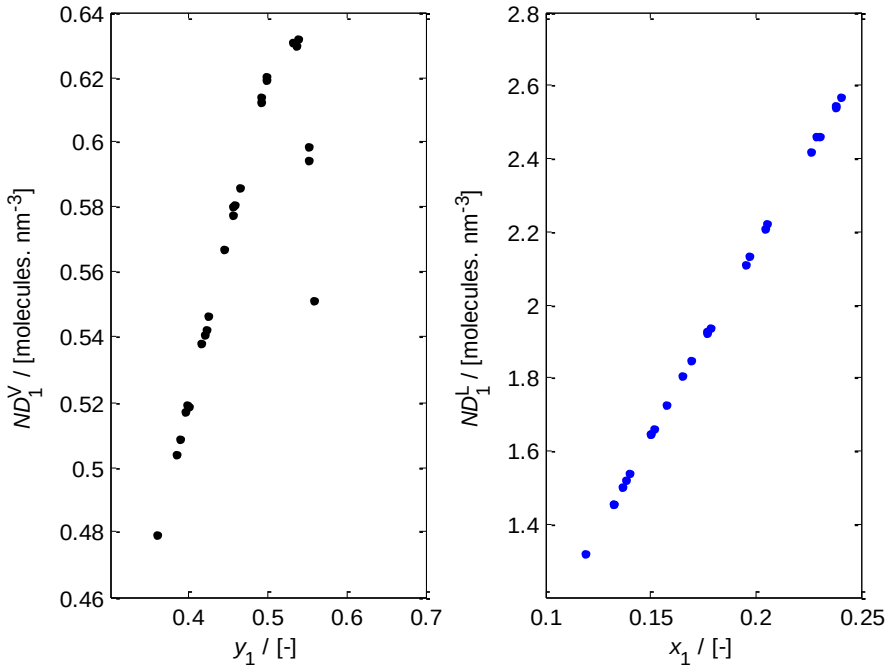

Figure 5–20 - Solubility-number density relationships in the vapour and liquid phase at (236.17 K, 3121 kPa)

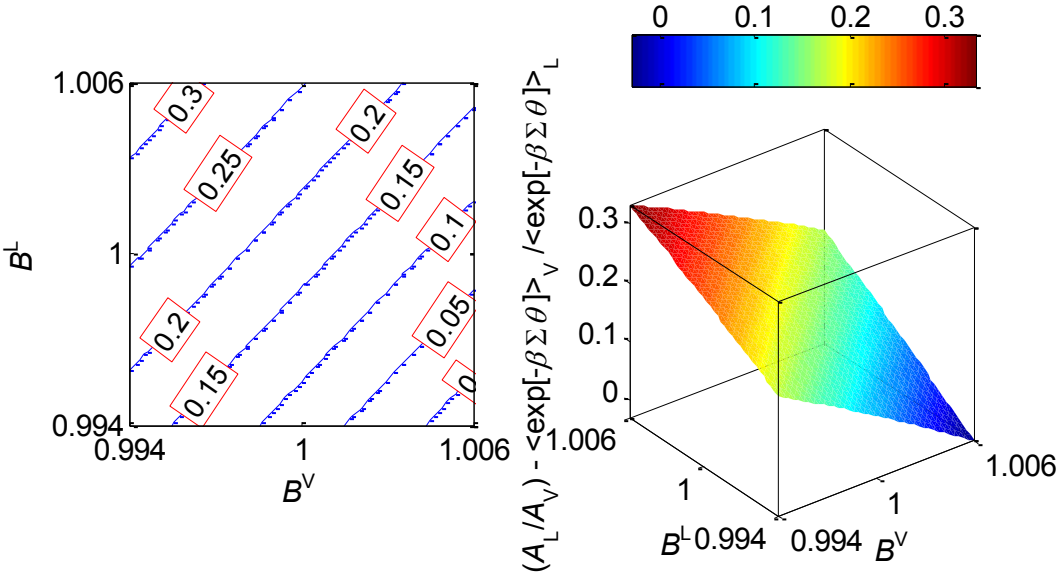

Figure 5–21 - Contour and surface plots depicting the difference between the ratio of number densities and phase energy ratio defined by Vlcek *et al*. (2011) and modified in this work for the methane/xenon system at (236.17 K, 4559 kPa).

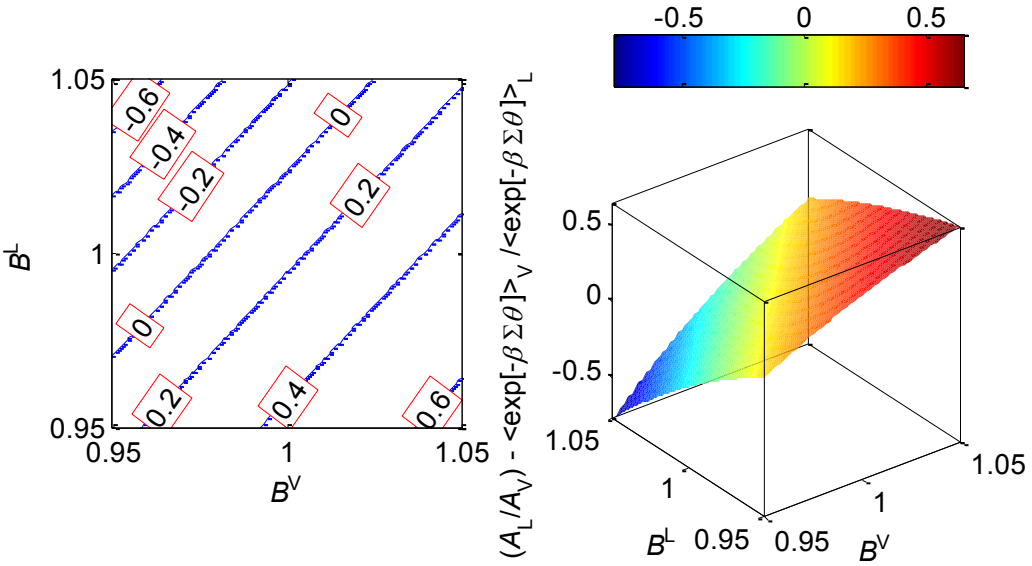

Figure 5–22 - Contour and surface plots depicting the difference between the ratio of number densities and phase energy ratio defined by Vlcek *et al*. (2011) and modified in this work for the methane/xenon system at (236.17 K, 3121 kPa).

6. CONCLUSIONS

This work has proved to be a good step for addressing the inadequacies of conventional mixing rules in molecular simulations. The reason for this is two-fold. Firstly, the introduction of an additional parameter to any parametric model (if one considers a mixing rule to be a model) that attempts to reproduce experimental data ("reality") usually decreases the relative error between the model system and reality. Secondly, in the present case by modelling the interactions between unlike molecules, which in this case are completely described by the Lennard-Jones potential, in each phase uniquely, a more solid physical foundation is naturally implied because the effective range of the intermolecular interactions that are expected in a liquid and a vapour are better-represented (e.g. the short-range order that characterises a liquid phase is dependent on the configurational energy of the phase). In other words, the multiplying factors that adjust the LJ unlike-energy parameter (ε_{12}) in this work scaled the overall potential energy, especially the contribution of the $(\sigma/r)^6$ term that makes the predominant contribution to the attractive dispersion interaction energy of neutral systems (Kaplan, 2006) in each phase uniquely, as opposed to using a single value for the same parameter in both phases. The necessity of the heterogeneous scaling can also be ascribed to the 'effective' contribution of the three-body (and higher terms) in each phase. For example, three-body dispersion interactions weaken the pair dispersion interactions in methane by approximately 20% (Kaplan, 2006). It was shown in Chapter 5 that a single-valued scaling (homogeneous correction factor) for the system methane/xenon (vapour and liquid phases) is inadequate for simultaneous satisfactory prediction of vapour and liquid compositions.

Obviously, one can argue that the LJ parameters of the pure components were the same in each phase and that if the potential models of the pure components were first given a treatment such as the one presented in this work, then the Lorentz-Berthelot or another set of mixing rules would suffice for the mixture of the two components. This, however, is still an incorrect approach (even if the simulation error bars might have extended over the experimental values of the properties of interest, for example, on a phase diagram) since any attempts to explain or calculate the properties of mixtures from knowledge of their pure components' properties and hence, parameters only, do not include any information about the mixtures (Rowlinson &

Swinton, 1982), and yet again it is only via mixing rules that the mixture interactions and subsequent properties can be approximated. Thus, experimental information must be used in order to obtain good models for mixtures (Haslam *et al*., 2008). As explained Chapter 4, in the broader context of intermolecular forces, the present study focused on a relatively simple, neutral-molecules chemical mixture, consisting of monoatoms, that was modelled by the simple Lennard-Jones 12-6 potential energy model. This is certainly a caveat since a lot of systems of practical interest cannot be adequately modelled as such. On the contrary a lot of important asymmetric, non-polar, non-ideal mixtures (e.g. n-alkane-perfluoroalkane) can benefit from the approach presented here. Indeed, several other potential energy models of higher complexity that are essentially variations of the Lennard-Jones model, for example, the 12–6–4 (Mason & Schamp, 1958), m–6–8 (Klein & Hanley, 1970) and Stockmayer (1941) potential models, and which still assume pair-wise additivity of interactions (some of which modify the neutral-system dominant dispersion interaction energy term) do provide a more rigid physical foundation for modelling different types molecules, but such complex models that are associated with more complex molecules and higher computational costs do not take into account the mixture properties and hence still rely on homogeneous mixing rules.

It was also shown numerically, and then proved by using a model that was developed in the latter part of this study, that the heterogeneous parameter approach gives no unique solution for a given NpT state point. This is also a caveat of the approach in that if a global heterogeneous parameter fitting was done for a single temperature (by using the weighted-relative volatilities corresponding to each pressure for the isotherm) then there would have been multiple solutions for each NpT simulation to choose. However, it was shown that along the energy contours on the $B^{\mathrm{V}} - B^{\mathrm{L}}$ plane (for a given NpT state point) that the correction factor used in one phase was everywhere either less than or greater than the correction factor used in the other phase. This means that with judicious selection of heterogeneous parameters, one may obtain chemically-sensible trends at a given temperature with respect to these parameters.

7. RECOMMENDATIONS

One application of the method presented here could be towards obtaining accurate prediction of hydrocarbon/water phase equilibrium especially to better represent TraPPE-UA alkanes and SPC/E water interactions. The study of Johansson *et al*. (2007) that used an empirical multiplying factor of 1.30 between water and alkanes to improve water solubility in alkanes, after the unmodified geometric average gave water solubilities in alkanes that were much lower than experimental values, also worsened alkane solubility in water. Thus as a first step in trying to obtain simultaneous good predictions of compositions in both phases, the heterogeneous unlike-energy parameter approach can be used. Further refinement, if necessary, can be done by varying the unlike-size parameter.

Another possible extension of this work would be to vary the repulsive exponent of the Lennard-Jones potential independently in each phase, which is also an extension of the work of Potoff & Bernard-Brunel (2009). Effectively, the range of the potential would be altered directly in each phase, unlike in this work where the overall potential energy was scaled linearly by the B^{L} and B^{V} multiplying correction factors.

8. REFERENCES

1. Allen, M. P. & Tildesley, D. J., "Computer Simulation of Liquids 2nd edition", Claredon Press, Oxford, 1987.
2. Al-Matar, A.K. & Rockstraw, D.A., "A generating equation for mixing rules and two new mixing rules for interatomic potential energy parameters", *Journal of Computational Chemistry* **25**(5) (2004) 660-668.
3. Berendsen, H. J. C., Grigera, J. R. and Straatsma, T. P., "The Missing Term in Effective Pair Potentials" *Journal of Physical Chemistry* **91** (1987) 6269-6271.
4. Berendsen, H. J. C., Postma, J. P. M., van Gunsteren, W. F. and Hermans, J. 1981, "Interaction Models for Water in Relation to Protein Hydration", in B. Pullmann, (ed.), *Intermolecular Forces*, Reidel, Dordrecht, , pp. 331-342.
5. Berthelot, M., "Sur le Mélange des Gaz", *Comptes Rendus de l'Académie des Sciences Paris* **126** (1889) 1703-1706.
6. Boda, D. & Henderson, H., "The effects of deviations from Lorentz–Berthelot rules on the properties of a simple mixture", *Molecular Physics* **106**(20) (2008) 2367–2370.
7. Boublik, T., "Statistical thermodynamics of nonspherical molecule fluids", *Ber. Bunsenges. Phys. Chem.* **85** (1981) 1038–1041.
8. Boulougouris, G. C., Economou, I. G. and Theodorou, D. N., "Engineering a Molecular Model for Water Phase Equilibrium over a Wide Temperature Range", *Journal of Physical Chemistry B* **102** (1998) 1029-1035.
9. Bourasseau, E., Haboudou, M., Boutin, A., Fuchs, A. H. and Ungerer, P., "New optimization method for intermolecular potentials: Optimization of a new anisotropic united atoms potential for olefins: Prediction of equilibrium properties", *Journal of Chemical Physics* **118** (2003) 3020-3034.
10. Buckingham, R. A., "The Classical Equation of State of Gaseous Helium, Neon and Argon", *Proceedings of the Royal Society of London. Series A, Mathematical and Physical Sciences* **168** (1938) 264.
11. Canongia Lopes, J. N. & Tildesley, D. J., "Multiphase equilibria using the Gibbs ensemble Monte Carlo Method", *Molecular Physics* **92**(2) (1997) 187–195.

12. Carnahan, N. F. & Starling, K. E., "Equation of State for Nonattracting Rigid Spheres", *Journal of Chemical Physics* **51** (1969) 635-636.

13. Chandrasekhar, J., Spellmeyer, D. and Jorgensen, W. L., "Energy component analysis for dilute aqueous solutions of Li+, Na+, F- and Cl- Ions", *Journal of the American Chemical Society* **106** (1984) 903-910.

14. Chen, B. & Siepmann, J. I., "Transferable Potentials for Phase Equilibria. 3. Explicit-Hydrogen Description of Normal Alkanes", *Journal of Physical Chemistry B* **103**(25) (1999) 5370–5379.

15. Chen, B., Potoff, J. J. and Siepmann, J. I., "Monte Carlo calculations for alcohols and their mixtures with alkanes. Transferable potentials for phase equilibria. 5. United-atom description of primary, secondary and tertiary alcohols", *Journal of Physical Chemistry B* **105** (2001) 3093-3104.

16. Chialvo, A. A., "Excess properties of liquid mixtures from computer simulation: a coupling-parameter approach to the determination of their dependence on molecular symmetry", *Molecular Physics* **73**(1) (1991), 127-140.

17. Cournoyer, M. E. & Jorgensen, W. L., "Solvent Effects on the Relative Energies of Carbonium Ions. Solvation and Internal Rotation for the Allyl Cation in Liquid Hydrogen Fluoride", *Journal of the American Chemical Society* **106** (1984) 5104-5112.

18. Damm, W., Frontera, A., Tirado-Rives, J., Jorgensen, W. L., "OPLS all-atom force field for carbohydrates", *Journal of Computational Chemistry* **18** (1997) 1955-1970.

19. de Leeuw, S. W., Perram, J. W. and Smith, E. R., "Simulation of Electronic Systems in Periodic Boundary Conditions. I. Lattice Sums and Dielectric Constants", *Proceedings of the Royal Society of London. Series A, Mathematical and Physical Sciences* **373**(1752) (1980*a*) 27–56.

20. de Leeuw, S. W., Perram, J. W. and Smith, E. R., "Simulation of Electronic Systems in Periodic Boundary Conditions. II. Equivalence of Boundary Conditions", *Proceedings of the Royal Society of London. Series A, Mathematical and Physical Sciences* **373**(1752) (1980*b*) 57–66.

21. de Leeuw, S. W., Perram, J. W. and Smith, E. R., "Simulation of Electronic Systems in Periodic Boundary Conditions. III. Further Theory and Applications", *Proceedings of the Royal Society of London. Series A, Mathematical and Physical Sciences* **388**(1794) (1980*c*) 173–193.

22. de Pablo, J. J., Prausnitz, J. M., Strauch, H. J. and Cummings, P. T., "Molecular simulation of water along the liquid-vapor coexistence curve from 25 °C to the critical point", *Journal of Chemical Physics* **93** (1990), pp. 7355-7359.

23. Delhommelle, J. & Millié, P., "Inadequacy of the Lorentz± Berthelot combining rules for accurate predictions of equilibrium properties by molecular simulation", *Molecular Physics* **99**(8) (2001) 619-625.

24. Docherty, H., Galindo, A., Vega, C. and Sanz, E., "A potential model for methane in water describing correctly the solubility of the gas and the properties of the methane hydrate", *Jounal of Chemical Physics* **125** (2006) 074510-074519.

25. Errington, J. R. & Panagiotopoulos, A. Z., "A Fixed Point Charge Model for Water Optimized to the Vapor−Liquid Coexistence Properties", *Journal of Physical Chemistry B* **102** (1998) 7470-7475.

26. Errington, J. R. & Panagiotopoulos, A. Z., "A New Intermolecular Potential Model for the *n*-Alkane Homologous Series", *Journal of Physical Chemistry B* **103** (1999) 6314-6322.

27. Errington, J. R. & Panagiotopoulos, A. Z., "Phase equilibria of the modified Buckingham exponential-6 potential from Hamiltonian scaling grand canonical Monte Carlo" *Journal of Chemical Physics* **109** (1998) 1093-1100.

28. Errington, J. R., Boulougouris, G. C., Economou, I. G., Panagiotopoulos, A. Z. And Theodorou, D. N., "Molecular Simulation of Phase Equilibria for Water−Methane and Water−Ethane Mixtures", *Journal of Physical Chemistry B* **102**(44) 8865–8873.

29. Escobedo, F. A., "Tracing coexistence lines in multicomponent fluid mixtures by molecular simulation", *Journal of Chemical Physics* **110** (1999) 11999-12010.

30. Faller, R., Schmitz, H., Biermann, O. and Müller-Plathe, F., "Automatic Parameterization of Force Fields for Liquids by Simplex Optimization", *Journal of Computational Chemistry* **20**(10) (1999) 1009-1017.

31. Fender, B.E.F. & Halsey, G.D., "Second Virial Coefficients of Argon, Krypton, and Argon-Krypton Mixtures at Low Temperatures", *Journal of Chemical Physics* **36** (1962) 1881-1888.

32. Fischer, J., Mller, D., Chialvo, A. A., Haile, J. M., "The influence of unlike molecule interaction parameters on liquid mixture excess properties", *Fluid Phase Equilibria* **48** (1989) 161-176.

33. Forbes, R. J., "A short history of the art of distillation: from the beginnings up to the death of Cellier Blumenthal (2nd edition)", Brill, Leiden, 1970.

34. Frenkel, D. & Smit, B., "Understanding Molecular Simulations: From Algorithms to Applications, Vol. 1 of Computational Science Series (2nd edition)", Academic Press, San Diego, 2002.

35. Gil-Villegas, A., Galindo, A., Whitehead, P. J., Mills, S. J., Jackson, G., and Burgess, A. N., "Statistical associating fluid theory for chain molecules with attractive potentials of variable range", *Journal of Chemical Physics* **106** (1997) 4168-4186.

36. Gross, J. & Sadowski, G., "Perturbed-Chain SAFT: An Equation of State Based on a Perturbation Theory for Chain Molecule", *Industrial & Engineering Chemistry Research* **40**(4) (2001) 1244-1260.

37. Halgren, T.A., "The representation of van der Waals (vdW) interactions in molecular mechanics force fields: potential form, combination rules, and vdW parameters", *Journal of the American Chemical Society* **114**(20) (1992) 7827–7843.

38. Haslam, A. J., Galindo, A. and Jackson. G., "Prediction of binary intermolecular potential parameters for use in modelling fluid mixtures", *Fluid Phase Equilibria* **266** (2008) 105–128.

39. Henderson, D. D. D. & Rowley, R. L., "Some effects of deviations from the Lorentz-Berthelot combining rules for mixtures of Lennard-Jones fluids", *Molecular Physics* **91**(6) (1997) 1143-1147.

40. Hiza, M. J. & Duncan, A. G., "A correlation for the prediction of interaction energy parameters for mixtures of small molecules", *AIChE Journal* **16**(5) (1970) 733-738.

41. Hiza, M. J. & Duncan, A. G., "Intermolecular Forces: Thermal Diffusion and Diffusion in He-Kr and H_2-Kr", *Physics of Fluids* **12** (1969) 1531.

42. Hiza, M. J. & Robinson, R. L., "Comment on "Intermolecular forces in mixtures of helium with the heavier noble gases", *Journal of Chemical Physics* **68** (1978) 4768-4769.

43. Hudson, G. H. & McCoubrey, J. C., "Intermolecular forces between unlike molecules. A more complete form of the combining rules", *Transactions of the Faraday Society* **56** (1960) 761-766.

44. Jensen, F., "Introduction to computational chemistry 2nd edition", Wiley, Chichester, 2007.

45. Jorgensen, W. L. & Briggs, J. M., "Monte Carlo simulations of liquid acetonitrile with a three-site model", *Molecular Physics* **63** (1988) 547-558.

46. Jorgensen, W. L. & McDonald, N. A., "Development of an all-atom force field for heterocycles. Properties of liquid pyridine and diazenes", *Journal of Molecular Structure: THEOCHEM* **424** (1998) 145-155.

47. Jorgensen, W. L. & Swenson C. J., "Optimized Intermolecular Potential Functions for Amides and Peptides. Structure and Properties of Liquid Amides", *Journal of the American Chemical Society* **107** (1985) 569-578.

48. Jorgensen, W. L., "Intermolecular Potential Functions and Monte Carlo Simulations for Liquid Sulfur Compounds", *Journal of Physical Chemistry* **90** (1986b) 6379-6388.

49. Jorgensen, W. L., "Optimized Intermolecular Potential Functions for Liquid Alcohols", *Journal of Physical Chemistry* **90** (1986a) 1276-1284.

50. Jorgensen, W. L., Briggs, J. M. and Contreras, M. L., "Relative Partition Coefficients for Organic Solutes from Fluid Simulations", *Journal of Physical Chemistry* **94** (1990) 1683-1686.

51. Jorgensen, W. L., J. D. Madura and Swenson, C. J., "Optimized Intermolecular Potential Functions for Liquid Hydrocarbons", *Journal of the American Chemical Society* **106** (1984) 6638-6646.

52. Jorgensen, W. L., Maxwell, D. S., Tirado-Rives, J., "Development and testing of the OPLS all-atom force field on conformational energetics and properties of organic liquids", *Journal of the American Chemical Society* **118** (1996) 11225-11236.

53. Joseph, M. A., Raal, J. D. and Ramjugernath, D., "Phase equilibrium properties of binary systems with diacetyl from a computer controlled vapour–liquid equilibrium still", *Fluid Phase Equilibria* **182**(1–2) (2001) 157-176.

54. Kamath, G., Cao, F. and Potoff, J. J., "An Improved Force Field for the Prediction of the Vapor-Liquid Equilibria for Carboxylic Acids", *Journal of Physical Chemistry B* **108** (2004) 14130-14136.

55. Kaminski, G. A., Friesner, R. A., Tirado-Rives, J., Jorgensen, W. L., "Evaluation and Reparametrization of the OPLS-AA Force Field for Proteins via Comparison with Accurate Quantum Chemical Calculations on Peptides", *Journal of Physical Chemistry B* **105** 6474-6487.

56. Kaminski, G., Duffy, E. M., Matsui, T. and Jorgensen, W. L., "Free energies of hydration and pure liquid properties of hydrocarbons from the OPLS all-atom model", *Journal of Physical Chemistry* **98** (1994) 13077-13082.

57. Kaplan, I. G., "Intermolecular interactions : physical picture, computational methods and model potentials", John Wiley & Sons Ltd, Chichester, 2006.

58. Khare, R., Sum, A. K., Nath, S. K. and de Pablo, J. J., "Simulation of Vapor-Liquid Phase Equilibria of Primary Alcohols and Alchol-Alkane Mixtures", *Journal of Physical Chemistry B* **108** (2004) 10071-10076.

59. Kofke, D. A., "Direct evaluation of phase coexistence by molecular simulation via integration along the saturation line", *Journal of Chemical Physics* **98** (1993a) 4149-4163.

60. Kofke, D. A., "Gibbs-Duhem integration: A new method for direct evaluation of phase coexistence by molecular simulations", *Molecular Physics* **78** (1993b) 1331-1336.

61. Kohler. F., "Zur Berechnung der Wechselwirkungsenergie zwischen ungleichen Molekülen in binären flüssigen Mischungen", *Monatshefte für Chemie* **88** (1957) 857-877.

62. Kong, C.L., "Combining rules for intermolecular potential parameters. II. Rules for the Lennard-Jones (12–6) potential and the Morse potential", *Journal of Chemical Physics* **59** (1973) 2464-2467.

63. Landau, L. D. & Lifshitz, E. M., "Course of Theoretical Physics Volume 5 Statistical Physics. Part 1 3rd edition", Pergamon, Oxford, 1980.

64. Lenart, P. J. & Panagiotopoulos, A. Z., "Tracing the Critical Loci of Binary Fluid Mixtures Using Molecular Simulation", *Journal of Physical Chemistry B* **110** (2006) 17200-17206.

65. Lennard-Jones, J. E, "Cohesion", *Proceedings of the Physical Society* **43**(5) (1931) 461-482.

66. Lennard-Jones, J. E., "On the Determination of Molecular Fields", *Proceedings of the Royal Society of London. Series A* **106**(738) (1924) 463–477.

67. Levey, M., "Perfumery in ancient Babylonia", *Journal of Chemical Education* **31**(7) (1954) 373.

68. Lorentz, H.A., "Ueber die Anwendung des Satzes vom Virial in der kinetischen Theorie der Gase", *Annalen der Physik* **12** (1881) 127-136.

69. Lubansky, A. S., Yeow, Y. L., Leong, Y. -K., Wickramasinghe, S. R. and Han, B., "A general method of computing the derivative of experimental data", *AIChE Journal* **52** (2006) 323–332.

70. MacKerell Jr., A. D., Bashford, D., Bellott, M., Dunbrack Jr., R. L., Evanseck, J. D., Field, M. J., Fischer, S., Gao, J., Guo, H., Ha, S., Joseph-McCarthy, D., Kuchnir, L., Kuczera, K., Lau, F. T. K., Mattos, C., Michnick, S., Ngo, T., Nguyen, D. T., Prodhom, B., Reiher III, W. E., Roux, B., Schlenkrich, M., Smith, J. C., Stote, R., Straub, J., Watanabe, M., Wiorkiewicz-Kuczera, J., Yin, D. and Karplus, M., "All-Atom Empirical Potential for Molecular Modeling and Dynamics Studies of Proteins", *Journal of Physical Chemistry B* **102** (1998) 3586-3616.

71. Mahoney, M. W. & Jorgensen, W. L., "A five-site model for liquid water and the reproduction of the density anomoly by rigid, nonpolarizable potential functions", *Journal of Chemical Physics* **112** (2000) 8910-8922.

72. Martin, M. G. & Siepmann, J. I., "Calculating Gibbs free energies of transfer from Gibbs ensemble Monte Carlo simulations", *Theoretical Chemistry Accounts* **99** (1998b) 347-350.

73. Martin, M. G. & Siepmann, J. I., "Novel configurational-bias Monte Carlo method for branched molecules. Transferable potentials for phase equilibria. 2. United-atom description of branched alkanes", *Journal of Physical Chemistry B* **103** (1999) 4508-4517.

74. Martin, M. G. & Siepmann, J. I., "Transferable potentials for phase equilibria. 1. United-atom description of n-alkanes", *Journal of Physical Chemistry B* **102** (1998a) 2569-2577.

75. Martin, M. G. & Thompson, A. P., "Industrial property prediction using Towhee and LAMMPS", *Fluid Phase Equilibria* **217** (2004) 105-110.

76. McDonald, N. A. & Jorgensen, W. L., "Development of an all-atom force field for heterocycles. Properties of liquid pyrrole, furan, diazoles, and oxazoles", *Journal of Physical Chemistry B* **102** (1998) 8049-8059.

77. McDonald, N. A., Duffy, E. M. and Jorgensen, W. L., "Monte Carlo investigations of selective anion complexation by a bis(phenylurea)p-tert-butylcalix[4]arene", *Journal of the American Chemical Society* **120** (1998) 5104-5111.

78. Metropolis, N., Rosenbluth, A. W., Rosenbluth, M., Teller, A. H. and Teller, E., "Equation of state calculations by fast computing machines", *Journal of Chemical Physics* **21** (1953) 1087–1092.

79. Mie, G., "Zur kinetischen Theorie der einatomigen Körper", *Annalen der Physik* **316**(8) (1903) 657-697.

80. Möller D., Oprzynski J., Müller A. and Fischer J., "Prediction of thermodynamic properties of fluid mixtures by molecular dynamics simulations: Methane-ethane.", *Molecular Physics* **75** (1992) 363–378.

81. Moodley, S., "Molecular Simulation of Vapour-Liquid-Liquid Equilibrium", MScEng Thesis, University of KwaZulu-Natal, 2008.

82. Moodley, S., Johansson, E., Bolton, K. and Ramjugernath, D., "Gibbs ensemble Monte Carlo simulations of binary vapour–liquid–liquid equilibrium: application to n-hexane–water and ethane–ethanol systems", *Molecular Simulation* **36**(10) (2010a) 758-762.

83. Moodley, S., Bolton, K. and Ramjugernath, D., "Monte Carlo simulations of vapor–liquid–liquid equilibrium of some ternary petrochemical mixtures", *Fluid Phase Equilibria* **15**(1) (2010b) 24-31.

84. Moučka, F. & Nezbeda, I., "Water-methanol mixtures with non-Lorentz–Berthelot combining rules: A feasibility study", *Journal of Molecular Liquids* **159**(1) (2011) 47-51.

85. Müller, T. J., Roy, S., Zhao, W., Maaß, A. and Reith, D., "Economic simplex optimization for broad range property prediction: Strengths and weaknesses of an automated approach for tailoring of parameters", *Fluid Phase Equilibria* **274** (2008) 27–35.

86. Foloe, N. and MacKerell Jr., A. D., "All-Atom Empirical Force Field for Nucleic Acids: I. Parameter Optimization Based on Small Molecule and Condensed Phase Macromolecular Target Data", *Journal of Computational Chemistry* **21** (2000) 86-104.

87. Naidoo, P., Ramjugernath, D. and Raal, J. D., "A new high-pressure vapour-liquid equilibrium apparatus", *Fluid Phase Equilibria*, **269**(1-2) (2008) 104-112.

88. Nath, S. K. & de Pablo, J. J., "Simulation of vapour-liquid equilibria for branched alkanes", *Molecular Physics* **98** (2000) 231-238.

89. Nath, S. K. & Khare, R., "New forcefield parameters for branched hydrocarbons", *Journal of Chemical Physics* **115** (2001b) 10837-10844.

90. Nath, S. K., “Molecular Simulation of Vapor-Liquid Phase Equilibria of Hydrogen Sulfide and Its Mixtures with Alkanes”, *Journal of Physical Chemistry B* **107** (2003) 9498-9504.

91. Nath, S. K., Banaszak, B. J. and de Pablo, J. J., “A new united atom force field for alpha-olefins”, *Journal of Chemical Physics* **114** (2001a) 3612-3616.

92. Nath, S. K., Escobedo, F. A. and de Pablo, J. J., “On the simulation of vapour-liquid equilibria for alkanes”, *Journal of Chemical Physics* **108** (1998) 9905-9911.

93. Nath, S. K., Escobedo, F. A. and de Pablo, J. J., “On the simulation of vapor-liquid equilibria for alkanes”, *Journal of Chemical Physics* **108** (1998) 9905-9911.

94. Nelder, J.A. & Mead, R., “A simplex method for function minimization.” *Computer Journal* **7** (1965) 308–313.

95. Norman, G. E. & Filinov, F. S., "Investigation of phase transitions by a Monte-Carlo method", *High Temperature*, **7** (1969) 216-222.

96. Panagiotopoulos, A. Z., “Direct determination of phase coexistence properties of fluids by Monte Carlo simulation in a new ensemble”, *Molecular Physics* **61** (1987) 813-826.

97. Panagiotopoulos, A. Z., Quirke, N., Stapleton, M. and Tildesley D. J., “Phase equilibria by simulation in the Gibbs ensemble”, *Molecular Physics* **63**(4) (1988) 527-545.

98. Parrinello, M. & Rahman, R., "Crystal structure and pair potentials: A molecular-dyanmics study", *Physical Review Letters* **45** (1980) 1196-1199.

99. Parrinello, M. & Rahman, R., “Polymorphic transitions in single crystals: A new molecular-dyanmics method”, *Journal of Applied Physics* **52** (1981) 7182-7190.

100. Peng, D. & Robinson, D. B., “A New Two-Constant Equation of State”, *Industrial & Engineering Chemistry Fundamentals* **15** (1976) 59-64.

101. Perry, R. H. & Green, D. W., “Perry’s Chemical Engineers’ Handbook (8^{th} edition)”, McGraw-Hill, New York, 2007.

102. Petrucci, R. H., Harwood, W. S., Herring, G. E. and Madura, J., “General Chemistry: Principles & Modern Applications (9^{th} edition)”, Prentice-Hall, New Jersey, 2006.

103. Pranata, J., Wierschke, S. G. and Jorgensen, W. L., “OPLS potential functions for nucleotide bases. Relative association constants of hydrogen-bonded base pairs in chloroform”, *Journal of the American Chemical Society* **113** (1991) 2810-2819.

104. Rai, N. & Siepmann, J.I., "Transferable potentials for phase equilibria. 9. Explicit-hydrogen description of benzene and 5-membered and 6-membered heterocyclic aromatic compounds", *Journal of Physical Chemistry B* **111** (2007) 10790-10799.

105. Rizzo, R. C. & Jorgensen, W. L., "OPLS all-atom model for amines: resolution of the amine hydration problem", *Journal of the American Chemical Society* **121** (1999) 4827-4836.

106. Rouha, M. & Nezbeda, I., "Non-Lorentz–Berthelot Lennard-Jones mixtures: A systematic study", *Fluid Phase Equilibria* **277** (2009) 42-48.

107. Rowlinson, J. S. & Swinton, F. L., 'Liquid and Liquid mixtures (3rd edition)', Butterworth Scientific, London, 1982.

108. Sadus, R. J., "Influence of combining rules and molecular shape on the high pressure phase equilibria of binary fluid mixtures", *Journal of Physical Chemistry* **97**(9) (1993) 1985-1992.

109. Sandler, S. I., "Quantum mechanics: a new tool for engineering thermodynamics", *Fluid Phase Equilibria* **210** (2003) 147–160.

110. Schnabel, T., Vrabec, J. and Hasse, H., "Unlike Lennard–Jones parameters for vapor–liquid equilibria", *Journal of Molecular Liquids* **135** (2007) 170–178.

111. Shetty, R. & Escobedo, F. A., "On the application of virtual Gibbs ensembles to the direct simulation of fluid–fluid and solid–fluid phase coexistence", *Journal of Chemical Physics* **116**(18) (2002) 7957-7966.

112. Siepmann, J. I. & Frenkel, D., "Configurational bias Monte Carlo: a new sampling scheme for flexible chains", *Molecular Physics* **75** (1992) 59-70.

113. Sikora, P. T., "Combining rules for spherically symmetric intermolecular potentials", *Journal of Physics B: Atomic and Molecular Physics* **3**(11) (1970) 1475.

114. Smith, F. T., "Atomic Distortion and the Combining Rule for Repulsive Potentials", *Physical Review A* **5** (1972) 1708-1713.

115. Smith, J. M., Van Ness, H. C. and Abbott, M. M., "Introduction to Chemical Engineering Thermodynamics (6th edition)", McGraw-Hill, Singapore, 2001.

116. Song, W., Rossky, P. J. and Maroncelli, M., "Modeling alkane¿perfluoroalkane interactions using all-atom potentials: Failure of the usual combining rules", *Journal of Chemical Physics* **119** (2003) 9145-9162.

117. Stone, A. J., "Intermolecular Potentials", *Science* **321** (2008) 787-789.

118. Strauch, H. J. & Cummings, P. T., "Comment on: Molecular simulation of water along the liquid-vapor coexistence curve from 25 °C to the critical point", *Journal of Chemical Physics* **96** (1992) 864-865.

119. Stubbs, J. M., Potoff, J. J. and Siepmann, J. I., "Transferable Potentials for Phase Equilibria. 6. United-Atom Description for Ethers, Glycols, Ketones, and Aldehydes", *Journal of Physical Chemistry B* **108** (2004) 17596-17605.

120. Sweatman, M. B. & Quirke, N., "Simulating Fluid–Solid Equilibrium with the Gibbs Ensemble", *Molecular Simulation* **30**(1) (2004) 23-28.

121. Ungerer, P., Beauvais, C., Delhommelle, J., Boutin, A., Rousseau, B. and Fuchs, A. H., "Optimization of the anisotropic united atoms intermolecular potential for n-alkanes", *Journal of Chemical Physics* **112** (2000) 5499-5510.

122. Ungerer, P., Tavitian, B., and Boutin, A., "Applications of Molecular Simulation in the Oil and Gas Industry: Monte Carlo Methods", Editions TECHNIP, Paris, 2005.

123. Valtz, A., Coquelet, C. and Richon, D., "Vapor–liquid equilibrium data for the sulfur dioxide (SO_2) + 1,1,1,2,3,3,3-heptafluoropropane (R227ea) system at temperatures from 288.07 to 403.19 K and pressures up to 5.38 MPa Representation of the critical point and azeotrope temperature dependence", Fluid Phase Equilibria **220** (2004) 77–83.

124. Valtz, A., Coquelet, C., Baba-Ahmed, A. and Richon, D., "Vapor–liquid equilibrium data for the CO_2 + 1,1,1,2,3,3,3,-heptafluoropropane (R227ea) system at temperatures from 276.01 to 367.30 K and pressures up to 7.4 MPa", Fluid Phase Equilibria **207** (2003) 53–67.

125. Vesely, F. J., "Statistical Physics. Course material with JAVA applets", Franz Vesely Personal Home Page (2005) University of Vienna. 9 September 2009 <http://homepage.univie.ac.at/franz.vesely/sp_english/sp/sp.html>.

126. Vlcek, L., Chialvo, A. A. and Cole, D. R., "Optimized Unlike-Pair Interactions for Water_Carbon Dioxide Mixtures Described by the SPC/E and EPM2 Models", *Journal of Physical Chemistry B* **115** (2011) 8775–8784.

127. Vrabec, J., Huang, Y. and Hasse, H., "Molecular models for 267 binary mixtures validated by vapor–liquid equilibria: A systematic approach." *Fluid Phase Equilibria* **279** (2009) 120–135.

128. Vrabec, J., Stoll, J. and Hasse, H., "Molecular models of unlike interactions in fluid mixtures", *Molecular Simulation* **31**(4) (2005) 215-221.

129. Vrabec., J. & Hasse, H., "Grand Equilibrium: vapour-liquid equilibria by a new molecular simulation method", *Molecular Physics* **100**(21) (2002) 3375-3383.

130. Waldman, M. & Hagler, A.T., "New combining rules for rare gas van der Waals parameters", *Journal of Computational Chemistry* **14**(9) (1993) 1077-1084.

131. van Westen, T., Vlugt, T. J. H., and Gross, J., "Determining Force Field Parameters Using a Physically Based Equation of State", *Journal of Physical Chemistry B* **115** (2011) 7872-7880.

132. Wick, C. D., Martin, M. G. and Siepmann, J. I., "Transferable potentials for phase equilibria. 4. United-atom description of linear and branched alkenes and alkylbenzenes", *Journal of Physical Chemistry B* **104** (2000) 8008-8016.

133. Widom, B., "Statistical Mechanics A Concise Introduction for Chemists", Cambridge University Press, New York, 2002.

134. Zhang, L. & Siepmann, J. I., "Pressure Dependence of the Vapor-Liquid-Liquid Phase Behavior in Ternary Mixtures Consisting of n-Alkanes, n-Perfluoroalkanes, and Carbon Dioxide", *Journal of Physical Chemistry B* **109** (2005) 2911-2919.

135. Zhang, Z. & Duan, Z., "Phase equilibria of the system methane–ethane from temperature scaling Gibbs Ensemble Monte Carlo simulation", *Geochimica et Cosmochimica Acta*, **66**(19) (2002) 3431–3439.

Appendix A

Selected representative numerical data, and MATLAB® routines

A.1 Numerical data

T / [K]	p / [kPa]	B	y_1		x_1		B^{opt}
150	130.235	0.97	0.7035	0.016	0.0482	0.0051	0.9864
y_1^{exp}	0.69901	0.98	0.7005	0.006	0.057	0.0006	
x_1^{exp}	0.06	0.99	0.7065	0.0159	0.0616	0.0017	
		1	0.6942	0.0059	0.0731	0.0029	
		1.01	0.7196	0.0075	0.084	0.0038	
		1.02	0.7008	0.0113	0.0908	0.0035	
		1.03	0.7146	0.0106	0.104	0.006	
		1.04	0.7218	0.0059	0.1159	0.007	
	348.2978	0.97	0.8975	0.0068	0.1996	0.007	0.9879
y_1^{exp}	0.89901	0.98	0.9015	0.0018	0.2182	0.0039	
x_1^{exp}	0.24	0.99	0.9019	0.0014	0.2441	0.0072	
		1	0.9049	0.0028	0.2673	0.0094	
		1.01	0.9063	0.0089	0.2885	0.0215	
		1.02	0.9147	0.0031	0.3101	0.0092	
		1.03	0.9131	0.007	0.3274	0.014	
	702.351	0.95	0.9547	0.0017	0.5068	0.0139	1.0077
y_1^{exp}	0.96675	0.96	0.9582	0.0011	0.5443	0.0211	
x_1^{exp}	0.64	0.97	0.9589	0.0021	0.5482	0.0179	
		0.98	0.9653	0.0026	0.6103	0.016	
		0.99	0.9669	0.0005	0.6258	0.0076	
		1	0.9679	0.0022	0.6257	0.0142	
		1.01	0.9722	0.0009	0.6458	0.0135	
		1.02	0.974	0.0012	0.6519	0.014	
	900.9612	0.97	0.982	0.0008	0.8309	0.0056	1.0041
y_1^{exp}	0.98721	0.975	0.9825	0.0004	0.8278	0.0079	
x_1^{exp}	0.87	0.98	0.985	0.0007	0.8502	0.0066	
		0.985	0.9862	0.0012	0.853	0.0156	
		0.99	0.9845	0.0011	0.8271	0.012	
		0.995	0.986	0.0007	0.8364	0.0093	
		1	0.987	0.0015	0.8439	0.0195	
		1.005	0.9876	0.0015	0.844	0.0168	
		1.01	0.989	0.0006	0.8555	0.0101	
		1.015	0.9891	0.0004	0.8507	0.0039	
		1.02	0.9893	0.0006	0.8438	0.0091	
		1.025	0.989	0.0005	0.832	0.0082	

Table A-1 - Numerical data obtained from *NpT*-GEMC at 150 K simulations that were used for calculating the optimum homogeneous *B* for each pressure-temperature pair by fitting the *SSQD*s to quadratic polynomials and then determining the *B* that gave the minimum error.

T / [K]	p / [kPa]	B	y_1		x_1		B^{opt}
165	320.7	0.955	0.6708	0.0248	0.0581	0.0099	0.9847
y_1^{exp}	0.69183	0.96	0.6812	0.0141	0.067	0.0025	
x_1^{exp}	0.09	0.97	0.6744	0.0323	0.0692	0.007	
		0.98	0.6839	0.0298	0.0809	0.01	
		0.99	0.6831	0.0239	0.0929	0.0046	
		1	0.6865	0.0092	0.109	0.0036	
		1.01	0.7019	0.0224	0.1215	0.0074	
		1.02	0.7081	0.0196	0.1307	0.0088	
		1.03	0.7054	0.018	0.1482	0.0063	
		1.04	0.7164	0.0142	0.1578	0.0052	
		1.05	0.7097	0.0094	0.1701	0.0063	
		1.06	0.7365	0.0319	0.1932	0.0126	
	701.5	0.955	0.8656	0.012	0.208	0.0201	0.9873
y_1^{exp}	0.87112	0.97	0.8646	0.0099	0.2366	0.0282	
x_1^{exp}	0.28	0.98	0.8696	0.0143	0.2686	0.0236	
		0.99	0.8722	0.0111	0.2799	0.0217	
		1	0.872	0.0123	0.2942	0.0212	
		1.01	0.8808	0.0088	0.3292	0.0156	
		1.02	0.8877	0.0099	0.3567	0.0191	
	1200	0.88	0.9055	0.0065	0.1997	0.0199	0.9961
y_1^{exp}	0.9415	0.92	0.9158	0.0073	0.353	0.0562	
x_1^{exp}	0.5881	0.94	0.9216	0.0025	0.4254	0.0163	
		0.955	0.9263	0.0009	0.4888	0.0088	
		0.97	0.9349	0.0022	0.5445	0.009	
		0.985	0.9397	0.0007	0.5654	0.0188	
		1	0.9436	0.0022	0.5798	0.0043	
		1.015	0.947	0.0009	0.5869	0.0031	
		1.03	0.9488	0.0009	0.5912	0.0006	
	1600	1	0.9753	0.0015	0.8192	0.0123	1.0625
y_1^{exp}	0.9253	1.01	0.978	0.0012	0.8262	0.0087	
x_1^{exp}	0.8363	1.02	0.9816	0.0012	0.8434	0.0105	
		1.03	0.9823	0.0007	0.8386	0.009	
		1.04	0.9841	0.0003	0.844	0.0046	
		1.05	0.9855	0.0007	0.8485	0.0076	
		1.06	0.9879	0.0015	0.8615	0.0151	
		1.07	0.9875	0.0011	0.8472	0.0125	
		1.08	0.99	0.0005	0.8639	0.0073	
		1.09	0.9903	0.0009	0.8602	0.0111	
		1.1	0.9911	0.0007	0.8616	0.0088	

Table A-2 –Numerical data obtained from *NpT*-GEMC simulations at 165 K that were used for calculating the optimum homogeneous *B* for each pressure-temperature pair by fitting the *SSQD*s to quadratic polynomials and then determining the *B* that gave the minimum error.

T / [K]	p / [kPa]	B	y_1		x_1		B^{opt}
180 K	790	0.955	0.734	0.0077	0.1294	0.008	0.9794
y_1^{exp}	0.7301	0.96	0.731	0.0021	0.1393	0.0018	
x_1^{exp}	0.1618	0.98	0.7314	0.0077	0.1587	0.0069	
		0.99	0.7332	0.0042	0.1709	0.0055	
		1	0.7331	0.008	0.1828	0.0056	
		1.01	0.7373	0.0063	0.1975	0.007	
		1.02	0.7517	0.0064	0.2223	0.0097	
		1.03	0.7437	0.0058	0.2281	0.0061	
		1.04	0.7681	0.011	0.2562	0.0098	
		1.05	0.7659	0.0085	0.2644	0.0089	
		1.06	0.766	0.0139	0.2771	0.0114	
	1001.8	0.955	0.7837	0.0045	0.1823	0.0094	0.9845
y_1^{exp}	0.79137	0.97	0.7832	0.0101	0.2051	0.0064	
x_1^{exp}	0.23	0.98	0.7907	0.0083	0.2216	0.0144	
		0.99	0.7891	0.0136	0.2343	0.0104	
		1	0.7962	0.0022	0.2519	0.0045	
		1.01	0.8005	0.0049	0.272	0.005	
		1.02	0.8028	0.0036	0.2888	0.0066	
	1750	0.955	0.8792	0.0027	0.4158	0.0117	0.9946
y_1^{exp}	0.8955	0.97	0.8882	0.0055	0.4589	0.027	
x_1^{exp}	0.5017	0.985	0.898	0.0037	0.5016	0.018	
		1	0.9048	0.0026	0.5335	0.0057	
		1.01	0.9093	0.0017	0.5447	0.0082	
		1.02	0.9146	0.0027	0.5606	0.0069	
		1.03	0.9169	0.0025	0.5685	0.0095	
		1.075	0.9291	0.004	0.5886	0.0041	
		1.1	0.9349	0.0041	0.5918	0.0023	
		1.15	0.9421	0.0051	0.5941	0.0011	
	2500	0.96	0.9406	0.0013	0.7559	0.0065	0.992
y_1^{exp}	0.9492	0.97	0.9456	0.0028	0.7674	0.0146	
x_1^{exp}	0.7819	0.98	0.9496	0.0021	0.7804	0.0089	
		0.99	0.9504	0.0022	0.7714	0.0119	
		1	0.9548	0.003	0.7824	0.0161	
		1.01	0.9581	0.0029	0.7901	0.0158	
		1.02	0.9628	0.0013	0.8044	0.0073	
		1.03	0.9653	0.0038	0.8078	0.0217	

Table A-3 –Numerical data obtained from *NpT*-GEMC simulations at 180 K that were used for calculating the optimum homogeneous *B* for each pressure-temperature pair by fitting the *SSQD*s to quadratic polynomials and then determining the *B* that gave the minimum error.

T / [K]	p / [kPa]	B	y_1		x_1		B^{opt}
189.78	693	0.96	0.4923	0.0149	0.0598	0.0023	0.999
y_1^{exp}	0.4877	0.97	0.4921	0.0097	0.0654	0.0033	
x_1^{exp}	0.088	0.98	0.494	0.0142	0.0705	0.0035	
		0.99	0.5075	0.0161	0.08	0.0037	
		1	0.4991	0.0089	0.0846	0.0038	
		1.01	0.5052	0.0087	0.0935	0.0018	
		1.02	0.5135	0.005	0.1018	0.0016	
		1.03	0.5119	0.0126	0.1105	0.0027	
		1.04	0.5126	0.0075	0.1195	0.003	
	1128	0.97	0.6929	0.0102	0.1551	0.0053	0.9981
y_1^{exp}	0.6913	0.98	0.7	0.0105	0.1724	0.0053	
x_1^{exp}	0.1994	0.99	0.6997	0.0039	0.1837	0.0045	
		1	0.7095	0.011	0.2034	0.006	
		1.01	0.7163	0.0093	0.2183	0.0067	
		1.02	0.7105	0.0053	0.2267	0.0019	
		1.03	0.7263	0.0087	0.2481	0.0058	
		1.04	0.7374	0.0067	0.2691	0.0043	
	1592	0.96	0.7868	0.002	0.2549	0.0031	1.0002
y_1^{exp}	0.785	0.97	0.7811	0.0055	0.2587	0.0102	
x_1^{exp}	0.3239	0.98	0.7941	0.009	0.2898	0.0089	
		0.99	0.7981	0.0037	0.3115	0.007	
		1	0.8005	0.0051	0.3248	0.0113	
		1.01	0.8086	0.0049	0.3446	0.0091	
		1.02	0.8153	0.0064	0.3622	0.0101	
		1.03	0.8195	0.0034	0.3763	0.0076	
	2632	0.95	0.8737	0.004	0.5216	0.0157	0.9976
y_1^{exp}	0.88	0.96	0.8784	0.0042	0.5471	0.018	
x_1^{exp}	0.6186	0.97	0.8859	0.0025	0.5647	0.0051	
		0.98	0.8946	0.0016	0.5945	0.0058	
		0.99	0.8984	0.0013	0.6039	0.0044	
		1	0.9036	0.0038	0.6196	0.014	
		1.01	0.9075	0.0025	0.6286	0.0062	
		1.02	0.9122	0.0026	0.6384	0.0109	
		1.03	0.92	0.001	0.6577	0.0029	
		1.04	0.9246	0.0021	0.6668	0.0076	
	3231	0.95	0.9142	0.0042	0.7269	0.0198	0.9866
y_1^{exp}	0.9214	0.96	0.9188	0.0018	0.7367	0.0095	
x_1^{exp}	0.7645	0.97	0.9235	0.0033	0.7449	0.0133	
		0.98	0.9293	0.0026	0.7583	0.0122	
		0.99	0.9345	0.0007	0.7691	0.0036	
		1	0.9381	0.0014	0.7726	0.0066	
		1.01	0.9424	0.0021	0.7807	0.0077	
		1.02	0.9455	0.0014	0.7845	0.0054	
		1.03	0.948	0.0003	0.7858	0.0028	
	3743	0.96	0.9531	0.004	0.8765	0.0135	0.9437
y_1^{exp}	0.947	0.97	0.9566	0.0032	0.8804	0.011	
x_1^{exp}	0.8822	0.98	0.9571	0.0023	0.8759	0.008	
		0.99	0.9618	0.0025	0.8855	0.009	
		1	0.963	0.0015	0.8831	0.0066	
		1.01	0.967	0.0014	0.8918	0.0054	
		1.02	0.9679	0.0013	0.8894	0.005	
		1.03	0.9716	0.0015	0.898	0.0065	
		1.04	0.9654	0.0144	0.9004	0.0098	

Table A-4 –Numerical data obtained from *NpT*-GEMC simulations at 189.78 K that were used for calculating the optimum homogeneous *B* for each pressure-temperature pair by fitting the *SSQD*s to quadratic polynomials and then determining the *B* that gave the minimum error.

T / [K]	p / [kPa]	B	y_1		x_1		B^{opt}
223.81	1726	0.96	0.2909	0.0047	0.0538	0.0012	0.989
y_1^{exp}	0.2961	0.97	0.2944	0.0098	0.0577	0.0026	
x_1^{exp}	0.067	0.98	0.2938	0.0101	0.0611	0.0024	
		0.99	0.3102	0.0129	0.0703	0.0039	
		1	0.305	0.0136	0.0725	0.005	
		1.01	0.3055	0.0112	0.077	0.0046	
		1.02	0.3166	0.0081	0.0846	0.0028	
		1.03	0.3255	0.0087	0.0926	0.0033	
		1.04	0.3344	0.0065	0.1022	0.0019	
	2345	0.92	0.4609	0.0061	0.0934	0.0015	0.9915
y_1^{exp}	0.4713	0.93	0.4593	0.0087	0.098	0.0038	
x_1^{exp}	0.1477	0.94	0.4623	0.0044	0.1067	0.0022	
		0.95	0.4662	0.0062	0.1137	0.0024	
		0.96	0.4679	0.0104	0.1213	0.0048	
		0.97	0.4788	0.0075	0.1329	0.0034	
		0.98	0.4829	0.007	0.1419	0.004	
		0.99	0.4816	0.0098	0.1474	0.0049	
		1.01	0.5023	0.013	0.1738	0.0079	
		1.02	0.5062	0.0074	0.1827	0.0046	
		1.03	0.5108	0.0081	0.1928	0.0056	
	2961	0.97	0.5784	0.0043	0.2064	0.0025	0.9995
y_1^{exp}	0.5716	0.98	0.5755	0.0052	0.2126	0.0032	
x_1^{exp}	0.2444	0.99	0.5902	0.0062	0.2317	0.0055	
		1	0.6001	0.0067	0.2472	0.0047	
		1.01	0.6031	0.0062	0.2592	0.0049	
		1.02	0.6118	0.0041	0.2728	0.0047	
		1.03	0.6189	0.0035	0.2852	0.0038	
	3656	0.97	0.654	0.0028	0.2979	0.0035	0.9869
y_1^{exp}	0.6508	0.98	0.6605	0.0066	0.3114	0.0096	
x_1^{exp}	0.3264	0.99	0.6669	0.0031	0.3284	0.0036	
		1	0.671	0.007	0.3393	0.0088	
		1.01	0.6825	0.0024	0.3596	0.0042	
		1.02	0.6946	0.0034	0.3798	0.0054	
		1.03	0.6988	0.0036	0.3889	0.004	
	4330	0.97	0.7035	0.0031	0.3912	0.0042	0.9939
y_1^{exp}	0.6887	0.98	0.7101	0.0045	0.4043	0.0077	
x_1^{exp}	0.4353	0.99	0.7191	0.0022	0.4244	0.006	
		1	0.7277	0.0027	0.44	0.0046	
		1.01	0.7357	0.0038	0.4573	0.0053	
		1.02	0.7438	0.0027	0.4705	0.005	
		1.03	0.7509	0.0055	0.4808	0.0078	
	5017	0.97	0.7365	0.0067	0.4815	0.0119	0.9958
y_1^{exp}	0.7281	0.98	0.7502	0.0062	0.5085	0.0119	
x_1^{exp}	0.5308	0.99	0.7614	0.0027	0.5289	0.0034	
		1	0.7642	0.0026	0.5345	0.0066	
		1.01	0.7711	0.0066	0.5446	0.0133	
		1.02	0.7754	0.0034	0.5515	0.0049	
		1.03	0.7873	0.0023	0.5726	0.005	
		1.04	0.7973	0.0055	0.5916	0.0072	
		1.05	0.6998	0.0998	0.6891	0.1047	
	5516	0.94	0.734	0.0044	0.5157	0.0115	0.9808

y_1^{exp}	0.7376	0.95	0.5485	0.0391	0.729	0.0296	
x_1^{exp}	0.5948	0.96	0.5607	0.0093	0.7583	0.0034	
		0.97	0.6071	0.0812	0.727	0.0714	
		0.98	0.7617	0.0012	0.5637	0.0045	
		0.99	0.5903	0.0175	0.7672	0.0142	
		1	0.6067	0.0084	0.7861	0.0039	
		1.01	0.6191	0.0084	0.7816	0.0137	
		1.02	0.7844	0.0083	0.6365	0.0031	

Table A-5 –Numerical data obtained from *NpT*-GEMC simulations at 223.81 K that were used for calculating the optimum homogeneous *B* for each pressure-temperature pair by fitting the *SSQD*s to quadratic polynomials and then determining the *B* that gave the minimum error.

T / [K]	p / [kPa]	B	y_1		x_1		B^{opt}
248.15	3109	0.96	0.2254	0.0105	0.0615	0.0039	0.98
y_1^{exp}	0.2226	0.97	0.228	0.0072	0.0653	0.0028	
x_1^{exp}	0.0706	0.98	0.2369	0.0109	0.0714	0.0039	
		0.99	0.235	0.0124	0.0742	0.0041	
		1	0.2413	0.0034	0.0807	0.0011	
		1.01	0.2495	0.0088	0.0868	0.0036	
		1.02	0.2499	0.0107	0.0908	0.0046	
		1.03	0.2512	0.0114	0.0955	0.0054	
		1.04	0.2638	0.0134	0.1045	0.0067	
		1.05	0.1401	0.0006	0.1399	0.0004	
	4020	0.96	0.3815	0.0048	0.1409	0.0026	0.9798
y_1^{exp}	0.3733	0.97	0.3846	0.0087	0.1485	0.0059	
x_1^{exp}	0.1591	0.98	0.3963	0.0104	0.1598	0.0068	
		0.99	0.3959	0.0069	0.1644	0.0044	
		1	0.4037	0.0053	0.1737	0.0033	
		1.01	0.4089	0.0085	0.183	0.0053	
		1.02	0.4151	0.0091	0.193	0.006	
		1.03	0.4232	0.009	0.2037	0.0059	
		1.04	0.4286	0.0043	0.2136	0.0029	
		1.05	0.4344	0.007	0.2214	0.0038	
	4895	0.96	0.4628	0.0045	0.2128	0.0031	0.988
y_1^{exp}	0.4563	0.965	0.4766	0.0067	0.2272	0.0064	
x_1^{exp}	0.2545	0.97	0.4742	0.0067	0.2297	0.0056	
		0.975	0.4806	0.0073	0.2369	0.0067	
		0.98	0.4796	0.0047	0.2391	0.0042	
		0.985	0.4829	0.0056	0.2454	0.004	
		0.99	0.4886	0.0032	0.252	0.0034	
		0.995	0.4849	0.0022	0.2521	0.0029	
		1	0.4944	0.0055	0.2621	0.0044	
		1.005	0.4982	0.0048	0.2683	0.0048	
		1.015	0.51	0.0048	0.2843	0.0043	
		1.02	0.5098	0.0038	0.2859	0.0042	
		1.025	0.5118	0.0064	0.2896	0.006	
	5482	0.95	0.5053	0.0128	0.2621	0.0133	0.9814
y_1^{exp}	0.4947	0.96	0.5084	0.0158	0.2711	0.0152	
x_1^{exp}	0.3086	0.97	0.5188	0.0137	0.2878	0.0144	
		0.975	0.5184	0.0144	0.2903	0.0137	
		0.98	0.5251	0.0097	0.2997	0.013	
		0.985	0.5319	0.0127	0.3084	0.0126	
		0.99	0.5331	0.0127	0.313	0.0139	
		0.995	0.5367	0.0123	0.3182	0.0143	
		1	0.5394	0.013	0.3235	0.0142	
		1.01	0.5488	0.0109	0.339	0.0124	
	5976	0.94	0.5239	0.0075	0.2982	0.0096	0.9908

y_1^{exp}	5145	0.95	0.5275	0.0032	0.3073	0.0042
x_1^{exp}	0.36	0.96	0.5335	0.0051	0.3184	0.0055
		0.97	0.5455	0.0029	0.337	0.003
		0.975	0.5506	0.0055	0.3484	0.007
		0.98	0.547	0.007	0.3451	0.0075
		0.985	0.5432	0.0076	0.3432	0.0071
		0.99	0.4663	0.097	0.4565	0.1004
		1	0.5222	0.0812	0.4183	0.0783
		1.015	0.4401	0.0708	0.5208	0.0824

Table A-6 –Numerical data obtained from *NpT*-GEMC simulations at 248.15 K that were used for calculating the optimum homogeneous *B* for each pressure-temperature pair by fitting the *SSQD*s to quadratic polynomials and then determining the *B* that gave the minimum error.

T / [K]	B_{RV}^{opt}	B_W^{opt}
150	0.9922	0.9929
165	0.9961	0.9914
180	0.9859	0.9858
189	0.9959	0.9941
223	0.9927	0.9922
248	0.9824	0.9832

Table A-7 - Optimum global homogeneous parameters obtained from weighted relative volatility (B_{RV}^{opt}) and weighted phase envelope width (B_W^{opt}), and plotted in Figure 5-5.

T / [K]	p / [MPa]	y_1		x_1	
223.81	1.726	0.3001	0.0074	0.0680	0.0023
	2.345	0.4818	0.0091	0.1503	0.0056
	2.961	0.5901	0.0034	0.2328	0.0031
	3.656	0.6713	0.0043	0.3344	0.0036
	4.33	0.7184	0.0030	0.4254	0.0050
	5.017	0.7542	0.0049	0.5158	0.0110
248.15	3.109	0.2308	0.0088	0.0708	0.0017
	4.02	0.3894	0.0052	0.1574	0.0024
	4.895	0.4778	0.0040	0.2398	0.0029
	5.482	0.5246	0.0073	0.2997	0.0077
	5.976	0.5464	0.0088	0.3487	0.0096

Table A-8 - Numerical data obtained from *NpT*-GEMC simulations, using the optimum temperature-dependent B parameters obtained from the relative volatility-weighted fitting and plotted in Figure 5-4.

B^V	B^L	$U^{(V+L)}$ *x* 1 x 10^4/ [K]
1	1	0
0.9985	1	-35001
1.0015	1	23743
1	0.9985	17898
1	1.0015	-38868

Table A-9 - Heterogeneous B simulation (4559 kPa, 236.17 K) data used in the multivariable linear regression to obtain heterogeneous potential energy model parameters.

T / [K]	U^V x 1x10^4/ [K]		U^L x 1x10^5/ [K]	
172.5	-1.9562	0.1160	-3.2780	0.1126
180	-1.9998	0.1425	-3.4787	0.1413
185	-1.8669	0.0718	-3.8323	0.0452
189.79	-1.9731	0.0501	-3.7419	0.0541
208.29	-2.1834	0.0982	-3.7143	0.1124
228.81	-2.3049	0.0989	-4.0017	0.1230

Table A-10 - Total potential energies obtained from *NpT*-GEMC simulations for the vapour (U^V) and liquid (U^L) phases using the standard Berthelot parameter (B = 1) and plotted in Figure 5-7.

T / [K]	ρ^V x 1x10^4/ [kg m^{-3}]		ρ^L x 1x10^5/ [kg m^{-3}]	
172.5	33.85	0.3043	1030.60	23.40
180	39.505	0.4946	1468.50	32.00
185	43.726	0.6032	1665.00	28.40
189.78	49.883	2.0351	1858.60	58.10
208.29	75.438	1.5444	2202.30	15.30
223.81	109.38	3.1087	2378.00	20.20

Table A-11 - Phase densities obtained from *NpT*-GEMC simulations for the vapour (ρ^V) and liquid (ρ^L) phases using the standard Berthelot parameter (B = 1) and plotted in Figure 5-8.

Simulation number	B^V	B^L	$U^{(V+L)}$ / 1 x 10^4 [K]
3	0.999	0.994	-7.94022
4	1.002	0.994	-9.4625
8	0.999	0.997	-4.4154
9	1.002	0.997	-8.52507
11	0.993	1	6.1131
13	0.999	1	-1.5918
14	1.002	1	-5.4354
18	0.999	1.003	3.3583
19	1.002	1.003	-1.2639
23	0.999	1.006	5.9384
24	1.002	1.006	2.2509
	1	1	0

Table A-12 - Heterogeneous B simulation (3121 kPa, 236.17 K) data used in the multivariable linear regression to obtain heterogeneous potential energy model parameters.

B^V	B^L	$U^{(V+L)}$ x 1 x 10^4/ [K]
1	1	0
0.9985	1	-35001
1.0015	1	23743
1	0.9985	17898
1	1.0015	-38868

Table A-13 - Heterogeneous B simulation (4559 kPa, 236.17 K) data used in the multivariable linear regression to obtain heterogeneous potential energy model parameters.

T / [K]	B^V	B^L	x_1	y_1	T / [K]	B^V	B^L	x_1	y_1	T / [K]	B^V	B^L	x_1	y_1
165	1.0285	1.0285	0.5853	0.9496	180	0.9801	0.9801	0.4704	0.8888	185	0.98	0.98	0.4907	0.8827
	1.0293	1.0285	0.5792	0.9464		0.9825	0.9801	0.4218	0.874		0.98	0.9825	0.5789	0.9062
	1.03	1.0285	0.5806	0.9456		0.985	0.9801	0.3679	0.8515		0.98	0.985	0.5933	0.9155
	1.0308	1.0285	0.5296	0.9361		0.9875	0.9801	0.3483	0.8481		0.98	0.9875	0.5952	0.9183
	1.0315	1.0285	0.5287	0.9348		0.9899	0.9801	0.3468	0.8427		0.98	0.99	0.5964	0.9197
	1.0285	1.0293	0.5934	0.949		0.9801	0.9825	0.5738	0.915		0.9825	0.98	0.4164	0.8597
	1.0293	1.0293	0.5794	0.9467		0.9825	0.9825	0.4854	0.8915		0.9825	0.9825	0.489	0.8787
	1.03	1.0293	0.5852	0.9482		0.985	0.9825	0.4295	0.8749		0.9825	0.985	0.5796	0.9074
	1.0308	1.0293	0.5702	0.9439		0.9875	0.9825	0.3928	0.8662		0.9825	0.9875	0.5932	0.9154
	1.0315	1.0293	0.56	0.942		0.9899	0.9825	0.3551	0.8508		0.9825	0.99	0.5955	0.9184
	1.0285	1.03	0.5934	0.9478		0.9801	0.985	0.5901	0.9227		0.985	0.98	0.3791	0.8385
	1.0293	1.03	0.5921	0.9481		0.9825	0.985	0.5784	0.9193		0.985	0.9825	0.4132	0.8544
	1.03	1.03	0.5892	0.9483		0.985	0.985	0.5079	0.8998		0.985	0.985	0.5009	0.8833
	1.0308	1.03	0.5865	0.9476		0.9875	0.985	0.44	0.8791		0.985	0.9875	0.583	0.9084
	1.0315	1.03	0.5681	0.9418		0.9899	0.985	0.3835	0.857		0.985	0.99	0.5933	0.9153
	1.0285	1.0308	0.5944	0.9514		0.9801	0.9875	0.5943	0.9249		0.9875	0.98	0.3474	0.8286
	1.0293	1.0308	0.5932	0.9501		0.9825	0.9875	0.5908	0.9236		0.9875	0.9825	0.3703	0.8365
	1.03	1.0308	0.5884	0.9513		0.985	0.9875	0.5798	0.9157		0.9875	0.985	0.4235	0.8562
	1.0308	1.0308	0.5896	0.9477		0.9875	0.9875	0.5008	0.8953		0.9875	0.9875	0.4948	0.8829
	1.0315	1.0308	0.5871	0.9448		0.9899	0.9875	0.4375	0.8789		0.9875	0.99	0.5872	0.9082
	1.0285	1.0315	0.595	0.9525		0.9801	0.9899	0.5952	0.9266		0.99	0.98	0.3244	0.8185
	1.0293	1.0315	0.5934	0.9534		0.9825	0.9899	0.5941	0.926		0.99	0.9825	0.3486	0.827
	1.03	1.0315	0.5922	0.9482		0.985	0.9899	0.5917	0.9224		0.99	0.985	0.3879	0.8431
	1.0308	1.0315	0.5919	0.9512		0.9875	0.9899	0.5726	0.9151		0.99	0.9875	0.4395	0.8644
	1.0315	1.0315	0.5884	0.9499		0.9899	0.9899	0.5161	0.9003		0.99	0.99	0.4831	0.8781

Table A-14 – Heterogenous *B* "grid" simulation data for 165 K (1200 kPa), 180 K (1750 kPa) and 185 K (2000 kPa).

T / [K]	B^V	B^L	x_1	y_1	T / [K]	B^V	B^L	x_1	y_1	T / [K]	B^V	B^L	x_1	y_1
189.78	1.008	1.008	0.4622	0.8601	208.29	0.9779	0.9779	0.2703	0.7039	260.62	0.9844	0.9844	0.3403	0.1633
	1.009	1.008	0.4538	0.8554		0.9863	0.9779	0.256	0.6893		0.9844	0.9847	0.3358	0.164
	1.01	1.008	0.4262	0.8444		0.9948	0.9779	0.253	0.6833		0.9844	0.985	0.3389	0.1681
	1.011	1.008	0.4193	0.8394		1.0032	0.9779	0.2555	0.6778		0.9844	0.9853	0.3489	0.1677
	1.012	1.008	0.4063	0.8354		1.0117	0.9779	0.2581	0.6751		0.9844	0.9856	0.3479	0.1682
	1.008	1.009	0.507	0.877		0.9779	0.9863	0.3852	0.7774		0.9847	0.9844	0.3129	0.1608
	1.009	1.009	0.4804	0.8661		0.9863	0.9863	0.2862	0.7089		0.9847	0.9847	0.3389	0.1621
	1.01	1.009	0.4499	0.8534		0.9948	0.9863	0.2644	0.6884		0.9847	0.985	0.3292	0.1579
	1.011	1.009	0.4312	0.8465		1.0032	0.9863	0.2598	0.6812		0.9847	0.9853	0.3416	0.1648
	1.012	1.009	0.4192	0.8409		1.0117	0.9863	0.2636	0.6772		0.9847	0.9856	0.3482	0.1671
	1.008	1.01	0.539	0.8883		0.9779	0.9948	0.5954	0.8772		0.985	0.9844	0.2811	0.1739
	1.009	1.01	0.5106	0.8766		0.9863	0.9948	0.4529	0.8095		0.985	0.9847	0.3341	0.1603
	1.01	1.01	0.4742	0.8649		0.9948	0.9948	0.2899	0.7076		0.985	0.985	0.3277	0.1654
	1.011	1.01	0.4533	0.855		1.0032	0.9948	0.272	0.6871		0.985	0.9853	0.3241	0.1626
	1.012	1.01	0.432	0.8461		1.0117	0.9948	0.2658	0.6814		0.985	0.9856	0.3455	0.1659
	1.008	1.011	0.5727	0.8998		0.9779	1.0032	0.5973	0.8847		0.9853	0.9844	0.3015	0.1596
	1.009	1.011	0.5387	0.8888		0.9863	1.0032	0.5956	0.8789		0.9853	0.9847	0.3395	0.1659
	1.01	1.011	0.5132	0.8791		0.9948	1.0032	0.4677	0.8172		0.9853	0.985	0.3192	0.1641
	1.011	1.011	0.4871	0.8679		1.0032	1.0032	0.3118	0.7212		0.9853	0.9853	0.3196	0.1643
	1.012	1.011	0.4461	0.8531		1.0117	1.0032	0.279	0.6906		0.9853	0.9856	0.3194	0.165
	1.008	1.012	0.5878	0.9057		0.9779	1.0117	0.5982	0.8808		0.9856	0.9844	0.3494	0.1688
	1.009	1.012	0.577	0.902		0.9863	1.0117	0.5973	0.8873		0.9856	0.9847	0.3445	0.1666
	1.01	1.012	0.5441	0.8898		0.9948	1.0117	0.5956	0.8819		0.9856	0.985	0.3415	0.1665
	1.011	1.012	0.5205	0.8813		1.0032	1.0117	0.4936	0.8298		0.9856	0.9853	0.3147	0.1586
	1.012	1.012	0.4673	0.8631		1.0117	1.0117	0.3268	0.7251		0.9856	0.9856	0.3263	0.1624

Table A-15 – Heterogenous *B* "grid" simulation data for 189.78 K (2073 kPa), 208.29 K (2411 kPa) and 260.62 K (5105 kPa).

A.2 Matlab routines

Subroutine 1 - Generating the false-colour surfaces for heterogeneous simulation data using 165 K (Table A-14) as an example.

```
load grid165.txt
ppp = length(grid165);
ydim = sqrt(ppp);
Bvmat=[grid165(1:ydim,1),grid165(ydim+1:2*ydim,1),grid165(2*ydim+1:3*ydim,1),.
..
    grid165(3*ydim+1:4*ydim,1),grid165(4*ydim+1:5*ydim,1)];
Blmat=[grid165(1:ydim,2),grid165(ydim+1:2*ydim,2),grid165(2*ydim+1:3*ydim,2),.
..
    grid165(3*ydim+1:4*ydim,2),grid165(4*ydim+1:5*ydim,2)];

xlin = linspace(min(Blmat(1,:)),max(Blmat(1,:)),800);
ylin = linspace(min(Blmat(1,:)),max(Blmat(1,:)),800);
[X165, Y165]=meshgrid(xlin,ylin);

Z165 = griddata(grid165(:,1),grid165(:,2),grid165(:,5),X165,Y165,'cubic');
h=fig('units','inches','width',9.724,'height',5.9,'font','Helvetica','fontsize
',10)
subplot(2,4,1)
pcolor(X165,Y165,Z165)

% colorbar('location','northoutside')
shading interp
% axis tight
% axis equal
axis square
```

Subroutine 2 – Heterogeneous potential energy model data regression, using 236.17 K (4559 kPa) as an example.

```
% SURFACE REGRESSION TO THOSE POINTS JUST AROUND (1.00,1.00)
% indexvec contains the numbers ("identities") of the simulations that gave
good linear trends with respect to the base-case Lorentz-Berthelot
simulation(BV = Bl = 1)

indexvec=[3 4 8 9 11 13 14 18 19 23 24];

energv=fv;
energl=fl;

zetaV=[zetav(indexvec); 1];
zetaV=zetaV-1;
zetaL=[zetal(indexvec); 1];
zetaL=zetaL-1;
% linear regression without interaction term
X=[ones(12,1) zetaV zetaL];

% vapour
yv=[energv(indexvec)./1e4; 0];
% liquid
yl=[energl(indexvec)./1e4; 0];
% total
y=yv+yl;
bv=regress(yv,X)
bl=regress(yl,X)
bt=regress(y,X);
```

```
% use a 95% confidence interval
alpha = 0.05;
[betahat,Ibeta,res,Ires,stats] = regress(y,X,alpha);

figure
% residual plot
rcoplot(res,Ires)
sumofresids=sum(res)
% extract R-squared value
stats1=stats(1)


h1=fig('units','centimeters','width',20.0,'height',6.0,'font','Helvetica','fon
tsize',10);
subplot(1,3,1)
scatter3(zetaV,zetaL,yv,'filled')
hold on
x1fit = linspace(min(zetaV),max(zetaV),100);
x2fit = linspace(min(zetaL),max(zetaL),100);
[X1FIT,X2FIT] = meshgrid(x1fit,x2fit);
YFIT = bv(1)+bv(2)*X1FIT + bv(3)*X2FIT;
meshc(X1FIT,X2FIT,YFIT)
axis tight
axis square
box on
grid off
xlabel('({\itB}^V - 1)')
ylabel('({\itB}^L - 1)')
zlabel('{\itU}_1_2^V / [K]')
hold on
%
subplot(1,3,2)
scatter3(zetaV,zetaL,yl,'filled')
hold on
x1fit = linspace(min(zetaV),max(zetaV),50);
x2fit = linspace(min(zetaL),max(zetaL),50);
[X1FIT,X2FIT] = meshgrid(x1fit,x2fit);
YFIT = bl(1)+bl(2)*X1FIT + bl(3)*X2FIT;
meshc(X1FIT,X2FIT,YFIT)
axis tight
axis square
box on
grid off
xlabel('({\itB}^V - 1)')
ylabel('({\itB}^L - 1)')
zlabel('{\itU}_1_2^L / [K]')
hold on
%
subplot(1,3,3)
scatter3(zetaV,zetaL,y,'filled')
hold on
x1fit = linspace(min(zetaV),max(zetaV),50);
x2fit = linspace(min(zetaL),max(zetaL),50);
[X1FIT,X2FIT] = meshgrid(x1fit,x2fit);
YFIT = bt(1)+bt(2)*X1FIT + bt(3)*X2FIT;
meshc(X1FIT,X2FIT,YFIT)
axis tight
axis square
box on
grid off
xlabel('({\itB}^V - 1)')
ylabel('({\itB}^L - 1)')
zlabel('{\itU}_1_2 / [K]')
hold on
```

Appendix B

Supplementary figures

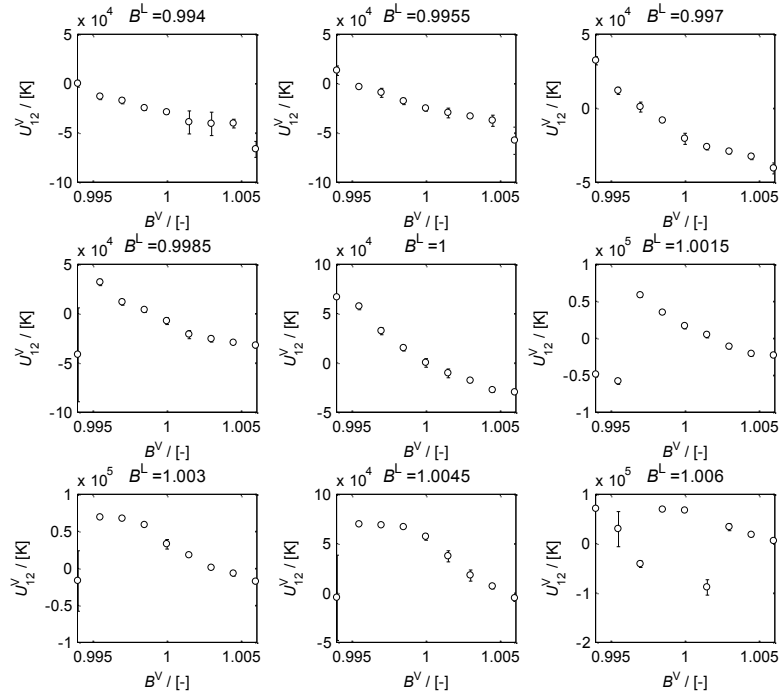

Figure B-1 – Variations of the vapour-phase energy contributions to the base-case Lorentz-Berthelot system ($B^V = B^L = 1$) at (236.17 K, 4559 kPa).

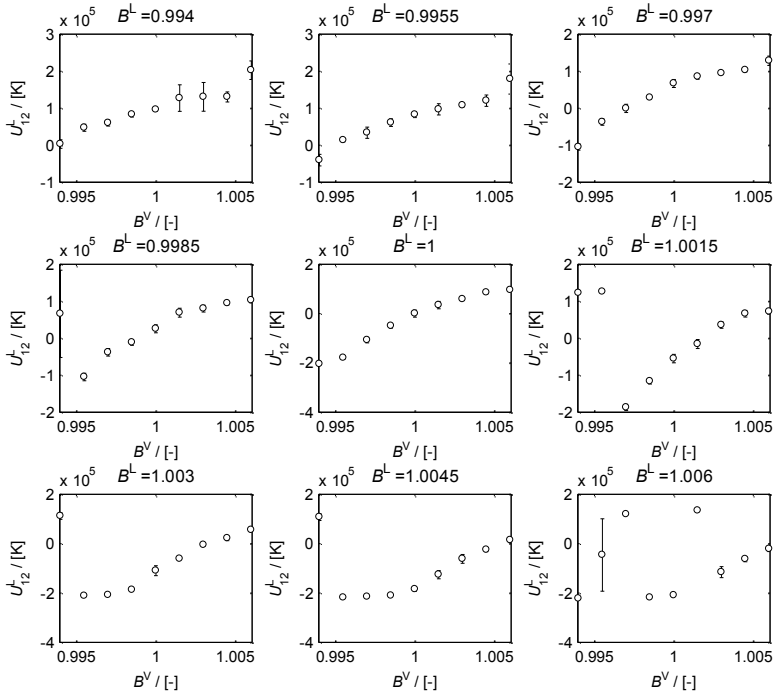

Figure B-2 – Variations of the liquid-phase energy contributions to the base-case Lorentz-Berthelot system ($B^V = B^L = 1$) at (236.17 K, 4559 kPa).

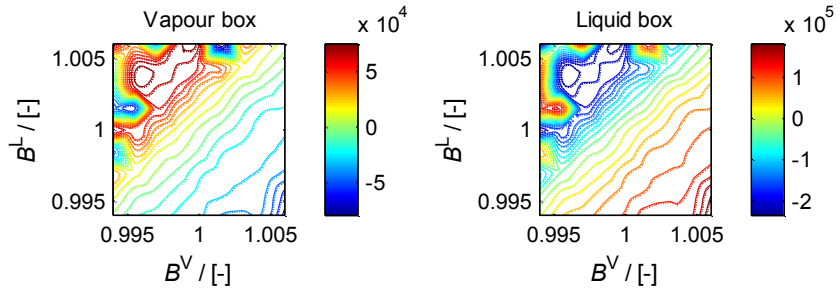

Figure B-3 – Contours of the vapour- and liquid-phase energy contributions to the base-case Lorentz-Berthelot system ($B^V = B^L = 1$) at (236.17 K, 4559 kPa). The energy unit is Kelvin [K].

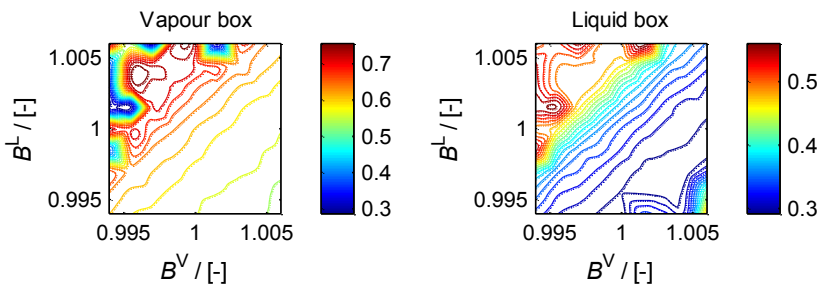

Figure B-4 – Contours of the vapour- and liquid-phase compositions (mole fractions) using methane as the reference component at (236.17 K, 4559 kPa).

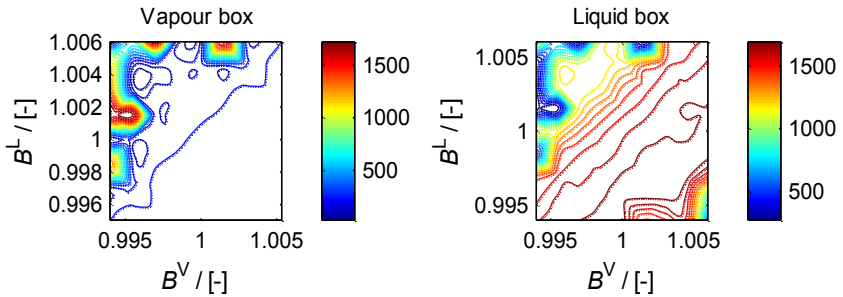

Figure B-5 – Contours of the vapour- and liquid-phase specific densities at (236.17 K, 4559 kPa) in [kg. m^{-3}]

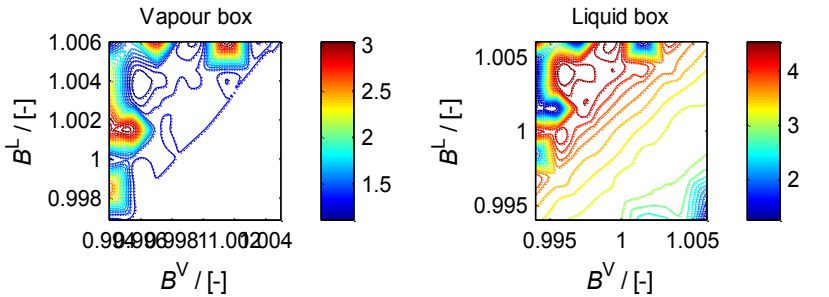

Figure B-6 – Contours of the vapour- and liquid-phase number densities of methane at (236.17 K, 4559 kPa) in [number of methane molecules. nm^{-3}]

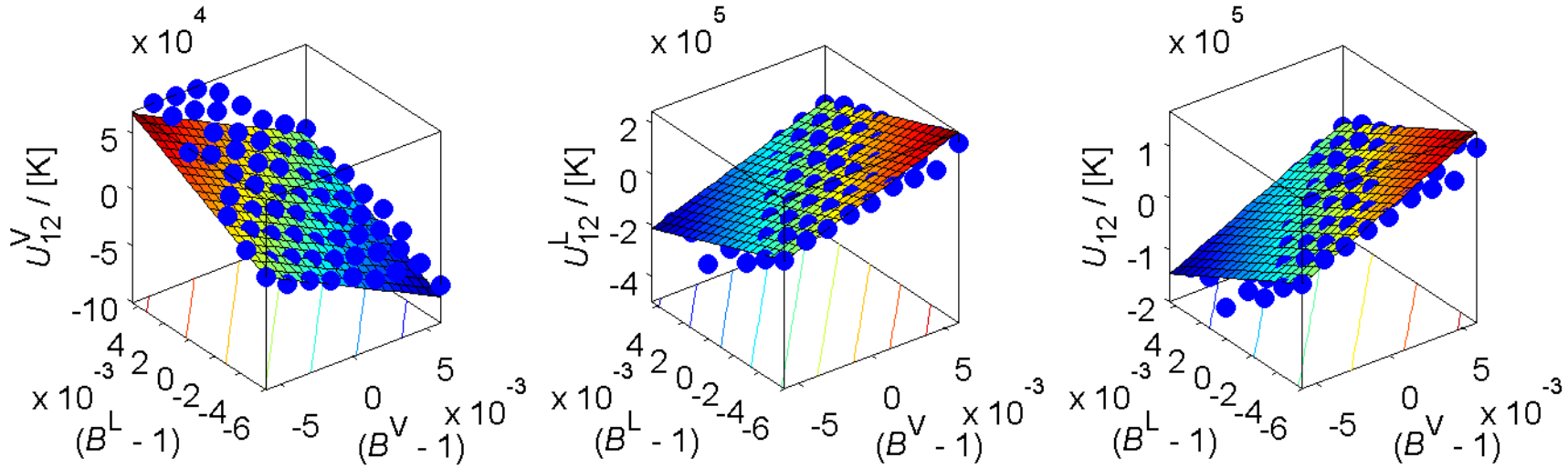

Figure B-7 – Comparison between the energy contributions at (236 K, 4559 kPa) in the vapour, liquid and overall system (vapour + liquid) due to heterogeneous perturbations from simulations (blue dots) with the surface predicted by the model proposed in this work (see Chapter 5), using results from the 81 simulations at this state point.

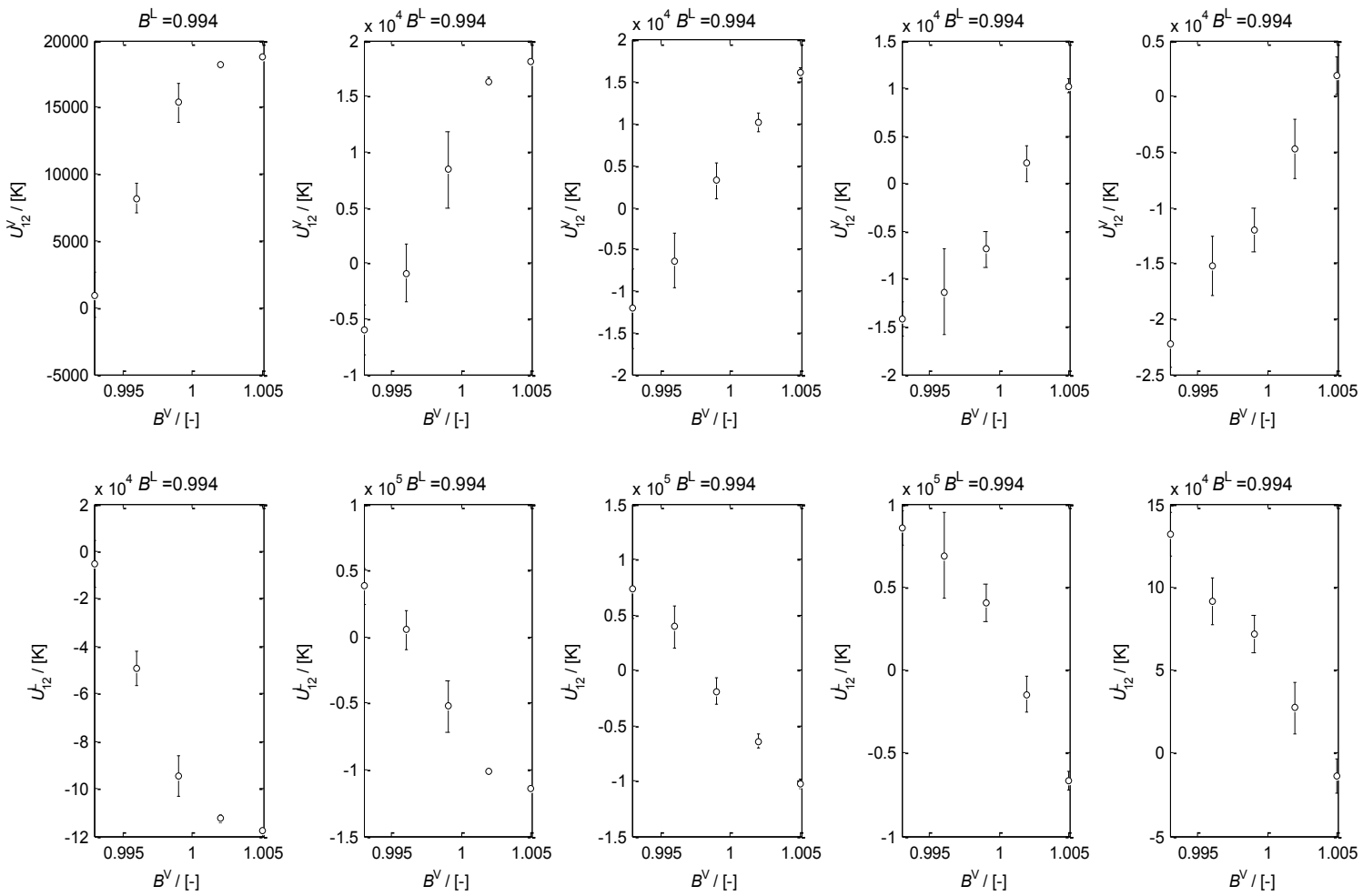

Figure B-8 – Variations of the vapour- and liquid-phase energy contributions to the base-case Lorentz-Berthelot system ($B^V = B^L = 1$) at (236.17 K, 3121 kPa).

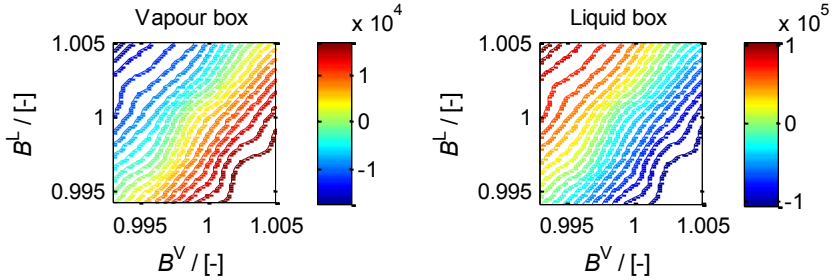

Figure B-9 – Contours of the vapour- and liquid-phase energy contributions to the base-case Lorentz-Berthelot system ($B^V = B^L = 1$) at (236.17 K, 3121 kPa). The energy unit is Kelvin [K].

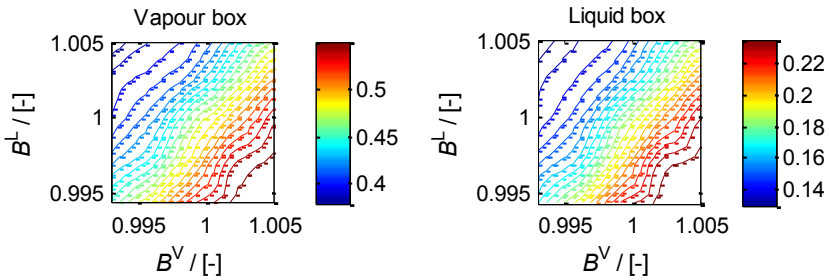

Figure B-10 – Contours of the vapour- and liquid-phase compositions (mole fractions) using methane as the reference component at (236.17 K, 3121 kPa).

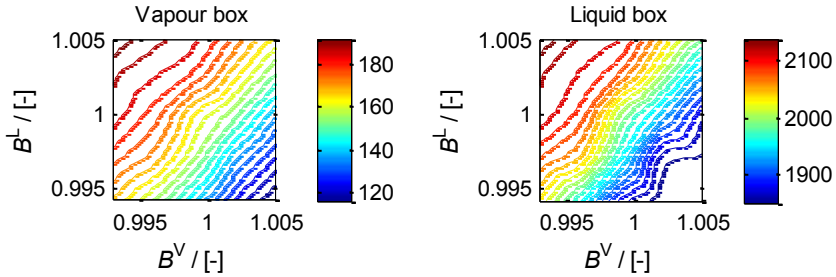

Figure B-11 – Contours of the vapour- and liquid-phase specific densities at (236.17 K, 3121 kPa) in [kg. m^{-3}]

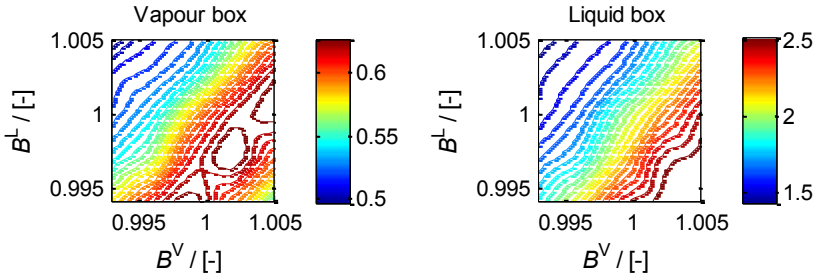

Figure B-12 – Contours of the vapour- and liquid-phase number densities of methane at (236.17 K, 3121 kPa) in [number of methane molecules. nm^{-3}]

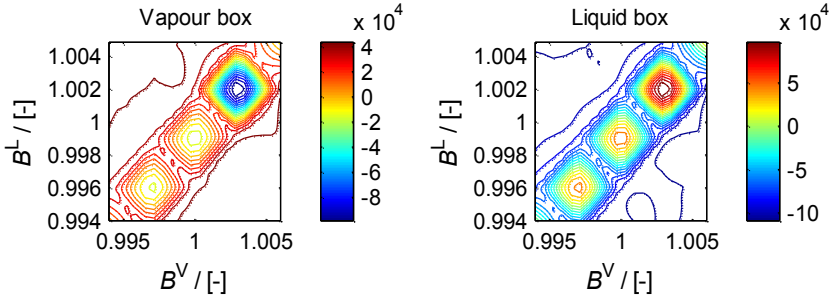

Figure B-13 – Contours of the vapour- and liquid-phase energy contributions to the base-case Lorentz-Berthelot system ($B^V = B^L = 1$) at (236.17 K, 5290 kPa). The energy unit is Kelvin [K].

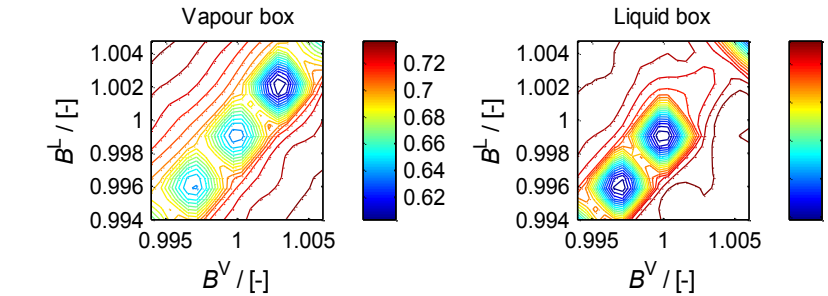

Figure B-14 – Contours of the vapour- and liquid-phase compositions (mole fractions) using methane as the reference component at (236.17 K, 5290 kPa).

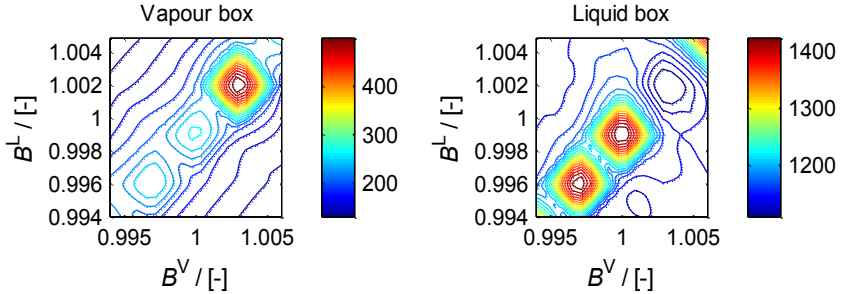

Figure B-15 – Contours of the vapour- and liquid-phase specific densities at (236.17 K, 5290 kPa) in [kg. m^{-3}]

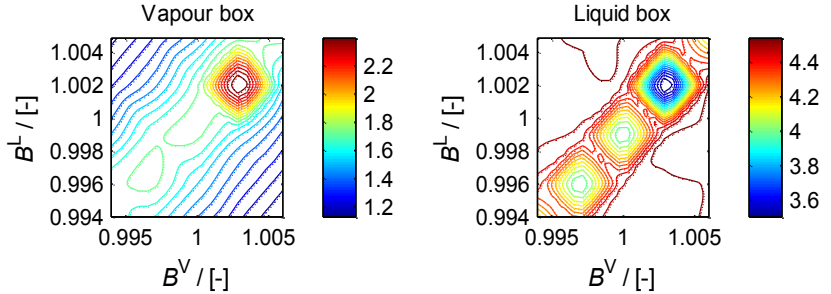

Figure B-16 – Contours of the vapour- and liquid-phase number densities of methane at (236.17 K, 5290 kPa) in [number of methane molecules. nm^{-3}]

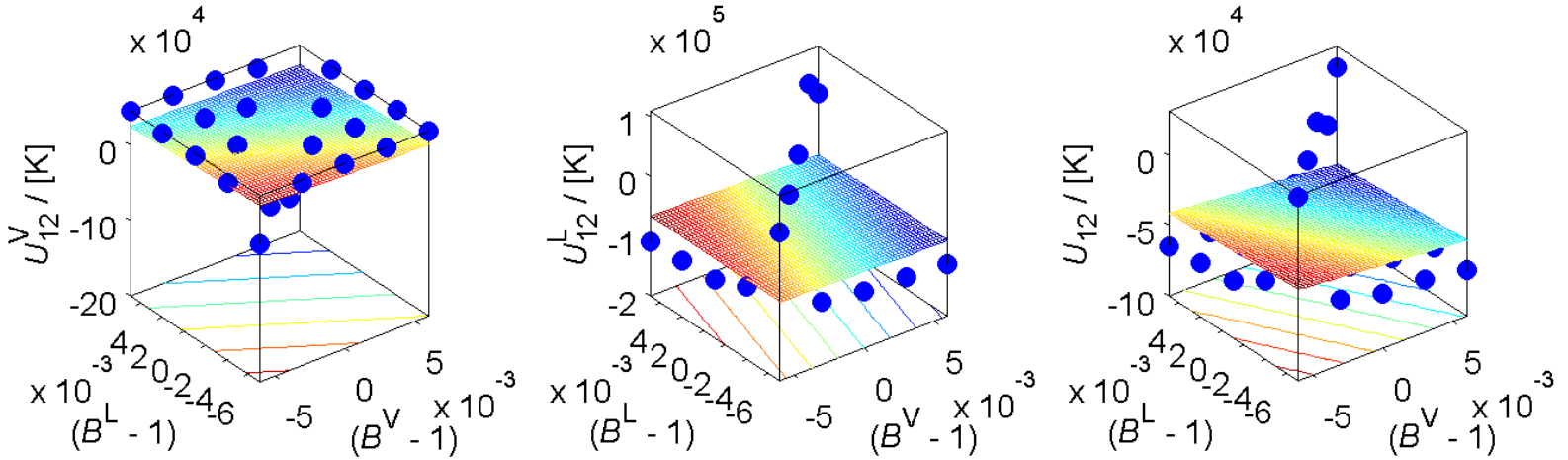

Figure B-17 – Comparison between the energy contributions at (236 K, 5290 kPa) in the vapour, liquid and overall system (vapour + liquid) due to heterogeneous perturbations from simulations (blue dots) with the surface predicted by the model proposed in this work (see Chapter 5), using results from the 25 simulations for this state point.

Appendix C

FORTRAN code modifications and subroutines written for this work

C1. Modifications of MCCCS Towhee code for implementation of heterogeneous cross-energies

File: *mymodule.F*
This file contains global variables and was added to the existing code for the purposes of this work.
N.B. Lines containing "c # ..." strings are comment lines.

```
      module mymodule
      implicit none
      save
c     # vapour phase LJ cross-energy multiplying factor
      double precision :: myBvalvb
c     # liquid phase LJ cross-energy multiplying factor
      double precision :: myBvallb
c     # array for storing simplex (in this case, a 2-dimensional
triangle) coordinates as (BV,BL)
      double precision Rsimplex(3,2)
c     # the box in which the energy is being computed
      integer :: CurrentBox
c     # the frequency at which the simplex is updated
      integer :: bupdate
      integer :: theInnerCycl
      logical :: lBresume
      end module mymodule
```

File: *engtotal.F*
Corrections to the tail cross-energies, except for inter-box molecule swaps, are done here.
N.B. Lines containing "c # ..." strings are comment lines.

```
      subroutine twh_engtotal_tail(vtail, ibox)
      use mymodule
...
[...other variable declarations]
...
      double precision [...some other variables], tailBf

...
c     # heterogenous tail energy corrections
      if (imolty .ne. jmolty) then
        if (ibox .eq. 1) then
          tailBf = myBvalvb
        elseif (ibox .eq. 2) then
          tailBf = myBvallb
        else
          write(777,*) 'SM: engtotal- vtail error: more than 2 boxes in
simulation
        endif
      else
          tailBf = 1.0d0
c     # initial debugging check
c         write(888,*) 'No correction'
      endif

c     ## end of B-factor correction
          vtail = vtail + dble(ncmt)*rho*coru*tailBf
...
[...other program statements]

...
      return
      end
```

On line 452:

```
          CurrentBox = ibox
```

File: *swapmoves.F*
Corrections to the tail cross-energies for inter-box molecule swaps are done here.
N.B. Lines containing "c # ..." strings are comment lines. The following code snippet was added on line 897.

```
      subroutine twh_swapmoves(lfailure,swaptype,inmoltype,inbox)
      use mymodule
...
[...other variable declarations]

...
      double precision [...some other variables], swapBf

 [...other program statements]
...
c     # heterogenous tail energy corrections for swap moves
                  if (imt .ne. jmt) then
                    if (activebox .eq. 1) then
                      swapBf = myBvalvb
                    elseif (activebox .eq. 2) then
                      swapBf = myBvallb
                    else
                      write(965,*) 'swapmoves.F: error > 3 boxes'
                    endif
                  else
                      swapBf = 1.0d0
                  endif
c     ## End of B-factor correction
                  if ( imt .eq. imolty ) then
                    vtailtest(icordflag) = vtailtest(icordflag) +
     &                   dble(ncmt + mcount)*rho*coru*swapBf
                  else
                    vtailtest(icordflag) = vtailtest(icordflag) +
     &                   dble(ncmt)*rho*coru*swapBf
                  endif
                enddo
              enddo
[...other program statements]
```

File: *vtwobody.F*
Modifications to the Lennard-Jones two-body potential energy.
N.B. Lines containing "c # ..." strings are comment lines.

```
      double precision function vtb_lennard_jones(ntij, rijsq, lonefour)
      use mymodule

      double precision srsix,tbljBf

c     # cross-energy multiplying factors. 407 and 404 are the
methane-xenon cross-energy
c     # "identity" integers generated within the Towhee source code.

      if ((ntij .eq. 407) .or. (ntij .eq. 404)) then
        if (CurrentBox .eq. 1) then
          tbljBf = myBvalvb
c           write(888,*) 'Box 1 407'
        elseif (CurrentBox .eq. 2) then
          tbljBf = myBvallb
c           write(888,*) 'Box 2 407'
        else
          write(777,*) 'SM: vtb_lennard_jones error'
        endif
```

```
      else
           tbljBf = 1.0d0
c            write(888,*) 'No correction'
      endif
c     ## End of B-factor correction

      if ( lonefour ) then
c      write(898,*) 'lonefour = true'

         srsix = twh_get_nbcoeff(15,ntij) / (rijsq**3)
         vtb_lennard_jones = srsix*(srsix-1.0d0)
     &        *twh_get_nbcoeff(16,ntij)*tbljBf

         call twh_lshift(GLB_GET,lshift)
         if ( lshift ) then
            vtb_lennard_jones = vtb_lennard_jones
     &           - twh_get_nbcoeff(0,ntij)
         endif
      else
c        write(889,*) 'tbljBf',tbljBf
         srsix = twh_get_nbcoeff(13,ntij) / (rijsq**3)
         vtb_lennard_jones = srsix*(srsix-1.0d0)
     &        *twh_get_nbcoeff(14,ntij)*tbljBf
         call twh_lshift(GLB_GET,lshift)
         if ( lshift ) then
            vtb_lennard_jones = vtb_lennard_jones
     &           - twh_get_nbcoeff(0,ntij)
         endif
      endif

      return
      end
```

File: *readtowhee.F*
Reads the energy correction factors which are then stored by mymodule(.F).
N.B. Lines containing "c # ..." strings are comment lines.

```
      subroutine twh_readtowhee(lfailure,atomcount)
      use mymodule

c     # Read B-factors
      myBvalvb = twh_read_labeled_float(4,'myBvalvb',.true.,
     &    idname)
      myBvallb = twh_read_labeled_float(4,'myBvallb',.true.,
     &    idname)
c     ## End
```

File: *stresstensor.F*
Tail cross-energy corrections to intermolecular pair virial function divided by r^2.
N.B. Lines containing "c # ..." strings are comment lines. The following code snippet was added on line 281.

```
      subroutine twh_stresstensor(lfailure,stress,ibox)
      use mymodule

      double precision boxvolume,tailpBf

c     ## SM2010 12-Aug
      if (imolty .ne. jmolty) then
        if (ibox .eq. 1) then
          tailpBf = myBvalvb
        elseif (ibox .eq. 2) then
          tailpBf = myBvallb
        else
          write(777,*) 'SM: stresstensor- more than 2 boxes'
        endif
      else
          tailpBf = 1.0d0
c           write(888,*) 'No correction'
      endif
c     ## End of B-factor correction
            stress(7) = stress(7) + rhosq*corp*tailpBf
          enddo
        enddo
        stress(7) = CON_PRESSCONST*stress(7)
      endif
```

On L185:
CurrentBox = ibox

File: *wtwobody.F*
Cross-energy corrections to intermolecular pair virial function divided by r^2.
N.B. Lines containing "c # ..." strings are comment lines.

```
      double precision function wtb_lennard_jones(ntij, rijsq)
      use mymodule

      double precision srsix,pvfljBf
```

```
c     ## SM2010 12-Aug
      if ((ntij .eq. 407) .or. (ntij .eq. 404)) then
        if (CurrentBox .eq. 1) then
          pvfljBf = myBvalvb
c           write(888,*) 'Box 1 407'
        elseif (CurrentBox .eq. 2) then
          pvfljBf = myBvallb
c           write(888,*) 'Box 2 407'
        else
          write(777,*) 'SM: wtb_lennard_jones err; > 2 boxes in sim'
        endif
      else
          pvfljBf = 1.00d0
c           write(888,*) 'No correction'
      endif
c     ## End of B-factor correction

      srsix = twh_get_nbcoeff(13,ntij) / (rijsq**3)
      wtb_lennard_jones = twh_get_nbcoeff(14,ntij)*pvfljBf
     &    *12.0d0*srsix*(0.5d0-srsix) / rijsq

      return
      end
```

C2. Modifications of MCCCS Towhee code for implementation of simplex algorithm to find optimum heterogeneous cross-energy correction factors

File: *readtowhee.F*
Reads the energy correction factors which are then stored by mymodule(.F), as well as the simplex update frequency.
N.B. Lines containing "c # ..." strings are comment lines.

```
      subroutine twh_readtowhee(lfailure,atomcount)
      use mymodule

c     # Read B-factors
      myBvalvb = twh_read_labeled_float(4,'myBvalvb',.true.,
     &    idname)
      myBvallb = twh_read_labeled_float(4,'myBvallb',.true.,
```

```
     &    idname)
      bupfreq = twh_read_labeled_integer(4,'bupfreq',.true.,
     &    idname)
c     ## End
```

File: *mainloop.F*

Contains the simplex algorithm and also determines when the simplex should be transformed (expansion, contraction, shrink or reflection).

N.B. Lines containing "c # ..." strings are comment lines.

```
c     On line 759
c     --- check whether we need to call the LJ epsilon modifier
c     --- subroutine //Suren Moodley
       iiii = nnn
c       myCycleCount = iiii
c       write(953,*) iiii
       if (mod(nnn,bupfreq)==0) then
c          if (Bcount .gt. 0) then
c            call twh_averages(lfailure,AVG_EXTRACT_BLOCK_VAL
c     &             ,keycode,1,1,currblksolu,Bcount)
             Bcount = Bcount + 1
c          endif
c            write(969,*) currblksolu
            call suren(nnn,Bcount)
       end if

      enddo

Line 99
      integer outputlocation,outputmode,pstyle,Bcount,iiii

c     On line 373
      Bcount = 0

      subroutine twh_mainloop(outputlocation,outputmode,
     &   lread_wrapper,pstyle)
c     ***********************************************************************
      use mymodule


c       ### Simplex optimization routine written by Suren Moodley
###
       subroutine suren(nnn,Bcount)
       use mymodule
```

```
       implicit none
#define FUNCTION_LIMITED_DOUBLE
#define FUNCTION_RANDOM
#include "functions.h"
c     ### variables passed to/from the subroutine
      logical lfailure,lBflag
      integer nnn,Bcount,iptrB,iB,jjjj
      integer nmolty,numboxes
c     ### local variables
c     ### logical scalars
      logical, save :: lReflDone,lExpndDone,lContrDone,lShrinkDone
      logical, save :: lCtOuter,lCtInner
c     ### integer scalars
      integer incount,keycode,xxbox,yymolty,Bcseed,nstep
      integer imolty,jmolty,ii,jj,ntii,ntjj,ntij,hbtype,classical_n
      integer numiunit,numjunit,molvcount,Bincr
      integer, save :: ShrinkCount
c     ### double precision scalars
      double precision xyzvalue,molfrave1,molfrave2,stddevmolf1
      double precision
termobj1,termobj2,relerror,ssqmoldev,stddevmolf2
      double precision rci3,ndub,overra,onepi,aaa,bbb,twopi,dvalue
      double precision rcut,LJEcorr,tempFeval,tempBB,ssqmoldev2
      double precision, parameter :: AlphaB = 0.50d0
      double precision, parameter :: BetaB = 0.80d0
      double precision, parameter :: GammaB = 1.1250d0
      double precision, parameter :: DeltaB = 0.8250d0
      double precision :: diffmolfrc
c     ### double precision arrays
      double precision molvector1(11),molvector2(11)
      double precision, save :: prvmolfrc(100)
      double precision, save :: molfold(2,2), molfnew(2,2)
      double precision, save :: Blast(2),SimHist(100,3)
      double precision, save ::
bFHI(1,3),bFMD(1,3),bFLO(1,3),bRef(1,3)
      double precision, save :: bExp(1,3),bCont(1,3),bShr(1,3)
      double precision, save :: bCentroid(1,2)
      double precision, save :: simplex(3,3),simpplus(4,3)
      double precision, save :: Bold(2),Bnew(2)
      double precision, save :: Bhistory(2,10),Chistory(2,10)
      double precision, save ::
Clatest(2),ReflectM(1,3),ExpandM(1,3)
      double precision, save :: CntrctM(1,3),ShrinkM1(1,3)
      double precision, save :: ShrinkM2(1,3)
      double precision, save :: ExpData(2)
```

```
c     ### retrieve constants
      call twh_numboxes(GLB_GET,numboxes)
      call twh_nmolty(GLB_GET,nmolty)
      call twh_nstep(GLB_GET,nstep)
      call twh_constant_pi(GLB_GET,onepi)
      call twh_constant_twopi(GLB_GET,twopi)
      call twh_nmolty(GLB_GET,nmolty)
      call twh_rcut(GLB_GET,rcut)
       write(994,*) 'u must nt c this if bupdate > than nsteps'
c     ### initialize parameters
       ExpData(1)=0.6310d0
       ExpData(2)=0.4340d0
c     ### these are the experimental solubilties of component 1 in
the
c     ### vapor (1) and liquid (2) phases.

c     ### algorithm-proper begins!

      if (Bcount .eq. 1) then

      molvcount = 1
      do Bincr = 20*Bcount, (20*Bcount-10), -1
        do xxbox = 1,numboxes
          do yymolty = 1,nmolty
            keycode = AC_MOL_FRACTION
              call
twh_averages(lfailure,AVG_EXTRACT_BLOCK_VAL
     &          ,keycode,xxbox,yymolty,xyzvalue,Bincr)
                molfnew(xxbox,yymolty) = xyzvalue
                molvector1(molvcount) = molfnew(1,1)
                molvector2(molvcount) = molfnew(2,1)
          enddo
        enddo
        molvcount = molvcount+1
      enddo

      molfrave1 = (molvector1(1) + molvector1(2) + molvector1(3)
     &          + molvector1(4) + molvector1(5) + molvector1(6)
     & + molvector1(7) + molvector1(8) + molvector1(9))/9.0d0
      ssqmoldev = ((molvector1(1) - molfrave1)**2.0d0
     &          + (molvector1(2) - molfrave1)**2.0d0
     &          + (molvector1(3) - molfrave1)**2.0d0
     &          + (molvector1(4) - molfrave1)**2.0d0
     &          + (molvector1(5) - molfrave1)**2.0d0
     &          + (molvector1(6) - molfrave1)**2.0d0
     &          + (molvector1(7) - molfrave1)**2.0d0
```

```
     &           + (molvector1(8) - molfrave1)**2.0d0
     &           + (molvector1(9) - molfrave1)**2.0d0)
      stddevmolf1 = dsqrt((1.0d0/9.0d0)*ssqmoldev)

      molfrave2 = (molvector2(1) + molvector2(2) + molvector2(3)
     &           + molvector2(4) + molvector2(5) + molvector2(6)
     &  + molvector2(7) + molvector2(8) + molvector2(9))/9.0d0
      ssqmoldev2 = ((molvector2(1) - molfrave2)**2.0d0
     &           + (molvector2(2) - molfrave2)**2.0d0
     &           + (molvector2(3) - molfrave2)**2.0d0
     &           + (molvector2(4) - molfrave2)**2.0d0
     &           + (molvector2(5) - molfrave2)**2.0d0
     &           + (molvector2(6) - molfrave2)**2.0d0
     &           + (molvector2(7) - molfrave2)**2.0d0
     &           + (molvector2(8) - molfrave2)**2.0d0
     &           + (molvector2(9) - molfrave2)**2.0d0)
      stddevmolf2 = dsqrt((1.0d0/9.0d0)*ssqmoldev2)

c    # write some vals to file
      open(963, file = 'out95.suren', position = 'append')
      write(963,*) 'Bcount: ',Bcount
      write(963,*) 'molvector1',molvector1(1),molvector1(2)
     &           ,molvector1(3),molvector1(4),molvector1(5)
      write(963,*) 'molvector2',molvector2(1),molvector2(2)
     &           ,molvector2(3),molvector2(4),molvector2(5)
      write(963,*) 'ave mole fraction Box
1',molfrave1,'Bvap',myBvalvb
      write(963,*) 'ave mole fraction Box 2',molfrave2,'Bliq',myBvallb
      write(963,*) 'sum of deviations squared',ssqmoldev
      write(963,*) 'standard deviation',stddevmolf1
      close(963)
c    # end of write
c    # must modify these when using reduced quantities (eij/e11
etc)
      if ((stddevmolf1 .gt. 0.0250d0) .or.
     & (stddevmolf2 .gt. 0.0250d0)) then
      open(963, file = 'out95.suren', position = 'append')
      write(963,*) 'sd1',stddevmolf1,'sd2',stddevmolf2,'...exiting'
      close(963)
        return
      else

c     ### will need to implement weight factors in future versions
       termobj1 = (1-(molfrave1/ExpData(1)))**2.0d0
       termobj2 = (1-(molfrave2/ExpData(2)))**2.0d0
       SimHist(Bcount,3) = dsqrt(termobj1 + termobj2)
       SimHist(Bcount,1) = myBvalvb
       SimHist(Bcount,2) = myBvallb
      write(709,*)  SimHist(Bcount,1),SimHist(Bcount,2)
       simplex(Bcount,1) = myBvalvb
       simplex(Bcount,2) = myBvallb
       simplex(Bcount,3) = SimHist(Bcount,3)

       myBvalvb = 0.9930d0
       myBvallb = 0.9910d0
      endif

      elseif (Bcount .eq. 2) then
      molvcount = 1
      do Bincr = 20*Bcount, (20*Bcount-10), -1
        do xxbox = 1,numboxes
          do yymolty = 1,nmolty
            keycode = AC_MOL_FRACTION
              call
twh_averages(lfailure,AVG_EXTRACT_BLOCK_VAL
     &          ,keycode,xxbox,yymolty,xyzvalue,Bincr)
                molfnew(xxbox,yymolty) = xyzvalue
                molvector1(molvcount) = molfnew(1,1)
                molvector2(molvcount) = molfnew(2,1)
          enddo
        enddo
        molvcount = molvcount+1
      enddo

      molfrave1 = (molvector1(1) + molvector1(2) + molvector1(3)
     &           + molvector1(4) + molvector1(5) + molvector1(6)
     & + molvector1(7) + molvector1(8) + molvector1(9))/9.0d0
      ssqmoldev = ((molvector1(1) - molfrave1)**2.0d0
     &           + (molvector1(2) - molfrave1)**2.0d0
     &           + (molvector1(3) - molfrave1)**2.0d0
     &           + (molvector1(4) - molfrave1)**2.0d0
     &           + (molvector1(5) - molfrave1)**2.0d0
     &           + (molvector1(6) - molfrave1)**2.0d0
     &           + (molvector1(7) - molfrave1)**2.0d0
     &           + (molvector1(8) - molfrave1)**2.0d0
     &           + (molvector1(9) - molfrave1)**2.0d0)

      molfrave2 = (molvector2(1) + molvector2(2) + molvector2(3)
     &           + molvector2(4) + molvector2(5) + molvector2(6)
     &  + molvector2(7) + molvector2(8) + molvector2(9))/9.0d0
      ssqmoldev2 = ((molvector2(1) - molfrave2)**2.0d0
     &           + (molvector2(2) - molfrave2)**2.0d0
     &           + (molvector2(3) - molfrave2)**2.0d0
     &           + (molvector2(4) - molfrave2)**2.0d0
     &           + (molvector2(5) - molfrave2)**2.0d0
     &           + (molvector2(6) - molfrave2)**2.0d0
     &           + (molvector2(7) - molfrave2)**2.0d0
     &           + (molvector2(8) - molfrave2)**2.0d0
     &           + (molvector2(9) - molfrave2)**2.0d0)
      stddevmolf2 = dsqrt((1.0d0/9.0d0)*ssqmoldev2)

c    # write some vals to file
      open(963, file = 'out95.suren', position = 'append')
      write(963,*) 'Bcount: ',Bcount
      write(963,*) 'molvector1',molvector1(1),molvector1(2)
     &           ,molvector1(3),molvector1(4),molvector1(5)
      write(963,*) 'molvector2',molvector2(1),molvector2(2)
     &           ,molvector2(3),molvector2(4),molvector2(5)
      write(963,*) 'ave mole fraction Box
1',molfrave1,'Bvap',myBvalvb
      write(963,*) 'ave mole fraction Box 2',molfrave2,'Bliq',myBvallb
      write(963,*) 'sum of deviations squared',ssqmoldev
      write(963,*) 'standard deviation',stddevmolf1
      close(963)
c    # end of write
      if ((stddevmolf1 .gt. 0.010d0) .or.
     & (stddevmolf2 .gt. 0.010d0)) then
      open(963, file = 'out95.suren', position = 'append')
      write(963,*) 'sd1',stddevmolf1,'sd2',stddevmolf2,'...exiting'
      close(963)
        return
      else
       termobj1 = (1-(molfrave1/ExpData(1)))**2.0d0
       termobj2 = (1-(molfrave2/ExpData(2)))**2.0d0

       SimHist(Bcount,3) = dsqrt(termobj1 + termobj2)

       SimHist(Bcount,1) = myBvalvb
       SimHist(Bcount,2) = myBvallb

       simplex(Bcount,1) = myBvalvb
       simplex(Bcount,2) = myBvallb
       simplex(Bcount,3) = SimHist(Bcount,3)
      write(709,*)  SimHist(Bcount,1),SimHist(Bcount,2)
       myBvalvb = 0.99150d0
       myBvallb = 0.99250d0
      endif
```

```
      elseif (Bcount .eq. 3) then
      molvcount = 1
      do Bincr = 20*Bcount, (20*Bcount-10), -1
        do xxbox = 1,numboxes
          do yymolty = 1,nmolty
            keycode = AC_MOL_FRACTION
              call
twh_averages(lfailure,AVG_EXTRACT_BLOCK_VAL
     &           ,keycode,xxbox,yymolty,xyzvalue,Bincr)
               molfnew(xxbox,yymolty) = xyzvalue
               molvector1(molvcount) = molfnew(1,1)
               molvector2(molvcount) = molfnew(2,1)
          enddo
        enddo
        molvcount = molvcount+1
      enddo

      molfrave1 = (molvector1(1) + molvector1(2) + molvector1(3)
     &           + molvector1(4) + molvector1(5) + molvector1(6)
     & + molvector1(7) + molvector1(8) + molvector1(9))/9.0d0
      ssqmoldev = ((molvector1(1) - molfrave1)**2.0d0
     &           + (molvector1(2) - molfrave1)**2.0d0
     &           + (molvector1(3) - molfrave1)**2.0d0
     &           + (molvector1(4) - molfrave1)**2.0d0
     &           + (molvector1(5) - molfrave1)**2.0d0
     &           + (molvector1(6) - molfrave1)**2.0d0
     &           + (molvector1(7) - molfrave1)**2.0d0
     &           + (molvector1(8) - molfrave1)**2.0d0
     &           + (molvector1(9) - molfrave1)**2.0d0)
       stddevmolf1 = dsqrt((1.0d0/9.0d0)*ssqmoldev)

      molfrave2 = (molvector2(1) + molvector2(2) + molvector2(3)
     &           + molvector2(4) + molvector2(5) + molvector2(6)
     &  + molvector2(7) + molvector2(8) + molvector2(9))/9.0d0
      ssqmoldev2 = ((molvector2(1) - molfrave2)**2.0d0
     &           + (molvector2(2) - molfrave2)**2.0d0
     &           + (molvector2(3) - molfrave2)**2.0d0
     &           + (molvector2(4) - molfrave2)**2.0d0
     &           + (molvector2(5) - molfrave2)**2.0d0
     &           + (molvector2(6) - molfrave2)**2.0d0
     &           + (molvector2(7) - molfrave2)**2.0d0
     &           + (molvector2(8) - molfrave2)**2.0d0
     &           + (molvector2(9) - molfrave2)**2.0d0)
       stddevmolf2 = dsqrt((1.0d0/9.0d0)*ssqmoldev2)
```

```
c     # write some vals to file
      open(963, file = 'out95.suren', position = 'append')
      write(963,*) 'Bcount: ',Bcount
      write(963,*) 'molvector1',molvector1(1),molvector1(2)
     &           ,molvector1(3),molvector1(4),molvector1(5)
      write(963,*) 'molvector2',molvector2(1),molvector2(2)
     &           ,molvector2(3),molvector2(4),molvector2(5)
      write(963,*) 'ave mole fraction Box
1',molfrave1,'Bvap',myBvalvb
      write(963,*) 'ave mole fraction Box 2',molfrave2,'Bliq',myBvallb
      write(963,*) 'sum of deviations squared',ssqmoldev
      write(963,*) 'standard deviation',stddevmolf1
      close(963)
c     # end of write
      if ((stddevmolf1 .gt. 0.010d0) .or.
     & (stddevmolf2 .gt. 0.010d0)) then
      open(963, file = 'out95.suren', position = 'append')
      write(963,*) 'sd1',stddevmolf1,'sd2',stddevmolf2,'...exiting'
      close(963)
        return
      else

        termobj1 = (1-(molfrave1/ExpData(1)))**2.0d0
        termobj2 = (1-(molfrave2/ExpData(2)))**2.0d0
        SimHist(Bcount,3) = dsqrt(termobj1 + termobj2)

        SimHist(Bcount,1) = myBvalvb
        SimHist(Bcount,2) = myBvallb

        simplex(Bcount,1) = myBvalvb
        simplex(Bcount,2) = myBvallb
        simplex(Bcount,3) = SimHist(Bcount,3)
      write(709,*)  SimHist(Bcount,1),SimHist(Bcount,2)

      do iB = 1,3
        iptrB = iB
        do jjjj = iB+1,3
          if (simplex(jjjj,3) .lt. simplex(iptrB,3)) then
            iptrB = jjjj
          endif
        enddo
        if (iB .ne. iptrB) then
          tempBB = simplex(iB,3)
          simplex(iB,3) = simplex(iptrB,3)
          simplex(iptrB,3) = tempBB
          tempBB = simplex(iB,1)
          simplex(iB,1) = simplex(iptrB,1)
          simplex(iptrB,1) = tempBB
          tempBB = simplex(iB,2)
          simplex(iB,2) = simplex(iptrB,2)
          simplex(iptrB,2) = tempBB
        endif
      enddo

      write(800,*) simplex(1,1), simplex(1,2), simplex(1,3)
      write(800,*) simplex(2,1), simplex(2,2), simplex(2,3)
      write(800,*) simplex(3,1), simplex(3,2), simplex(3,3)

      bCentroid(1,1) = 0.5d0*(simplex(1,1)+simplex(2,1))
      bCentroid(1,2) = 0.5d0*(simplex(1,2)+simplex(2,2))
      ReflectM(1,1)=bCentroid(1,1)+AlphaB*(bCentroid(1,1)-
simplex(3,1))
      ReflectM(1,2)=bCentroid(1,2)+AlphaB*(bCentroid(1,2)-
simplex(3,2))
      ReflectM(1,3)=0.0d0
       write(800,*) 'Reflected point:',ReflectM(1,1),ReflectM(1,2)
      myBvalvb = ReflectM(1,1)
      myBvallb = ReflectM(1,2)

      lReflDone = .true.
      lExpndDone = .false.
      lContrDone = .false.
      lShrinkDone = .false.
      lCtOuter = .false.
      lCtInner = .false.
      endif

      else
 595  molvcount = 1
      do Bincr = 20*Bcount, (20*Bcount-10), -1
        do xxbox = 1,numboxes
          do yymolty = 1,nmolty
            keycode = AC_MOL_FRACTION
              call
twh_averages(lfailure,AVG_EXTRACT_BLOCK_VAL
     &           ,keycode,xxbox,yymolty,xyzvalue,Bincr)
               molfnew(xxbox,yymolty) = xyzvalue
               molvector1(molvcount) = molfnew(1,1)
               molvector2(molvcount) = molfnew(2,1)
          enddo
        enddo
        molvcount = molvcount+1
```

```
      enddo
      molfrave1 = (molvector1(1) + molvector1(2) + molvector1(3)
     &           + molvector1(4) + molvector1(5) + molvector1(6)
     & + molvector1(7) + molvector1(8) + molvector1(9))/9.0d0
      ssqmoldev = ((molvector1(1) - molfrave1)**2.0d0
     &           + (molvector1(2) - molfrave1)**2.0d0
     &           + (molvector1(3) - molfrave1)**2.0d0
     &           + (molvector1(4) - molfrave1)**2.0d0
     &           + (molvector1(5) - molfrave1)**2.0d0
     &           + (molvector1(6) - molfrave1)**2.0d0
     &           + (molvector1(7) - molfrave1)**2.0d0
     &           + (molvector1(8) - molfrave1)**2.0d0
     &           + (molvector1(9) - molfrave1)**2.0d0)
       stddevmolf1 = dsqrt((1.0d0/9.0d0)*ssqmoldev)

      molfrave2 = (molvector2(1) + molvector2(2) + molvector2(3)
     &           + molvector2(4) + molvector2(5) + molvector2(6)
     &  + molvector2(7) + molvector2(8) + molvector2(9))/9.0d0
      ssqmoldev2 = ((molvector2(1) - molfrave2)**2.0d0
     &           + (molvector2(2) - molfrave2)**2.0d0
     &           + (molvector2(3) - molfrave2)**2.0d0
     &           + (molvector2(4) - molfrave2)**2.0d0
     &           + (molvector2(5) - molfrave2)**2.0d0
     &           + (molvector2(6) - molfrave2)**2.0d0
     &           + (molvector2(7) - molfrave2)**2.0d0
     &           + (molvector2(8) - molfrave2)**2.0d0
     &           + (molvector2(9) - molfrave2)**2.0d0)
       stddevmolf2 = dsqrt((1.0d0/9.0d0)*ssqmoldev2)

c     # write some vals to file
      open(963, file = 'out95.suren', position = 'append')
      write(963,*) 'Bcount: ',Bcount
      write(963,*) 'molvector1',molvector1(1),molvector1(2)
     &            ,molvector1(3),molvector1(4),molvector1(5)
      write(963,*) 'molvector2',molvector2(1),molvector2(2)
     &            ,molvector2(3),molvector2(4),molvector2(5)
      write(963,*) 'ave mole fraction Box
1',molfrave1,'Bvap',myBvalvb
      write(963,*) 'ave mole fraction Box 2',molfrave2,'Bliq',myBvallb
      write(963,*) 'sum of deviations squared',ssqmoldev
      write(963,*) 'standard deviation',stddevmolf1
      close(963)
c     # end of write
      if ((stddevmolf1 .gt. 0.006250d0) .or.
     & (stddevmolf2 .gt. 0.0062500d0)) then
      open(963, file = 'out95.suren', position = 'append')
      write(963,*) 'sd1',stddevmolf1,'sd2',stddevmolf2,'...exiting'
      close(963)
        return
      else

c     # write some vals to file
      open(963, file = 'out95.suren', position = 'append')
      write(963,*) 'Standard deviations are satisfactory'
      close(963)
c     # end of write

        termobj1 = (1-(molfrave1/ExpData(1)))**2.0d0
        termobj2 = (1-(molfrave2/ExpData(2)))**2.0d0

        SimHist(Bcount,3) = dsqrt(termobj1 + termobj2)
        SimHist(Bcount,1) = myBvalvb
        SimHist(Bcount,2) = myBvallb
       write(709,*)  SimHist(Bcount,1),SimHist(Bcount,2)
      &    ,SimHist(Bcount,3)
       write(800,*) 'This is Bcount:',Bcount
       write(800,*) 'Previous transformation results:'
       write(800,*) SimHist(Bcount,1),SimHist(Bcount,2)
      &            ,SimHist(Bcount,3)
c      ### More reflections,expansions,shrinks, and contractions!

        if (lReflDone .eqv. .true.) then

          ReflectM(1,3)=SimHist(Bcount,3)

          if ((ReflectM(1,3) .ge. simplex(1,3) .and.
     &        (ReflectM(1,3) .lt. simplex(2,3)))) then
            write(800,*) 'Reflection accepted; reflect again'
c       ## Accept the reflected point; do another reflection
              simplex(3,1)=ReflectM(1,1)
              simplex(3,2)=ReflectM(1,2)
              simplex(3,3)=ReflectM(1,3)

              do iB = 1,3
                iptrB = iB
                do jjjj = iB+1,3
                  if (simplex(jjjj,3) .lt. simplex(iptrB,3)) then
                    iptrB = jjjj
                  endif
                enddo
                if (iB .ne. iptrB) then
                  tempBB = simplex(iB,3)
                  simplex(iB,3) = simplex(iptrB,3)
                  simplex(iptrB,3) = tempBB
                  tempBB = simplex(iB,1)
                  simplex(iB,1) = simplex(iptrB,1)
                  simplex(iptrB,1) = tempBB
                  tempBB = simplex(iB,2)
                  simplex(iB,2) = simplex(iptrB,2)
                  simplex(iptrB,2) = tempBB
                endif
              enddo

              bCentroid(1,1) = 0.5d0*(simplex(1,1)+simplex(2,1))
              bCentroid(1,2) = 0.5d0*(simplex(1,2)+simplex(2,2))
      ReflectM(1,1)=bCentroid(1,1)+AlphaB*(bCentroid(1,1)-
simplex(3,1))
      ReflectM(1,2)=bCentroid(1,2)+AlphaB*(bCentroid(1,2)-
simplex(3,2))
              ReflectM(1,3)=0.0d0
           write(800,*) 'Reflected point: ',ReflectM(1,1),ReflectM(1,2)
              myBvalvb = ReflectM(1,1)
              myBvallb = ReflectM(1,2)
              lReflDone = .true.
             write(800,*) simplex(1,1), simplex(1,2), simplex(1,3)
             write(800,*) simplex(2,1), simplex(2,2), simplex(2,3)
             write(800,*) simplex(3,1), simplex(3,2), simplex(3,3)
              return
              write(800,*) 'Live long and prosper'

          elseif (ReflectM(1,3) .lt. simplex(1,3)) then
              write(800,*) 'Expand: FRefl = ', ReflectM(1,3)
c       ## Expansion
              simplex(3,1)=ReflectM(1,1)
              simplex(3,2)=ReflectM(1,2)
              simplex(3,3)=ReflectM(1,3)

              do iB = 1,3
                iptrB = iB
                do jjjj = iB+1,3
                  if (simplex(jjjj,3) .lt. simplex(iptrB,3)) then
                    iptrB = jjjj
                  endif
                enddo
                if (iB .ne. iptrB) then
                  tempBB = simplex(iB,3)
                  simplex(iB,3) = simplex(iptrB,3)
                  simplex(iptrB,3) = tempBB
```

```
                tempBB = simplex(iB,1)
                simplex(iB,1) = simplex(iptrB,1)
                simplex(iptrB,1) = tempBB
                tempBB = simplex(iB,2)
                simplex(iB,2) = simplex(iptrB,2)
                simplex(iptrB,2) = tempBB
              endif
            enddo

            bCentroid(1,1) = 0.5d0*(simplex(1,1)+simplex(2,1))
            bCentroid(1,2) = 0.5d0*(simplex(1,2)+simplex(2,2))

     ExpandM(1,1)=bCentroid(1,1)+(GammaB*(ReflectM(1,1)
    &    -bCentroid(1,1)))
     ExpandM(1,2)=bCentroid(1,2)+(GammaB*(ReflectM(1,2)
    &    -bCentroid(1,2)))
            ExpandM(1,3)=0.0d0
           write(800,*) 'Expanded
point',ExpandM(1,1),ExpandM(1,2)
            myBvalvb = ExpandM(1,1)
            myBvallb = ExpandM(1,2)

            lReflDone = .false.
            lExpndDone = .true.
           write(800,*) simplex(1,1), simplex(1,2), simplex(1,3)
           write(800,*) simplex(2,1), simplex(2,2), simplex(2,3)
           write(800,*) simplex(3,1), simplex(3,2), simplex(3,3)
            return
          write(800,*) 'May the Force be with you'
       elseif (ReflectM(1,3) .ge. simplex(2,3)) then
          write(800,*) 'Contract: FRefl = ',ReflectM(1,3)
c      ## Contraction

            do iB = 1,3
              iptrB = iB
               do jjj = iB+1,3
                 if (simplex(jjjj,3) .lt. simplex(iptrB,3)) then
                   iptrB = jjjj
                 endif
               enddo
              if (iB .ne. iptrB) then
                tempBB = simplex(iB,3)
                simplex(iB,3) = simplex(iptrB,3)
                simplex(iptrB,3) = tempBB
                tempBB = simplex(iB,1)
                simplex(iB,1) = simplex(iptrB,1)
                tempBB = simplex(iB,2)
                simplex(iB,2) = simplex(iptrB,2)
                simplex(iptrB,2) = tempBB
              endif
            enddo

            bCentroid(1,1) = 0.5d0*(simplex(1,1)+simplex(2,1))
            bCentroid(1,1) = 0.5d0*(simplex(1,1)+simplex(2,1))
            bCentroid(1,2) = 0.5d0*(simplex(1,2)+simplex(2,2))

            if ((ReflectM(1,3) .ge. simplex(2,3) .and.
    &           (ReflectM(1,3) .lt. simplex(3,3)))) then
              write(800,*) '-- Outide Contraction'
     CntrctM(1,1)=bCentroid(1,1)+BetaB*(ReflectM(1,1)-
bCentroid(1,1))
     CntrctM(1,2)=bCentroid(1,2)+BetaB*(ReflectM(1,2)-
bCentroid(1,2))
              lCtOuter = .true.
            elseif (ReflectM(1,3) .ge. simplex(3,3)) then
              write(800,*) '-- Inside Contraction'
     CntrctM(1,1)=bCentroid(1,1)+BetaB*(simplex(3,1)-
bCentroid(1,1))
     CntrctM(1,2)=bCentroid(1,2)+BetaB*(simplex(3,2)-
bCentroid(1,2))
              lCtInner = .true.
            else
              write(800,*) 'Contraction: not supposed to happen'
            endif

            CntrctM(1,3)=0.0d0
          write(800,*) 'Contracted point',CntrctM(1,1),CntrctM(1,2)
            myBvalvb = CntrctM(1,1)
            myBvallb = CntrctM(1,2)
           write(800,*) myBvalvb, myBvallb
            lReflDone = .false.
            lContrDone = .true.
           write(800,*) simplex(1,1), simplex(1,2), simplex(1,3)
           write(800,*) simplex(2,1), simplex(2,2), simplex(2,3)
           write(800,*) simplex(3,1), simplex(3,2), simplex(3,3)
            return
          write(800,*) 'Free your mind'
       endif
c      ## end of Contraction
       elseif (lExpndDone .eqv. .true.) then
            write(800,*) 'Last transformation: Expansion'
        ExpandM(1,3)=SimHist(Bcount,3)
       write(800,*) 'Ex:',ExpandM(1,3),'Rf:',ReflectM(1,3)

       if (ExpandM(1,3) .lt. ReflectM(1,3)) then
c      ## accept expansion and do another reflection
        write(800,*) 'Expansion accepted; calculate new Reflection'
            simplex(3,1) = ExpandM(1,1)
            simplex(3,2) = ExpandM(1,2)
            simplex(3,3) = ExpandM(1,3)

            do iB = 1,3
              iptrB = iB
               do jjj = iB+1,3
                 if (simplex(jjjj,3) .lt. simplex(iptrB,3)) then
                   iptrB = jjjj
                 endif
               enddo
              if (iB .ne. iptrB) then
                tempBB = simplex(iB,3)
                simplex(iB,3) = simplex(iptrB,3)
                simplex(iptrB,3) = tempBB
                tempBB = simplex(iB,1)
                simplex(iB,1) = simplex(iptrB,1)
                simplex(iptrB,1) = tempBB
                tempBB = simplex(iB,2)
                simplex(iB,2) = simplex(iptrB,2)
                simplex(iptrB,2) = tempBB
              endif
            enddo

            bCentroid(1,1) = 0.5d0*(simplex(1,1)+simplex(2,1))
            bCentroid(1,2) = 0.5d0*(simplex(1,2)+simplex(2,2))
     ReflectM(1,1)=bCentroid(1,1)+AlphaB*(bCentroid(1,1)-
simplex(3,1))
     ReflectM(1,2)=bCentroid(1,2)+AlphaB*(bCentroid(1,2)-
simplex(3,2))
            ReflectM(1,3)=0.0d0
          write(800,*) 'Reflected point:',ReflectM(1,1),ReflectM(1,2)
            myBvalvb = ReflectM(1,1)
            myBvallb = ReflectM(1,2)

            lReflDone = .true.
            lExpndDone = .false.

            return
       else
```

```
c      ## reject expansion; accept previous + do another reflection
       write(800,*) 'Expansion rejected; reverting to previous Reflct'
c                simplex(3,1) = ReflectM(1,1)
c                simplex(3,2) = ReflectM(1,2)
c                simplex(3,3) = ReflectM(1,3)

                 do iB = 1,3
                  iptrB = iB
                   do jjjj = iB+1,3
                     if (simplex(jjjj,3) .lt. simplex(iptrB,3)) then
                        iptrB = jjjj
                     endif
                   enddo
                  if (iB .ne. iptrB) then
                     tempBB = simplex(iB,3)
                     simplex(iB,3) = simplex(iptrB,3)
                     simplex(iptrB,3) = tempBB
                     tempBB = simplex(iB,1)
                     simplex(iB,1) = simplex(iptrB,1)
                     simplex(iptrB,1) = tempBB
                     tempBB = simplex(iB,2)
                     simplex(iB,2) = simplex(iptrB,2)
                     simplex(iptrB,2) = tempBB
                   endif
                 enddo

                 bCentroid(1,1) = 0.5d0*(simplex(1,1)+simplex(2,1))
                 bCentroid(1,2) = 0.5d0*(simplex(1,2)+simplex(2,2))

     ReflectM(1,1)=bCentroid(1,1)+AlphaB*(bCentroid(1,1)-
simplex(3,1))
     ReflectM(1,2)=bCentroid(1,2)+AlphaB*(bCentroid(1,2)-
simplex(3,2))
                 ReflectM(1,3)=0.0d0
              write(800,*) 'Reflected point',ReflectM(1,1),ReflectM(1,2)
                 myBvalvb = ReflectM(1,1)
                 myBvallb = ReflectM(1,2)

                 lReflDone = .true.
                 lExpndDone = .false.
                write(800,*) simplex(1,1), simplex(1,2), simplex(1,3)
                write(800,*) simplex(2,1), simplex(2,2), simplex(2,3)
                write(800,*) simplex(3,1), simplex(3,2), simplex(3,3)
                 return

          endif
```

```
        elseif (lContrDone .eqv. .true.) then
          CntrctM(1,3)=SimHist(Bcount,3)
          write(800,*) 'Cn:',CntrctM(1,3),'Rf:',ReflectM(1,3)

        if (lCtOuter .eqv. .true.) then
          if (CntrctM(1,3) .le. ReflectM(1,3)) then
c       ## accept contraction and do another reflection
          write(800,*) 'Outer-Contraction accepted; Reflecting again'
                 simplex(3,1) = CntrctM(1,1)
                 simplex(3,2) = CntrctM(1,2)
                 simplex(3,3) = CntrctM(1,3)

                 do iB = 1,3
                  iptrB = iB
                   do jjjj = iB+1,3
                     if (simplex(jjjj,3) .lt. simplex(iptrB,3)) then
                        iptrB = jjjj
                     endif
                   enddo
                  if (iB .ne. iptrB) then
                     tempBB = simplex(iB,3)
                     simplex(iB,3) = simplex(iptrB,3)
                     simplex(iptrB,3) = tempBB
                     tempBB = simplex(iB,1)
                     simplex(iB,1) = simplex(iptrB,1)
                     simplex(iptrB,1) = tempBB
                     tempBB = simplex(iB,2)
                     simplex(iB,2) = simplex(iptrB,2)
                     simplex(iptrB,2) = tempBB
                   endif
                 enddo

                 bCentroid(1,1) = 0.5d0*(simplex(1,1)+simplex(2,1))
                 bCentroid(1,2) = 0.5d0*(simplex(1,2)+simplex(2,2))
     ReflectM(1,1)=bCentroid(1,1)+AlphaB*(bCentroid(1,1)-
simplex(3,1))
     ReflectM(1,2)=bCentroid(1,2)+AlphaB*(bCentroid(1,2)-
simplex(3,2))
                 ReflectM(1,3)=0.0d0
              write(800,*) 'Reflected point:',ReflectM(1,1),ReflectM(1,2)
                 myBvalvb = ReflectM(1,1)
                 myBvallb = ReflectM(1,2)
                 lContrDone = .false.
                 lCtOuter = .false.
                 lReflDone = .true.
```

```
                 return

          else
c       ## reject contraction; do a Shrink transformation
          write(800,*) 'Outer-Contraction rejected; now Shrinking
simplex'

                 do iB = 1,3
                  iptrB = iB
                   do jjjj = iB+1,3
                     if (simplex(jjjj,3) .lt. simplex(iptrB,3)) then
                        iptrB = jjjj
                     endif
                   enddo
                  if (iB .ne. iptrB) then
                     tempBB = simplex(iB,3)
                     simplex(iB,3) = simplex(iptrB,3)
                     simplex(iptrB,3) = tempBB
                     tempBB = simplex(iB,1)
                     simplex(iB,1) = simplex(iptrB,1)
                     simplex(iptrB,1) = tempBB
                     tempBB = simplex(iB,2)
                     simplex(iB,2) = simplex(iptrB,2)
                     simplex(iptrB,2) = tempBB
                   endif
                 enddo

     ShrinkM1(1,1)=simplex(1,1)+DeltaB*(simplex(2,1)-
simplex(1,1))
     ShrinkM1(1,2)=simplex(1,2)+DeltaB*(simplex(2,2)-
simplex(1,2))
     ShrinkM2(1,1)=simplex(1,1)+DeltaB*(simplex(3,1)-
simplex(1,1))
     ShrinkM2(1,2)=simplex(1,2)+DeltaB*(simplex(3,2)-
simplex(1,2))
                 ShrinkM1(1,3)=0.0d0
                 ShrinkM2(1,3)=0.0d0
              write(800,*) 'Shrink co-ords
pt1',ShrinkM1(1,1),ShrinkM1(1,2)
              write(800,*) 'Shrink co-ords
pt2',ShrinkM2(1,1),ShrinkM2(1,2)
                 myBvalvb = ShrinkM1(1,1)
                 myBvallb = ShrinkM1(1,2)

                 lContrDone = .false.
```

```
              lCtOuter = .false.
              lShrinkDone = .true.
              ShrinkCount = 1
c     ## now replace 2nd n 3rd row of simplex matrix with ShrinkM1
n M2
          simplex(2,1) = ShrinkM1(1,1)
          simplex(2,2) = ShrinkM1(1,2)
          simplex(2,3) = ShrinkM1(1,3)
          simplex(3,1) = ShrinkM2(1,1)
          simplex(3,2) = ShrinkM2(1,2)
          simplex(3,3) = ShrinkM2(1,3)
               write(800,*) simplex(1,1), simplex(1,2), simplex(1,3)
               write(800,*) simplex(2,1), simplex(2,2), simplex(2,3)
               write(800,*) simplex(3,1), simplex(3,2), simplex(3,3)
          write(800,*) 'Note: simplex([2,3],3) still to be calculated'

               return
           endif

       elseif (lCtInner .eqv. .true.) then
          if (CntrctM(1,3) .lt. simplex(3,3)) then
c       ## accept contraction and do another reflection
           write(800,*) 'Inner-Contraction accepted; Reflecting again'
               simplex(3,1) = CntrctM(1,1)
               simplex(3,2) = CntrctM(1,2)
               simplex(3,3) = CntrctM(1,3)

               do iB = 1,3
                 iptrB = iB
                  do jjjj = iB+1,3
                     if (simplex(jjjj,3) .lt. simplex(iptrB,3)) then
                        iptrB = jjjj
                     endif
                  enddo
                 if (iB .ne. iptrB) then
                    tempBB = simplex(iB,3)
                    simplex(iB,3) = simplex(iptrB,3)
                    simplex(iptrB,3) = tempBB
                    tempBB = simplex(iB,1)
                    simplex(iB,1) = simplex(iptrB,1)
                    simplex(iptrB,1) = tempBB
                    tempBB = simplex(iB,2)
                    simplex(iB,2) = simplex(iptrB,2)
                    simplex(iptrB,2) = tempBB
                 endif
               enddo
```

```
               bCentroid(1,1) = 0.5d0*(simplex(1,1)+simplex(2,1))
               bCentroid(1,2) = 0.5d0*(simplex(1,2)+simplex(2,2))
     ReflectM(1,1)=bCentroid(1,1)+AlphaB*(bCentroid(1,1)-
simplex(3,1))
     ReflectM(1,2)=bCentroid(1,2)+AlphaB*(bCentroid(1,2)-
simplex(3,2))
               ReflectM(1,3)=0.0d0
           write(800,*) 'Reflected point:',ReflectM(1,1),ReflectM(1,2)
               myBvalvb = ReflectM(1,1)
               myBvallb = ReflectM(1,2)
               lContrDone = .false.
               lCtInner = .false.
               lReflDone = .true.

               return

           else
c       ## reject contraction; do a Shrink transformation
        write(800,*) 'Inner-Contraction rejected; now Shrinking
simplex'

               do iB = 1,3
                 iptrB = iB
                  do jjjj = iB+1,3
                     if (simplex(jjjj,3) .lt. simplex(iptrB,3)) then
                        iptrB = jjjj
                     endif
                  enddo
                 if (iB .ne. iptrB) then
                    tempBB = simplex(iB,3)
                    simplex(iB,3) = simplex(iptrB,3)
                    simplex(iptrB,3) = tempBB
                    tempBB = simplex(iB,1)
                    simplex(iB,1) = simplex(iptrB,1)
                    simplex(iptrB,1) = tempBB
                    tempBB = simplex(iB,2)
                    simplex(iB,2) = simplex(iptrB,2)
                    simplex(iptrB,2) = tempBB
                 endif
               enddo

     ShrinkM1(1,1)=simplex(1,1)+DeltaB*(simplex(2,1)-
simplex(1,1))
     ShrinkM1(1,2)=simplex(1,2)+DeltaB*(simplex(2,2)-
simplex(1,2))
```

```
     ShrinkM2(1,1)=simplex(1,1)+DeltaB*(simplex(3,1)-
simplex(1,1))
     ShrinkM2(1,2)=simplex(1,2)+DeltaB*(simplex(3,2)-
simplex(1,2))
               ShrinkM1(1,3)=0.0d0
               ShrinkM2(1,3)=0.0d0
          write(800,*) 'Shrink co-ords
pt1',ShrinkM1(1,1),ShrinkM1(1,2)
          write(800,*) 'Shrink co-ords
pt2',ShrinkM2(1,1),ShrinkM2(1,2)
               myBvalvb = ShrinkM1(1,1)
               myBvallb = ShrinkM1(1,2)

               lContrDone = .false.
               lCtInner = .false.
               lShrinkDone = .true.
               ShrinkCount = 1
c     ## now replace 2nd n 3rd row of simplex matrix with ShrinkM1
n M2
          simplex(2,1) = ShrinkM1(1,1)
          simplex(2,2) = ShrinkM1(1,2)
          simplex(2,3) = ShrinkM1(1,3)
          simplex(3,1) = ShrinkM2(1,1)
          simplex(3,2) = ShrinkM2(1,2)
          simplex(3,3) = ShrinkM2(1,3)
               write(800,*) simplex(1,1), simplex(1,2), simplex(1,3)
               write(800,*) simplex(2,1), simplex(2,2), simplex(2,3)
               write(800,*) simplex(3,1), simplex(3,2), simplex(3,3)
          write(800,*) 'Note: simplex([2,3],3) still to be calculated'

               return
           endif
       else
               write(800,*) 'Error:both Inner & Outer cntrcts false'
       endif

        elseif (lShrinkDone .eqv. .true.) then

        if (ShrinkCount .eq. 1) then
          write(800,*) 'meh...'

          ShrinkM1(1,3)=SimHist(Bcount,3)
          write(800,*) 'Shr1:',ShrinkM1(1,3)
c     ## now replace 2nd+3rd highest pt on simplex by ShrinkM1 n
M2
c     ## increment ShrinkCount by 1 and assign other set of Shrink
```

```
pts
c    ## to Bvapor and Bliquid

          ShrinkCount = ShrinkCount + 1
          simplex(2,3) = ShrinkM1(1,3)
          myBvalvb = ShrinkM2(1,1)
          myBvallb = ShrinkM2(1,2)

            write(800,*) simplex(1,1), simplex(1,2), simplex(1,3)
            write(800,*) simplex(2,1), simplex(2,2), simplex(2,3)
            write(800,*) simplex(3,1), simplex(3,2), simplex(3,3)
            write(800,*) 'Note: simplex(3,3) still to be calculated'

          return

        elseif (ShrinkCount .eq. 2) then
          ShrinkM2(1,3)=SimHist(Bcount,3)
          write(800,*) 'Shr2:',ShrinkM2(1,3)
          write(800,*) 'blah'
          ShrinkCount = 0
          simplex(3,3) = ShrinkM2(1,3)

c    ## reflect, n set Shrink logical to F and Refl logical to T...
                do iB = 1,3
                  iptrB = iB
                   do jjjj = iB+1,3
                     if (simplex(jjjj,3) .lt. simplex(iptrB,3)) then
                       iptrB = jjjj
                     endif
                   enddo
                  if (iB .ne. iptrB) then
                    tempBB = simplex(iB,3)
                    simplex(iB,3) = simplex(iptrB,3)
                    simplex(iptrB,3) = tempBB
                    tempBB = simplex(iB,1)
                    simplex(iB,1) = simplex(iptrB,1)
                    simplex(iptrB,1) = tempBB
                    tempBB = simplex(iB,2)
                    simplex(iB,2) = simplex(iptrB,2)
                    simplex(iptrB,2) = tempBB
                  endif
                enddo

                bCentroid(1,1) = 0.5d0*(simplex(1,1)+simplex(2,1))
                bCentroid(1,2) = 0.5d0*(simplex(1,2)+simplex(2,2))
      ReflectM(1,1)=bCentroid(1,1)+AlphaB*(bCentroid(1,1)-
simplex(3,1))
          ReflectM(1,2)=bCentroid(1,2)+AlphaB*(bCentroid(1,2)-
simplex(3,2))
                    ReflectM(1,3)=0.0d0
               write(800,*) 'Reflected point:',ReflectM(1,1),ReflectM(1,2)
                    myBvalvb = ReflectM(1,1)
                    myBvallb = ReflectM(1,2)

                    lShrinkDone = .false.
                    lReflDone = .true.

                  write(800,*) simplex(1,1), simplex(1,2), simplex(1,3)
                  write(800,*) simplex(2,1), simplex(2,2), simplex(2,3)
                  write(800,*) simplex(3,1), simplex(3,2), simplex(3,3)

                return
              else
                write(800,*) 'Error: ShrinkCount neq 1 or 2'
              endif

              endif
            endif
            endif

            return
            end
c    # End of simplex code // SM
```

File: *towhee_input.F*
This is the sample input file that is read by Towhee before execution.

```
inputformat
'Towhee'
randomseed
1321240
random_luxlevel
3
random_allow_restart
T
myBvalvb
1.0d0
myBvallb
1.0d0
ensemble
'npt'
temperature
236.17d0
pressure
4559.0d0
nmolty
2
nmolectyp
360 360
numboxes
2
stepstyle
'cycles'
nstep
200000
printfreq
0
blocksize
10000
moviefreq
0
backupfreq
0
runoutput
'full'
pdb_output_freq
0
loutdft
.false.
loutlammps
.false.
pressurefreq
0
trmaxdispfreq
2000
volmaxdispfreq
2000
chempotperstep
0 0
potentialstyle
'internal'
```

```
ffnumber
2
ff_filename
/home/suren/towhee-6.2.2/ForceFields/towhee_ff_TraPPE-
UA
/home/suren/towhee-
6.2.2/ForceFields/towhee_ff_Pana1989
classical_potential
'Lennard-Jones'
classical_mixrule
'Lorentz-Berthelot'
lshift
.false.
ltailc
.true.
rmin
1.0d0
rcut
11.10440d0
rcutin
5.0d0
electrostatic_form
'coulomb'
coulombstyle
'ewald_fixed_kmax'
kalp
5.6
kmax
5
dielect
1.0
nfield
0
solvation_style
'none'
linit
.FALSE.
initboxtype
'dimensions'
initstyle
```

```
'full cbmc' 'full cbmc'
'full cbmc' 'full cbmc'
initlattice
'simple cubic' 'simple cubic'
'simple cubic' 'simple cubic'
initmol
300 60
60 300
inix iniy iniz
8    8    8
8    8    8
hmatrix
100.0d0 0.0d0 0.0d0
0.0d0 100.0d0 0.0d0
0.0d0 0.0d0 100.0d0
38.00d0 0.0d0 0.0d0
0.0d0  38.00d0 0.0d0
0.0d0  0.0d0 38.00d0
pmvol
0.015d0
        pmvlpr
        0.5d0 1.0d0
        rmvol
        0.1d0
        tavol
        0.4d0
0.115d0
        pm2cbswmt
        0.4d0 1.0d0
        pm2cbswpr
        1.00d0
pmtracm
1.0d0
#(methane)
input_style
'basic connectivity map'
nunit
1
nmaxcbmc
1
lpdbnames
```

```
F
forcefield
'TraPPE-UA'
charge_assignment
'bond increment'
unit ntype
1    'CH4'
vibration
0
improper torsion
0
#(xenon)
input_style
'basic connectivity map'
nunit
1
nmaxcbmc
1
lpdbnames
F
forcefield
'Pana1989'
charge_assignment
'bond increment'
unit ntype
1    'Xe'
vibration
0
improper torsion
0
```

Appendix D

Experimental methane/xenon system

This appendix provides an outline of the experimental system, methane/xenon, with which the simulation results in this work were compared. As pointed out by the experimental workers (Dias *et al*., 2004), many types of molecular characteristics (e.g. shape, flexibility and size) add up to give the overall system's thermodynamic behaviour. The information presented here is based on the experimental investigation of Dias *et al*. (2004).

Mixtures of spherical and quasi-spherical molecules (e.g. noble gases and methane) are among the simplest types of systems that can be studied, and in the case of alkane/noble gas mixtures, a series of mixtures of light alkanes (ethane, propane, n-butane, or *i*-butane) and xenon have also been studied. This justified the study of the methane/xenon system, since methane was missing from the list of light alkanes used in previous such studies. The experimental measurements were performed in a recently-developed apparatus for the study of vapor-liquid or vapor-liquid-liquid equilibrium, which uses a static and analytical method. The phase compositions were analysed by use of a differential thermal conductivity method, using a catherometer. The following phase diagrams were obtained from experiment. For the numerical results that were obtained from the experiments, the reader is referred to Dias *et al*. (2004). The vapour-liquid phase diagram for the system (Figure D-1) is shown on the next page.

Dias *et al*. (2004) used the optimum k_{ij} interaction parameter from a best fit to the isotherm at 236.17 K (the mid-point of the temperature range) to generate all other EoS-predicted data. As can be seen, the PR-EoS provides an excellent representation of the experimental data, although at lower temperatures the vapour phase compositions is over-estimated and at higher temperatures, the liquid phase compositions are over-estimated.

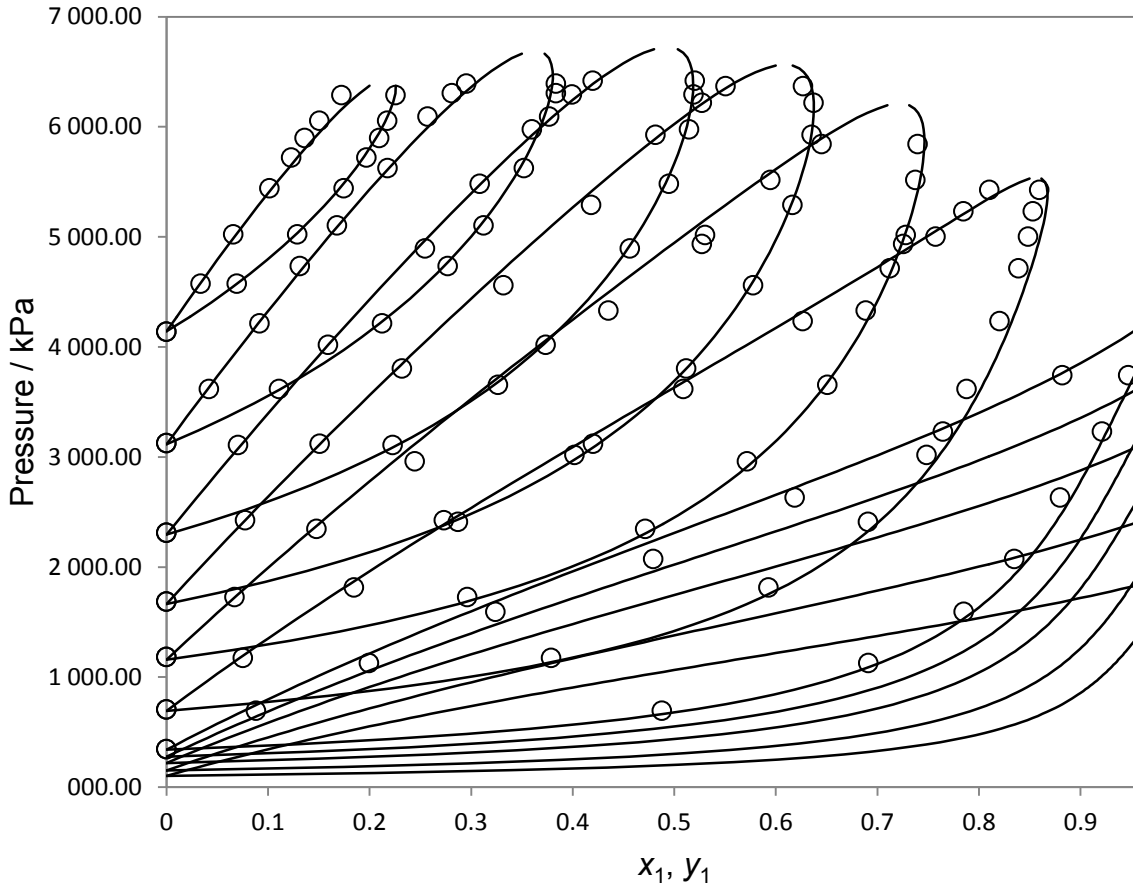

Figure D-1 ‑Isothermal (*P*, *x*, *y*) slices of the methane/xenon vapour-liquid phase diagram. Solid lines correspond to the results obtained with the Peng-Robinson equation of state (PR-EoS), and the symbols correspond to the experimental data – starting from the lower-most isotherm with symbols (experimental data), the experimental temperatures are 189.78 K, 208.29 K, 223.81 K, 236.17 K, 248.15 K, 260.62 K and 273.18 K. The isotherms below 189.78 K, from the lowest isotherm going up are 165 K, 172 K, 180 K and 185 K, which were generated using the PR-EoS.